理學博士學位論文

Mitosis 과정 중 chromosome bi-orientation 에 영향을 미치는 Rad52 의 새로운 기능들

Novel functions of Rad52 in chromosome bi-orientation during mitosis

2018 年 2 月

서울大學校 大學院

生命科學部

임 규 범

ABSTRACT

Novel functions of Rad52 in chromosome bi-orientation during mitosis

Gyubum Lim
The Graduate School
Seoul National University

Chromosome bi-orientation is essential to maintain chromosome number and cell viability. For accurate chromosome segregation, eukaryotic cell monitors the state of spindle-kinetochore attachment by Aurora B kinase, which is a crucial factor of the spindle assembly checkpoint (SAC). In *Saccharomyces cerevisiae*, SAC is regulated by the phosphorylation signal generated by budding yeast Aurora B kinase, Ipl1. When spindle-kinetochore attachment is damaged, Ipl1 recognizes aberrant spindle-kinetochore attachment and recruits SAC activator kinase Mps1 to unattached kinetochore. Kinetochore-accumulated Mps1 recruits SAC proteins such as Mad1, Mad2, and Bub1 to kinetochore and phosphorylates substrates in SAC pathway such as Knl1 and Bub1. Subsequently, activated SAC inhibits the anaphase progression to correct mis-linked spindle-kinetochore connections. Recent studies reported that various kinds of tumor in vertebrate have problem in SAC. Thus defining the details of SAC is helpful to understand mechanism of tumor generation.

Rad52 is key subunit in homologous recombination machinery. During DNA replication in S phase, DNA double strand breakage caused by internal or external reasons is recovered by Rad52-dependent repair pathway. Although the function of Rad52 in DNA damage repair pathway is well studied, other functions are not uncovered yet. Present study found evidences that Rad52 has genetic relationship with subunits of SAC and Ipl1 complex. By using *RAD52* deletion strain, it was clearly confirmed that Rad52 is crucial factor for SAC activation under spindle damage condition and chromosome bi-orientation under normal mitosis.

Mitotic functions of Rad52 are not related to previously reported functions of Rad52, which are homologous recombination activity in eukaryotic cells and kinetochore structure maintenance in *Candida albicans*. It was also verified that Rad52 is novel substrate of major mitotic kinase Ipl1 and SAC activator kinase Mps1 by in vitro kinase assay. To find regulatory mechanism of Rad52 functions in mitosis, physiological functions of Rad52 phosphorylation were examined. By using non-phosphorylable mutants and phospho-mimicking mutants, it was confirmed that Ipl1 phosphorylates Rad52 to recruit Mps1 to the kinetochore and Mps1 phosphorylates Rad52 to activate SAC under spindle damage condition. Based on the obtained results, present study suggests novel functions of Rad52 in accurate chromosome segregation.

Key words : Rad52, Mitosis, Spindle assembly checkpoint, Ipl1, Mps1, *Saccharomyces cerevisiae*.

CONTENTS

LIST OF FIGURES

CHAPTER 1

CHAPTER 2

LIST OF TABLES

BACK GROUND

CHAPTER 1

CHAPTER 2

LIST OF ABBREVIATIONS

CDK	Cyclin dependent kinase
PCNA	Proliferating cell nuclear antigen
SAC	Spindle Assembly Checkpoint
NLS	Nucleus Localization Signal
DNA	Deoxyribonucleic acid
A. A.	Amino Acid
SUMO	Small ubiquitin-like modifier
OD	Optical densiy
DAPI	4',6-diamidino-2-phenylindole
CEN5	Centromere V
GFP	Green Fluorescent Protein
RFP	Red Fluorescent Protein
TAP	Tandem affinity purification
UV	Ultraviolet light
MMS	Methyl methanesulfonate
DTT	Dithilthreitol
SDS	Sodium dodecyl sulfate
PAGE	Polyacrylamide gel eletrophoresis
Tris	Trishydrocymethylaminomethane
EDTA	Ethylenediaminetetraacetic acid
ChIP	Chromatin immunoprecipitation

BACKGROUND

1. Mitosis in *Saccharomyces cerevisiae*

All living cells repeat the cell cycle to product daughter cell that has identical genome information with mother cell. The cell cycle is classified to four phases. G1 phase means the period from end of previous M phase to the beginning of S phase. In this phase, cell growth and biosynthetic activities are accelerated to prepare DNA replication. DNA replication occurs in S phase. During S phase, each chromosome has two sister chromatids, which have identical genome information. After completion of DNA replication, the cell cycle enters G2 phase. In G2 phase, cells synthesize cellular organelles and proteins to prepare mitosis. Cell size is also remarkably increased for cell division in this phase. Duplicated chromosomes are separated to each daughter cell and two daughter cells are divided from each other in M phase. After finishing M phase, two daughter cells enter G1 phase again to prepare next cell division. Thus, The transmission of genetic information from one generation to the next requires the accurate replication of the DNA during S phase and the proper separation of chromosomes during M phase.

1.1. Cell cycle regulation by Cyclin-CDK complex

To faithfully progress cell division, cyclin-dependent kinase complex (CDKC) accurately regulates the each phase of cell cycle. CDKC is comprised to cyclin-dependent kinase CDK and regulatory subunit Cyclin. Depending on the cell phase, CDK associates with different Cyclin to recognize appropriate substrates for regulation of cell cycle. To provide substrate specificity to CDK, Cyclin is precisely regulated by synthesis and programmed proteolysis according to the cell phase. It had been reported that *Saccharomyces cerevisiae* has single CDK, which is known as Cdc28, and nine Cyclins (Andrews and Measday, 1998). Especially, Clb1-Cdc28 and Clb2-Cdc28 complex are well characterized to major regulators of mitosis progression. The list of Cyclin is summarized in **Table 1**.

Table 1 Composition of CDKC in *Saccharomyces cerevisiae*

CDK	cyclin	Phase of cell cycle
Cdc28	Cln3	Mid G1 phase to S phase
Cdc28	Cln1, Cln2	Late G1 phase to S phase
Cdc28	Clb5, Clb6	Early S phase to M phase
Cdc28	Clb3, Clb4	Last S phase to M phase
Cdc28	Clb1, Clb2,	G2 phase to M phase

1.2. Mitotic phase

Mitotic phase (M phase) is the cell cycle period for chromosome segregation and cell division. M phase is divided to mitosis, which is the period for chromosome segregation, and cytokinesis, which is the period for cell division. During the mitosis progression, nuclear envelope is broken at prophase and separated chromosomes are enveloped again at telophase. In contrast, S*accharomyces cerevisiae* progresses close mitosis, which means mitosis progression without breaking of nuclear envelope.

Mitosis is usually classified to four sub phases. After S phase, the cell prepares to progress chromosome segregation during prophase. In the period, replicated DNA is condensed to chromosome. In metaphase, sister chromatids are tethered to opposite spindle poles by mitotic spindles and erroneous attachment between kinetochores and spindles are monitored by mitotic kinase Ipl1 to prevent inaccurate segregation of chromosomes. In anaphase, cohesin, which is a protein complex for holding sister chromatids, is degraded by separase to separate sister chromatids and mitotic spindles are elongated to divide separated sister chromatids to each cell. In telophase, elongated mitotic spindles are degraded from the mid-zone of spindle and chromosomes are decondensed. After telophase, cytokinesis is progressed to divide daughter cell from mother cell.

1.3. Biological function of Ipl1

During mitosis, many mitotic kinases regulate spindle-kinetochore attachment and repair abnormal attachment to maintain the number of chromosomes. Among them, Ipl1 (Aurora B kinase in *Homo sapiens*) is known as a major regulator for monitoring spindle-kinetochore attachment and activating spindle assembly checkpoint (SAC) (Yamagishi et al., 2014). Ipl1 composes Ipl1 complex with Sli15 (INCENP in *Homo sapiens*) and Bir1 (Survivin in *Homo sapiens*) (Carmena et al., 2012). Sli15 acts as a scaffold for other subunits and also assists kinase activity of Ipl1. Bir1 provides binding affinity to the centromeres but is not necessary for

kinase activity of Ipl1 complex. Because, Ipl1 complex is tightly bound to centromere by Bir1, most target proteins of Ipl1 complex are localized close to centromere.

The mechanism of monitoring accurate spindle attachment by Ipl1 complex is well characterized in many eukaryotic organisms. Ipl1 complex localizes between sister kinetochores during metaphase (Ruchaud et al., 2007) and phosphorylates target proteins in a distance-dependent manner (Wang et al., 2011). Ipl1 dependent phosphorylation of substrates at kinetochore destabilizes spindle-kinetochore interaction (Kalantzaki et al., 2015; Liu et al., 2009). When tension is generated by bi-directional attachment of spindles, the distance between Ipl1 and its substrates increases. Increasing distance from Ipl1 complex helps that substrates are dephosphorylated by PP1 phosphatase, resulting in stabilization of spindle-kinetochore interaction (Emanuele et al., 2008; Liu et al., 2010). All spindle-kinetochore attachment are stabilized by bi-directional tension, the cell cycle progresses to anaphase to separate sister chromatids. By contrast, when kinetochores are not connected properly to spindles, substrates in kinetochore are stayed close to centromere and continuously phosphorylated by Ipl1 complex. The kinetochore including phosphorylated substrates loses the stability of spindle attachment and it is sequentially detached from mitotic spindle. Because unattached kinetochore acts as a signal for SAC activation, anaphase transition is suppressed to recover accurate attachment between spindle and unattached kinetochore.

1.4. Biological function of Mps1

Mps1 was identified originally in *Saccharomyces cerevisiae* as a gene required for duplication of the spindle pole body. Subsequently, kinase activity for SAC regulation was also defined. When unattached kinetochores are generated by kinase activity of Ipl1 complex, Mps1 is accumulated to unattached kinetochores to activate SAC. Kinetochore-accumulated Mps1 recruits SAC proteins such as Mad1, Mad2, and Bub1 to kinetochore and phosphorylates substrates in SAC pathway such as Knl1 and Bub1 (London and Biggins, 2014; London et al.,

2012). SAC protein complex suppresses APC/C activator Cdc20 by proteasome-dependent proteolysis and prevents metaphase to anaphase transition.

By the recent report, It is clearly confirmed that kinase activity of Ipl1 and outer kinetochore component Ndc80 are required for Mps1 localization to kinetochore (Heinrich et al., 2012). However, how localization of Mps1 can be regulated by kinase activity of centromere bound Ipl1 is not yet discovered.

2. Mitotic checkpoint in *Saccharomyces cerevisiae*

Mitotic checkpoint is a cell cycle checkpoint that delays mitosis for accurate chromosome segregation and cell division. It is comprised of two pathways, which are spindle assembly checkpoint (SAC) and Bub2-dependent checkpoint. SAC suppresses anaphase-promoting complex APC/C that promotes metaphase to anaphase transition. When SAC is activated, the cell cycle is stopped in metaphase. Bub2-dependent checkpoint suppresses activation of anaphase phosphate Cdc14. Thus, it stops the cell cycle at the beginning of anaphase.

2.1. Spindle assembly checkpoint

To ensure accurate chromosome segregation, cells developed SAC to supervise chromosome bi-orientation and to control metaphase to anaphase transition. SAC suppresses APC/C complex, which is an E3 ubiquitin ligase for metaphase to anaphase transition. During the mitosis, APC/C binds to Cdc20, which is the activator of APC/C, and this complex degrades Securin (Pds1 in *S. cerevisiae*) and cyclin B by ubiquitination to activate seperase (Cohen-Fix et al., 1996; Glotzer et al., 1991; Visintin et al., 1997). When spindle damage occurs, Mps1 phosphorylates Knl1 (Spc105 in *S. cerevisiae*) to activate SAC (London et al., 2012). Phosphorylated Knl1 accumulates SAC components such as Mad1, Mad2, and Bub1 (Shepperd et al., 2012; Yamagishi et al., 2012). Mad2 composes mitotic checkpoint complex (MCC) with Cdc20 (Hwang et al., 1998; Sudakin et al., 2001), and Cdc20 in MCC is degraded by Mad2 and APC/C dependent manner to inactivate APC/C^{Cdc20} (Ge et al., 2008).

2.2. Bub2-depedent checkpoint

Bub2-dependent checkpoint suppresses release of Cdc14 to inhibit mitotic exit (Alexandru et al., 1999; Fraschini et al., 1999). Cdc14 is regulated by Cdc fourteen early anaphase release (FEAR) network and mitotic exit network (MEN) (Pereira et al., 2002; Shou et al., 1999; Stegmeier et al., 2002). Although FEAR network, which is activated by APC/C^{Cdc20},

initiates Cdc14 release from nucleolus, MEN is also important to maintain Cdc14 release and fully activate its phosphatase activity (Stegmeier et al., 2002). Bub2/Bfa1 suppresses Ras-like GTPase Tem1, which is a positive regulator of MEN, and suppression of MEN results cell cycle arrest to prevent anaphase promotion (Geymonat et al., 2002; Shirayama et al., 1994).

Although Bub2-dependent checkpoint can be activated by both of DNA damage and spindle damage, detailed mechanisms for activating checkpoint are clearly different. For DNA damage repair, The DNA damage checkpoint proteins such as Rad53 and Dun1 regulate Bfa1, which is binding partner of Bub2, to activate Bub2-dependent checkpoint (Liang and Wang, 2007). By contrast, Bub2-dependent checkpoint is activated by Cdc5-dependent phosphorylation of Bub2 in response to spindle damage to prevent inaccurate chromosome segregation (Hu and Elledge, 2002).

3. Rad52

3.1. Repair pathways for DNA double strand break

DNA double strand break (DSB) are one of severe damage that causes impaired genome stability. Thus, the repair of DSB is extremely important for the cell viability and the maintenance of genome integrity. DSB can be repaired by two pathways, non-homologous-end junction (NHEJ) and homologous recombination (HR). Non-homologous end-joining directly connects the broken DNA ends by ligation. In contrast, homologous recombination repairs damaged DNA by using undamaged homologous DNA template to restore all genomic information on damaged site. Thus, contrary to non-homologous end-joining, homologous recombination is error-free mechanism for DSB repair.

3.2. Role of Rad52 in *Saccharomyces cerevisiae*

In *saccharomyces cerevisiae*, DSB repair by homologous recombination is progressed in two steps, recognition of DSB by DNA damage checkpoint and DSB repair by *RAD52* epistasis group.

3.2.1. DNA damage checkpoint

To maintain genome integrity, DSB should be rapidly recognized by DNA damage checkpoint. When DNA damage occurs, sensor proteins such as Rad9, Rad17, Rad24, Mec3, and Ddc1 recognizes the presence of damaged DNA and initiates the DNA damage checkpoint to stop the progression of cell cycle until repair completion. The sensors activate the signal transducer kinase Mec1 and Mec1 phosphorylates several kinases including Rad53 and Chk1 (Alver et al., 2013; D'Amours and Jackson, 2002). Although the targets of Rad53 and Chk1 in cell cycle regulator have not clearly defined, recent studies presumed that proteins related to

mitosis such as Cdc5 and Pds1 can be regulated by DNA damage checkpoint (Liang and Wang, 2007).

3.2.2. DSB repair by *RAD52* epistasis group

After cell cycle inhibition by DNA damage checkpoint, DSB is repaired by *RAD52* epistasis group, which includes *RAD50*, *RAD51*, *RAD52*, *RAD54*, *RAD55*, *RAD57*, *RAD59*, *RDH54/TID1*, *MRE11* and *XRS2* genes (Dudáš and Chovanec, 2004). Single-stranded DNA (ssDNA) at DSB site is coated by spindle-stranded DNA binding protein RPA. Subsequently, Rad52 is accumulated to damage site and interacts with RPA. Accumulated Rad52 at damage site recruits Rad51 and promotes the binding of Rad51 to ssDNA by RPA replacement. The interaction between Rad51 and ssDNA is stabilized by binding of Rad55-Rad57 to Rad51 complex. Rad54 interacts with the Rad51-ssDNA nucleoprotein and promotes the unwinding of complementary double strand DNA to supply the template for synthesis of damaged DNA (Symington, 2002). After formation of DNA damage repair complex, ssDNA is replicated by PCNA and δ polymerase.

4. Aims of this study

Mitosis is the central process to transmit genomic information to next generation. To faithfully inherit replicated DNA from mother cell, all steps of mitosis are precisely regulated by mitotic regulators and monitored by mitotic checkpoint. Because improper regulation of mitosis results aneuploidy, which promotes tumorigenesis in mammalian system, defining of all details in regulatory mechanism is the major concern of the researchers.

Last few years, the functions of mitotic kinases such as Ipl1 and Mps1 have been highlighted in molecular mechanism of mitotic regulation. As a major kinase for mitotic regulation, Ipl1 monitors kinetochore-microtubule attachment and regulates accurate chromosome segregation (Yamagishi et al., 2014). Mps1 is known as SAC activating kinase. When spindle damage occurs, Mps1 is accumulated to kinetochore and phosphorylates SAC-related substrates to prevent metaphase to anaphase transition. In the recent studies, it was also demonstrated that Mps1 has a function for mitotic regulation during unperturbed mitosis (Heinrich et al., 2012; Maure et al., 2007; Nijenhuis et al., 2013). Although it has been discovered that precise regulation of Mps1 activity requires kinase activity of Ipl1, detailed mechanism has not been fully defined.

Present study attempts to define the novel functions of Rad52 in mitotic regulation. Because Rad51 and Rad52 play central role in regulation of homologous recombination, homologous recombination related features of Rad52 such as functional domain, interacting partners, and protein structure have been well characterized. By contrast, other functions of Rad52 have not been discovered. Thus, defining the functions in other biological process will help to expand the understandings of Rad52. Furthermore, the Rad52 functions in mitotic regulation provide further insights into the regulatory mechanism of mitosis.

CHAPTER 1

Rad52 is important for proper chromosome segregation and spindle assembly checkpoint activation

1. Introduction

Proper segregation of duplicated chromosomes during mitosis is most crucial step to maintain genome stability of next generation. To accurately regulate chromosome segregation, eukaryotic cells have evolutionally developed monitoring system for spindle-kinetochore interaction and mitotic checkpoint. Spindle-kinetochore interaction is monitored by measuring the tension between sister kinetochores, which is generated by pulling forces of mitotic spindles (Yamagishi et al., 2014). When the tension between sister kinetochores is not properly generated, cells suppress cell cycle progression and activate repair pathway to recover accurate spindle-kinetochore interaction.

Mitotic checkpoint is a cell cycle checkpoint that delays mitosis for accurate chromosome segregation and cell division. It is comprised of two pathways, which are spindle assembly checkpoint (SAC) and Bub2-dependent checkpoint. SAC is activated in metaphase to delay anaphase onset and suppresses APC/C complex, which is an E3 ubiquitin ligase for metaphase to anaphase transition. During the mitosis, APC/C binds to Cdc20, which is the activator of APC/C, and this complex degrades Securin (Pds1 in *S. cerevisiae*) and cyclin B by ubiquitination to activate seperase (Cohen-Fix et al., 1996; Glotzer et al., 1991; Visintin et al., 1997). When spindle damage occurs, Mps1 phosphorylates Knl1 (Spc105 in *S. cerevisiae*) to activate SAC (London et al., 2012). Phosphorylated Knl1 accumulates SAC components such as Mad1, Mad2, and Bub1 (Shepperd et al., 2012; Yamagishi et al., 2012). Mad2 composes mitotic checkpoint complex (MCC) with Cdc20 (Hwang et al., 1998; Sudakin et al., 2001), and Cdc20 in MCC is degraded by Mad2 and APC/C dependent manner to inactivate APC/C^{Cdc20} (Ge et al., 2008). Bub2-dependent checkpoint suppresses release of Cdc14 to inhibit mitotic exit (Alexandru et al., 1999; Fraschini et al., 1999). Cdc14 is regulated by Cdc fourteen early anaphase release (FEAR) network and mitotic exit network (MEN) (Pereira et al., 2002; Shou et al., 1999; Stegmeier et al., 2002). Although FEAR network, which is activated by APC/C^{Cdc20},

initiates Cdc14 release from nucleolus, MEN is also important to maintain Cdc14 release and fully activate its phosphatase activity (Stegmeier et al., 2002). Bub2/Bfa1 suppresses Ras-like GTPase Tem1, which is a positive regulator of MEN, and suppression of MEN results cell cycle arrest to prevent anaphase promotion (Geymonat et al., 2002; Shirayama et al., 1994).

Rad52 is a key factor for homologous recombination pathway. Because homologous recombination is crucial step to repair DNA double strand break (DSB), Rad52 is also important to maintain genome stability. In *saccharomyces cerevisiae*, DSB repair by homologous recombination is progressed in two steps, recognition of DSB by DNA damage checkpoint and DSB repair by *RAD52* epistasis group. When DNA damage occurs, sensor proteins such as Rad9, Rad17, Rad24, Mec3, and Ddc1 recognizes the presence of damaged DNA and initiates the DNA damage checkpoint to stop the progression of cell cycle until repair completion. The sensors activate the signal transducer kinase Mec1 and Mec1 phosphorylates several kinases including Rad53 and Chk1 (Alver et al., 2013; D'Amours and Jackson, 2002). Although the targets of Rad53 and Chk1 in cell cycle regulator have not clearly defined, recent studies presumed that proteins related to mitosis such as Cdc5 and Pds1 can be regulated by DNA damage checkpoint (Liang and Wang, 2007). After cell cycle inhibition by DNA damage checkpoint, DSB is repaired by *RAD52* epistasis group, which includes *RAD50*, *RAD51*, *RAD52*, *RAD54*, *RAD55*, *RAD57*, *RAD59*, *RDH54/TID1*, *MRE11* and *XRS2* genes (Dudáš and Chovanec, 2004). Single-stranded DNA (ssDNA) at DSB site is coated by spindle-stranded DNA binding protein RPA. Subsequently, Rad52 is accumulated to damage site and interacts with RPA. Accumulated Rad52 at damage site recruits Rad51 and promotes the binding of Rad51 to ssDNA by RPA replacement. The interaction between Rad51 and ssDNA is stabilized by binding of Rad55-Rad57 to Rad51 complex. Rad54 interacts with the Rad51-ssDNA nucleoprotein and promotes the unwinding of complementary double strand DNA to supply the template for synthesis of damaged DNA (Symington, 2002). After formation of DNA damage repair complex, ssDNA is replicated by PCNA and δ polymerase.

Although it has been discovered that details about homologous recombination activity of Rad52, other functions of Rad52 has not been defined. In this study, it was confirmed that Rad52 has novel functions for mitotic regulation. Rad52 is a key factor for SAC activation under spindle damage condition. Furthermore, Rad52 also regulates accurate chromosome bi-orientation. Finally, present study provides further insight for understanding the precise mechanism of mitotic regulation.

2. Results

Deletion of *RAD52* leads to cell growth defect

The optical density at wavelength 600nm is usually used to measure growth of yeast cells. According to the increase pattern of the optical density, growth of yeast is classified to four phases; lag phase, log (logarithmic) phase, stationary phase, and death phase. Among these four phases, log phase shows most efficient proliferation. To check the difference of growth rate between wild-type and *rad52*Δ cells, the optical density from lag phase to late log phase was measured. Compared to wild-type cells, *rad52*Δ cells showed growth defect in log phase (**Fig. 1A**). To identify cell cycle phase that was delayed in *rad52*Δ cells, DNA contents analysis was performed. Cell cycle is divided to four phases; G1, S, G2, and M phase. Because cell cycle phases represent procedures for cell division including DNA replication event, measurement of DNA contents can be used to examine the composition of cell cycle phases. As shown in **Fig. 1B**, wild-type cells in log phase were almost evenly distributed to G1 and G2/M phase. However, in *rad52*Δ cells, large numbers of cells were accumulated in G2/M phase. These results suggest that deletion of *RAD52* leads to cell growth defect, which is caused by cell cycle delay in G2/M phase.

Deletion of *RAD52* causes delay of mitosis progression

Because DNA contents analysis divides cell cycle phases based on amount of DNA in the cell, it cannot separate G2 and M phase, which have two copies of DNA. Furthermore, M phase is roughly separated to five detailed phases; prophase, metaphase, anaphase, telophase, and cytokinesis (Ruchaud et al., 2007). Thus, I examined that which detailed phase is delayed in *rad52*Δ cell to find the reason of growth defect. Consistent with DNA content data, large budded cell was frequently observed in *rad52*Δ cells. To obtain the information of delayed cell phase, nucleus was stained with blue-fluorescent DNA straining agent DAPI. Contrary to other

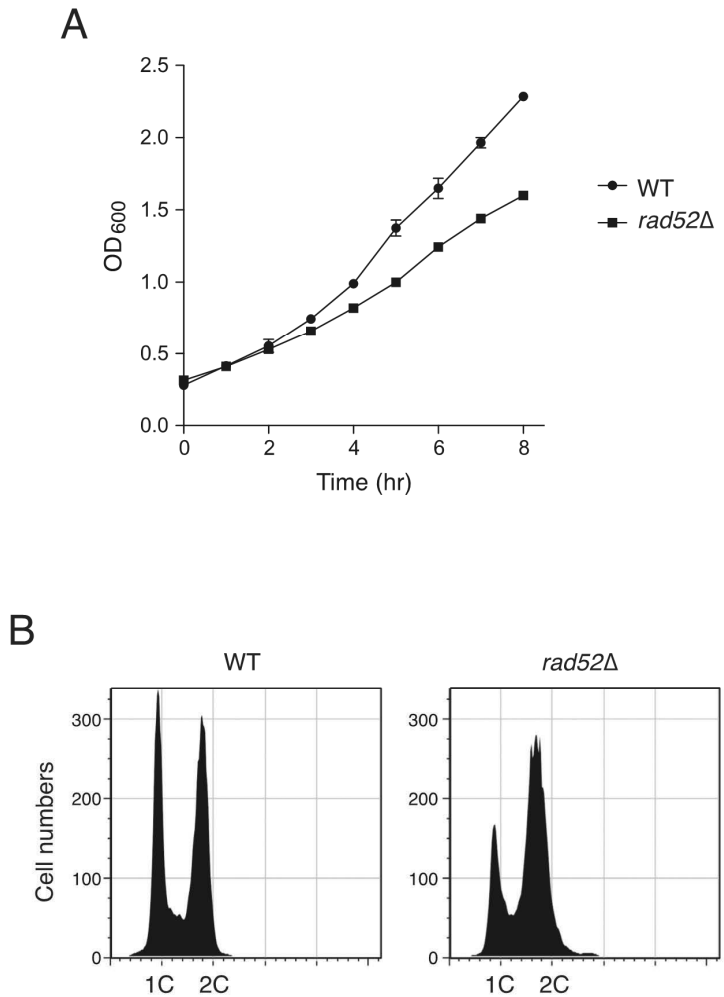

Fig. 1 *rad52*Δ cells show growth defect.

(A) Growth rate of *rad52*Δ cells was lower than wild-type strain in log phase. Wild-type and rad52Δ cells, which contain empty vector, were grown in SC-Leu media. Optical density was measured every 1 hr. Data represent the mean±SD of triplicate cultures. (B) Large numbers of *rad52*Δ cells were accumulated in G2/M phase. DNA contents of wild-type and *rad52*Δ cells were analyzed by flow cytometry. 1C and 2C indicate single and double DNA haploid content.

eukaryotic cells, nuclear envelope is not destructed in *Saccharomyces cerevisiae* during mitosis. Thus, DAPI staining visualizes morphology of nucleus in budding yeast. As shown in **Fig. 2 (upper panel)**, cell types were divided according to the budding index and nucleus morphology. Unbudded cell with single nucleus was considered as cell in G1 phase and budded cells were classified to three nucleus types, which are one nucleus, dumbbell-shaped nuclei, and two nuclei. Less than 3% of wild-type cells showed dumbbell-shaped nuclei and other nucleus types were mainly observed. In contrary, 20% of *rad52*Δ cells had undivided dumbbell-shaped nuclei (**Fig. 2; lower panel**). This result indicates that separation of duplicated chromosomes is delayed in *rad52*Δ cells.

Deletion of *RAD52* causes delay of Ipl1 complex localization to the mitotic spindle

To more confirm whether growth defect of *rad52*Δ cells is due to the delay in mitosis, I chased mitotic phase-dependent localization of Ipl1. According to the previous study (Buvelot et al., 2003), Ipl1 changes cellular localization during mitosis. First, Ipl1 localized to the kinetochores until metaphase to monitor kinetochore-microtubule attachment and regulate accurate chromosome segregation. Second, when tension between kinetochore and microtubule is generated by amphitelic attachment and mitosis is progressed to early anaphase, Ipl1 moves from kinetochore to the mitotic spindle. Third, Ipl1 moves again from the mitotic spindle to the spindle mid-zone at late anaphase to degrade elongated mitotic spindle (**Fig. 3A**). In *rad52*Δ cells, however, Ipl1 was released from the kinetochores and diffused to the nucleus during mitosis (**Fig. 3B**). In addition, Sli15, a subunit of Ipl1 complex, was also diffused to the nucleoplasm similarly to Ipl1 (**Fig. 3C**). It suggests that Ipl1 complex cannot properly localized to the mitotic spindle at the transition between metaphase and anaphase.

Mis-localization of Ipl1 can be caused by either disruption in spindle organization or uncoordinated regulation of Ipl1. To check whether mis-localization of Ipl1 complex is caused by the disruption in spindle organization, spindle morphology in these strains was examined by

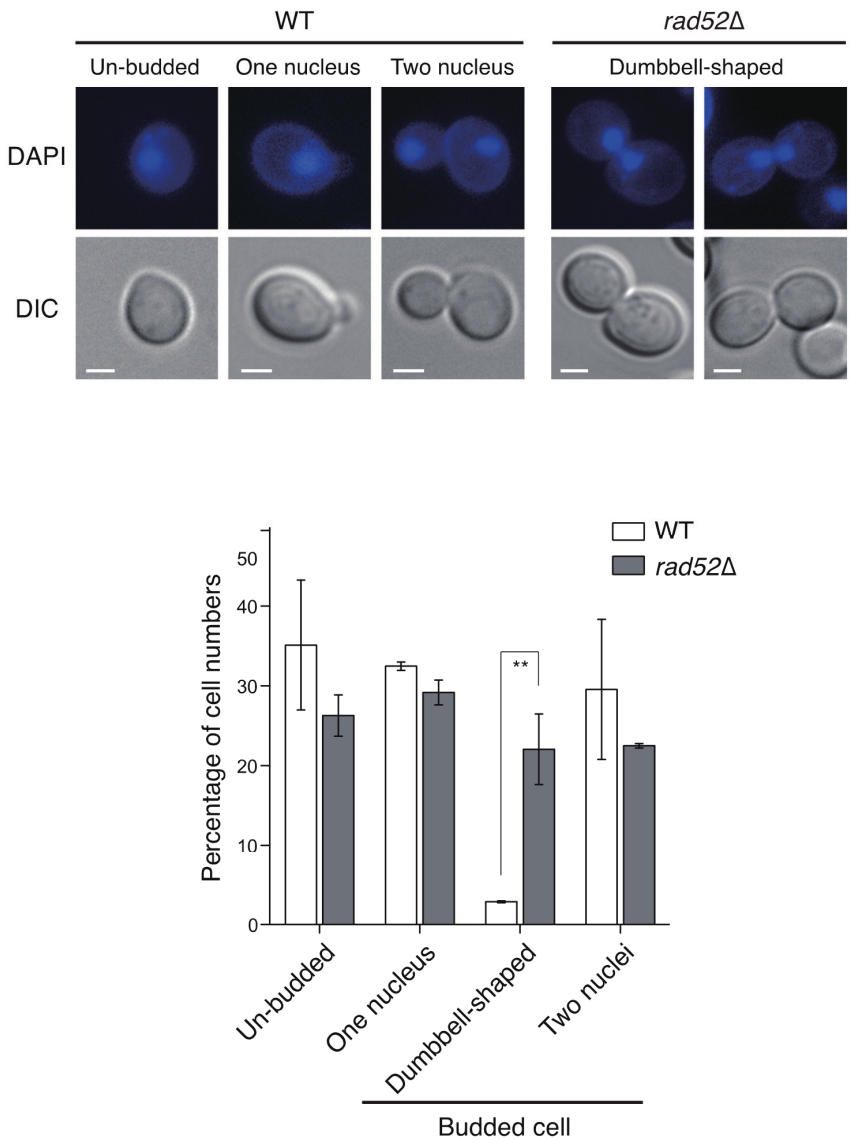

Fig. 2 Large numbers of *rad52*Δ cells showed undivided dumbbell-shaped nuclei.

Nuclei were visualized by 1 μg/ml DAPI staining at mid-log phase. Scale bars are 2 μm. More than 200 cells were counted in every trial (lower panel). Data represent the mean±SD of triplicate cultures. P-values were determined by the Student's t test (**$p < 0.01$).

using spindle-binding protein Bim1 (Schwartz et al., 1997). As shown in **Fig. 3D**, spindle was properly organized in *rad52*Δ cells, while Ipl1 was diffused to nucleus. These results suggest that the binding step of Ipl1 complex to the mitotic spindle is delayed in *rad52*Δ cells. It has been reported that Ipl1 complex is dephosphorylated by anaphase-promoting phosphatase Cdc14 to have binding affinity to the mitotic spindle in anaphase (Zimniak et al., 2012). Thus, this result suggested that growth defect of *rad52*Δ cells was due to the delay in Cdc14 activation.

Loss of Homologous recombination activity does not cause growth defect of *rad52*Δ cells

Because Rad52 is the major component of homologous recombination, *rad52*Δ cell cannot repair DNA damage. It has been also reported that DNA damage can cause G2/M arrest (Liang and Wang, 2007). Thus, the relationship growth defect and homologous recombination activity was examined. To check whether growth defect of *rad52*Δ cells was due to the loss of homologous recombination activity, I constructed a C-terminus-truncated mutant of Rad52 as previously described (Seong et al., 2008). Rad52 can be divided to three parts as shown in **Fig. 4A**. N-terminus part (N region) is from 1st A.A. to 136th A.A., including DNA binding domain and oligomerization domain for construction DNA repair complex with other Rad52 proteins. Middle part (M region) is from 137th A.A. to 294th A.A., including RPA binding domain for recognition of damaged DNA. C-terminus part (C region) is from 295th A.A. to 471st A.A., including Rad51 binding domain for construction of homologous recombination complex with other repair proteins and DNA binding domain. Because truncation of protein domain can result protein mis-folding or mis-regulation of cellular localization, I checked protein expression and localization of C-terminus-truncated Rad52 mutant by using RFP fusion. As shown in **Fig. 4B**, C-terminus-truncated Rad52 mutant was well expressed and localized to the nucleus. To confirm disruption of DNA repair activity in C-terminus-truncated Rad52 mutant, I checked the viability under stress condition by treatment of DNA damage agents such as MMS and UV. Compared to *rad52*Δ cells expressing wild-type Rad52, *rad52*Δ cells expressing C-terminus-

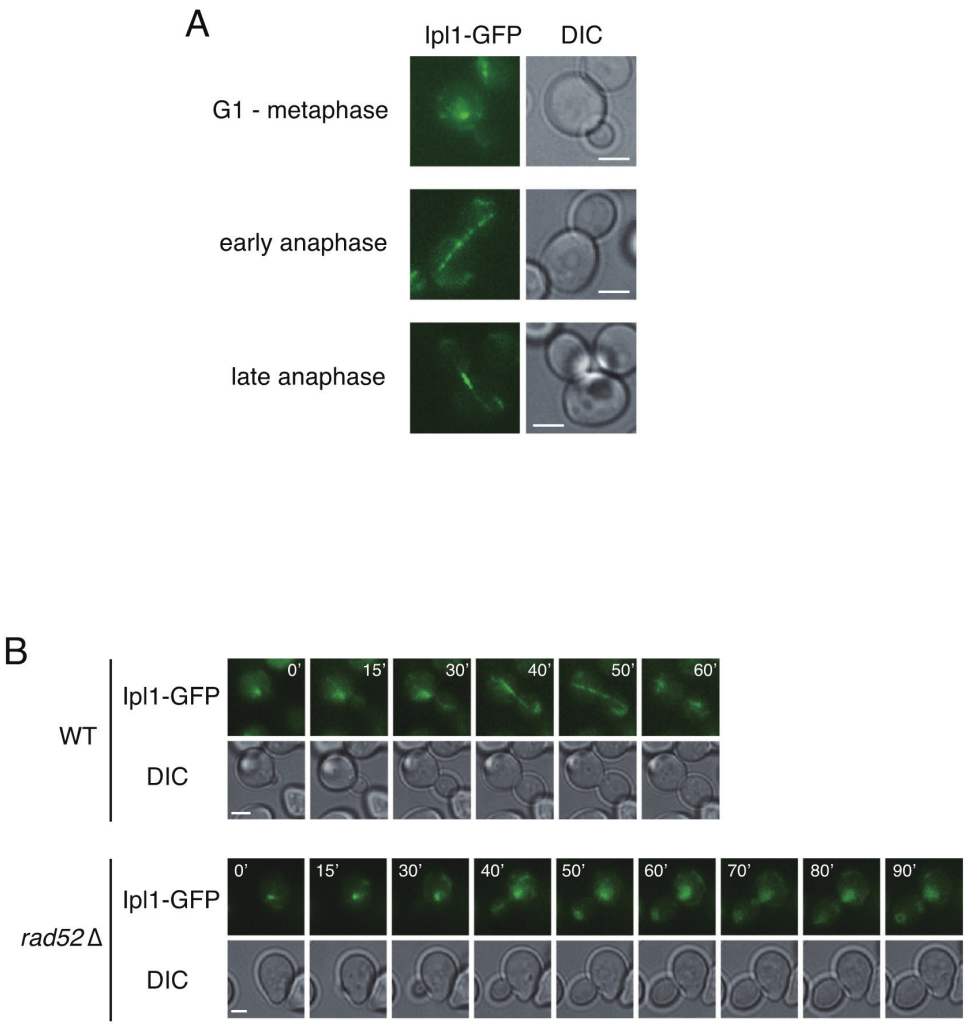
A
Ipl1-GFP
DIC
G1 - metaphase
early anaphase
late anaphase
B
WT
Ipl1-GFP
DIC
0'
15'
30'
40'
50'
60'
rad52Δ
Ipl1-GFP
DIC
0'
15'
30'
40'
50'
60'
70'
80'
90'

C

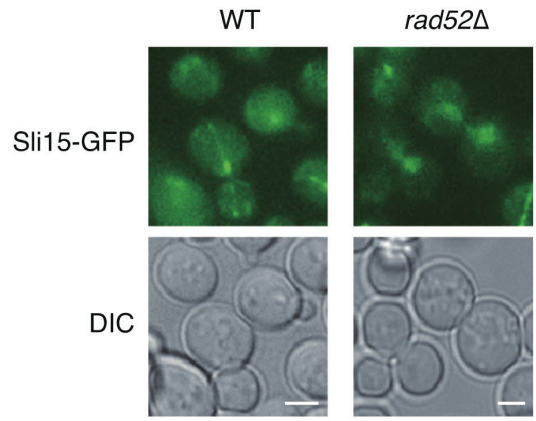
WT
rad52Δ
Sli15-GFP
DIC

D

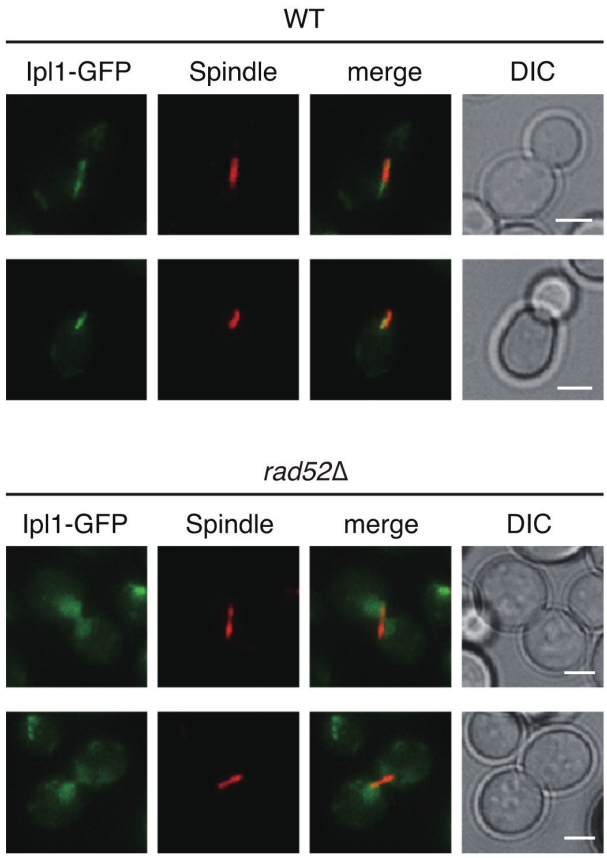
WT
Ipl1-GFP
Spindle
merge
DIC
rad52Δ
Ipl1-GFP
Spindle
merge
DIC

Fig. 3 Ipl1 complex was diffused from the kinetochore to the nucleoplasm in *rad52*Δ cells during mitosis.

(A) Ipl1 was localized to the kinetochore from G1 to metaphase, mitotic spindle at early anaphase, and spindle middle zone at late anaphase. Wild-type cells expressing GFP-tagged Ipl1 was imaged during asynchronous log phase in SC media. Scale bars are 2 μm. (B) Ipl1 in *rad52*Δ cells was diffused from the kinetochore to the nucleoplasm during mitosis. Wild-type and *rad52*Δ cells were grown in SC media, synchronized by 150 μM α-factor treatment, washed and released to fresh SC media. GFP-tagged Ipl1 was imaged every 5 min. Scale bars are 2 μm. (C) Ipl1 complex subunit Sli15 was also diffused to the nucleus in *rad52*Δ cells during mitosis. Wild-type cells expressing GFP-tagged Sli15 and *rad52*Δ cells expressing GFP-tagged Sli15 were imaged during asynchronous log phase in SC media. Scale bars are 2 μm. (D) Spindle morphology in *rad52*Δ cells was not different with that in wild-type cells, while Ipl1 was diffused to nucleus. Spindle was visualized by RFP tagged spindle-binding protein Bim1. Scale bars are 2 μm.

truncated Rad52 mutant showed hypersensitivity to MMS treatment and UV radiation (**Fig. 4C**). It suggests that C-terminus-truncated Rad52 mutant failed to recover DNA damage caused by UV and MMS and homologous recombination activity of Rad52 resides at the C-terminus. To check whether C-terminus-truncated Rad52 mutant recovers growth defect of *rad52*Δ cells, the optical density from lag phase to late log phase was measured using rad52Δ cells expressing wild-type Rad52 or C-terminus-truncated Rad52 mutant. As shown in **Fig. 4D**, the expression of C-terminus-truncated Rad52 mutant rescued growth defect of *rad52*Δ cells. To check whether cell cycle phase is also recovered in *rad52*Δ cells expressing C-terminus-truncated Rad52, DNA contents analysis was performed. Compared to *rad52*Δ cells including expression vector for wild-type Rad52 or empty vector, expression of C-terminus-truncated Rad52 did not represent G2/M phase accumulation phenotype of *rad52*Δ cells (**Fig. 4E**). These results suggest that growth defect of *rad52*Δ cells is not related to the loss of homologous recombination activity.

Domains for DNA damage repair and cell cycle regulation are definitely separated in Rad52

To identify Rad52 domain for cell cycle regulation, I made other truncated mutants of Rad52 as described in **Fig. 5A**. 137-471Δ mutant retained only N-terminus part of Rad52. To construct Middle part truncated mutants such as 137-272Δ and 137-294Δ, amplified N-terminus and C-terminus genomic DNAs were conjugated by SLIC method (Jeong et al., 2012). 137-294Δ mutant excluded all domains in Middle part of Rad52 and 137-272Δ mutant retained RPA binding domain to avoid disruption of DNA damage repair activity. For construction of N-terminus truncated Rad52 mutants such as 1-61Δ and 1-136Δ, NLS sequence from SV40 was inserted to 3'-end of *RAD52* sequence. 1-136Δ mutant excluded all domains in N-terminus part of Rad52 and 1-61Δ mutant retained oligomerization domain to avoid disruption of DNA damage repair activity. I checked the expression of all truncated mutants by fluorescence

intensity of C-terminally tagged RFP and confirmed that 137-272Δ mutant and 137-294Δ mutant were unstable in cells (**Fig. 5B**). To confirm the effect of truncated mutation on DNA damage repair activity, I checked the viability under stress condition by UV radiation. Compared to *rad52*Δ cell expressing wild-type Rad52, only 1-61Δ mutant was functionally active under DNA damage condition and effectively repair DNA damages (**Fig. 5C**). To check whether truncated Rad52 mutants recover growth defect of *rad52*Δ cells, the optical density from lag phase to late log phase was measured using rad52Δ cells expressing truncated Rad52 mutants. As shown in **Fig. 5D**, all types of truncated Rad52 mutant could not restore growth defect of *rad52*Δ cells. These results demonstrate that, although exact domain for cell cycle regulation is still unclear, domains for DNA damage repair and cell cycle regulation are definitely separated in Rad52.

DNA damage does not spontaneously occur in *rad52*Δ cells

Because DNA damage can cause G2/M phase arrest (Liang and Wang, 2007) and Rad52 is a key factor for DNA damage repair pathway, the confirmation that DNA damage does not cause growth defect of *rad52*Δ cells is most important information to define the novel functions of Rad52. Using domain-truncated Rad52 mutants, it was confirmed that the domains for DNA damage repair pathway are distinctly separated from the domain for cell growth regulation. To further confirm that DNA damage does not have responsibility to growth defect in *rad52*Δ cells, DNA damage occurrence during normal cell growth without treatment of DNA damage agents was examined. Rad53 is a regulatory kinase for DNA double-strand break repair pathway. When DNA damage occurs, DNA damage checkpoint kinases such as Mec1 and Rad9 phosphorylate Rad53 to activate DNA damage checkpoint and repair pathway (Hustedt et al., 2013). As a marker for endogenous DNA damage (Ohouo et al., 2013), I checked Rad53 phosphorylation in wild-type and *rad52*Δ cells. Rad53 phosphorylation was not detected in both of wild-type cells and *rad52*Δ cells during normal cell cycle (**Fig. 6 upper panel**),

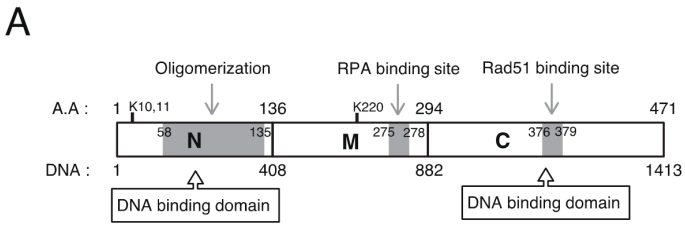
A
Oligomerization
RPA binding site
Rad51 binding site
A.A :
1
K10,11
136
K220
294
471
58
N
135
M
275
278
C
376
379
DNA :
1
408
882
1413
DNA binding domain
DNA binding domain

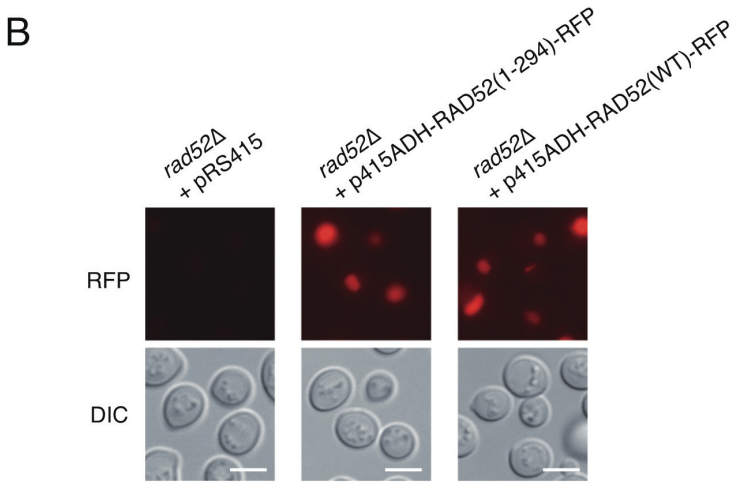
B
rad52Δ + pRS415
rad52Δ + p415ADH-RAD52(1-294)-RFP
rad52Δ + p415ADH-RAD52(WT)-RFP
RFP
DIC

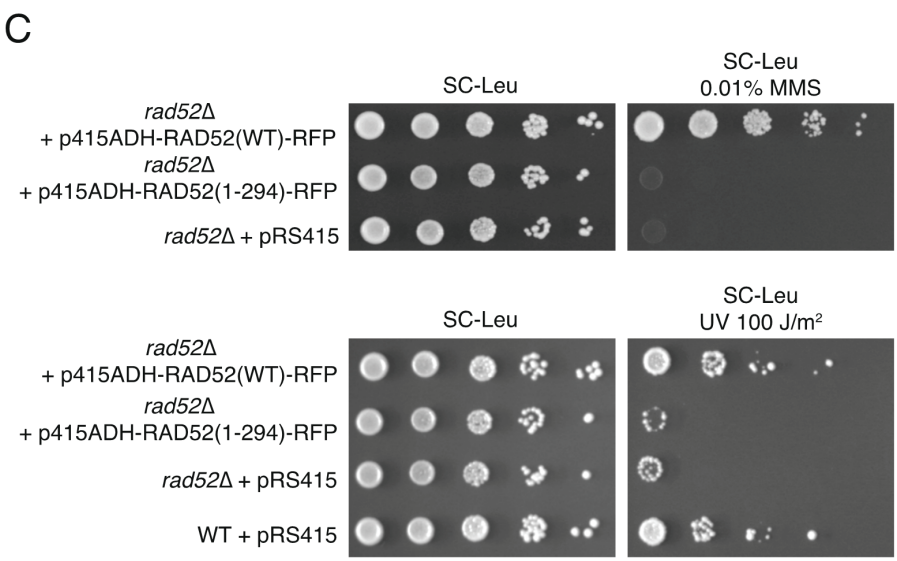
C
SC-Leu
SC-Leu 0.01% MMS
rad52Δ + p415ADH-RAD52(WT)-RFP
rad52Δ + p415ADH-RAD52(1-294)-RFP
rad52Δ + pRS415
SC-Leu
SC-Leu UV 100 J/m2
rad52Δ + p415ADH-RAD52(WT)-RFP
rad52Δ + p415ADH-RAD52(1-294)-RFP
rad52Δ + pRS415
WT + pRS415

D

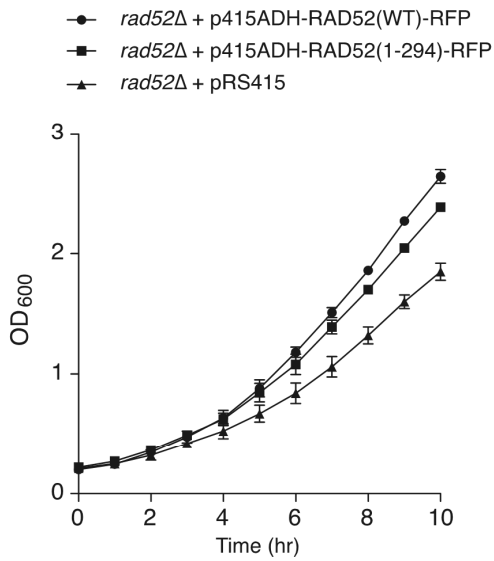
rad52Δ + p415ADH-RAD52(WT)-RFP
rad52Δ + p415ADH-RAD52(1-294)-RFP
rad52Δ + pRS415
OD600
Time (hr)
0
1
2
3
0
2
4
6
8
10

E

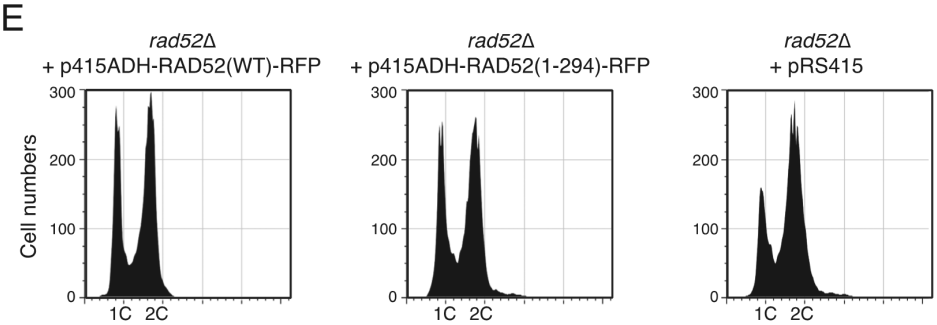
rad52Δ
+ p415ADH-RAD52(WT)-RFP
rad52Δ
+ p415ADH-RAD52(1-294)-RFP
rad52Δ
+ pRS415
Cell numbers
300
200
100
0
1C
2C

Fig. 4 Loss of homologous recombination activity is not responsible for growth defect in *rad52*Δ cells.

(A) Brief scheme of protein domains in Rad52. (B) The C-terminus-truncated Rad52 was well localized to the nucleus similarly to wild-type Rad52. *rad52*Δ cells containing indicated vectors were imaged during asynchronous log phase in SC-Leu medium. Scale bars are 4 μm. (C) The C-terminus-truncated Rad52 could not repair DNA damage. *rad52*Δ cells containing indicated vectors were serially diluted on SC-Leu agar plates in the absence or presence of 0.01% MMS (upper panel). Wild-type cells containing empty vector and *rad52*Δ cells containing indicated vectors were serially diluted on SC-Leu agar plates with or without exposure to 100 J/m2 ultraviolet light (lower panel). Plates were incubated at 30°C for 3 days. (D) Expression of the C-terminus-truncated Rad52 recovered growth defect of *rad52*Δ cells. *rad52*Δ cells containing indicated vectors were grown in SC-Leu medium. Optical density was measured every 1 hr. Data represent the mean±SD of triplicate cultures. (E) Expression of the C-terminus-truncated Rad52 recovered G2/M phase accumulation of *rad52*Δ cells. DNA contents of *rad52*Δ cells containing indicated vectors were analyzed by flow cytometry. 1C and 2C indicate single and double DNA haploid content.

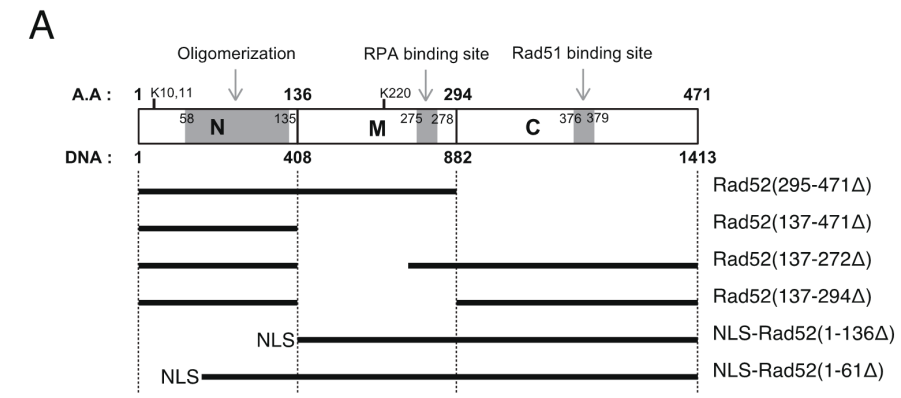
A
Oligomerization
RPA binding site
Rad51 binding site
A.A :
1
K10,11
136
K220
294
471
58
N
135
M
275
278
C
376
379
DNA :
1
408
882
1413
Rad52(295-471Δ)
Rad52(137-471Δ)
Rad52(137-272Δ)
Rad52(137-294Δ)
NLS
NLS-Rad52(1-136Δ)
NLS
NLS-Rad52(1-61Δ)

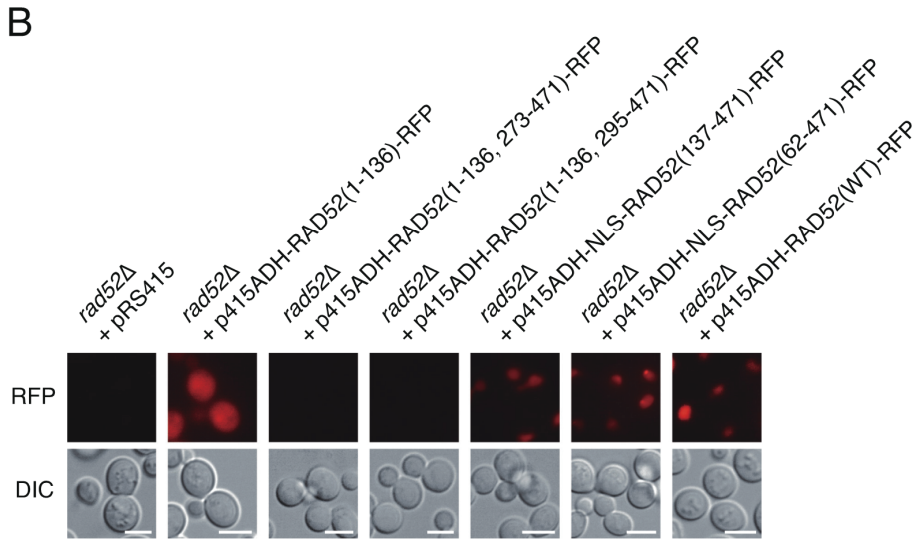
B
rad52Δ + pRS415
rad52Δ + p415ADH-RAD52(1-136)-RFP
rad52Δ + p415ADH-RAD52(1-136, 273-471)-RFP
rad52Δ + p415ADH-RAD52(1-136, 295-471)-RFP
rad52Δ + p415ADH-NLS-RAD52(137-471)-RFP
rad52Δ + p415ADH-NLS-RAD52(62-471)-RFP
rad52Δ + p415ADH-RAD52(WT)-RFP
RFP
DIC

C

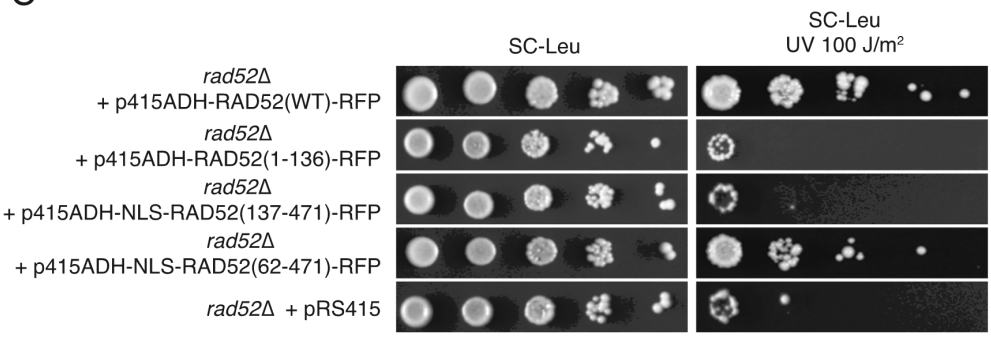
SC-Leu
SC-Leu
UV 100 J/m²
rad52Δ
+ p415ADH-RAD52(WT)-RFP
rad52Δ
+ p415ADH-RAD52(1-136)-RFP
rad52Δ
+ p415ADH-NLS-RAD52(137-471)-RFP
rad52Δ
+ p415ADH-NLS-RAD52(62-471)-RFP
rad52Δ + pRS415

D

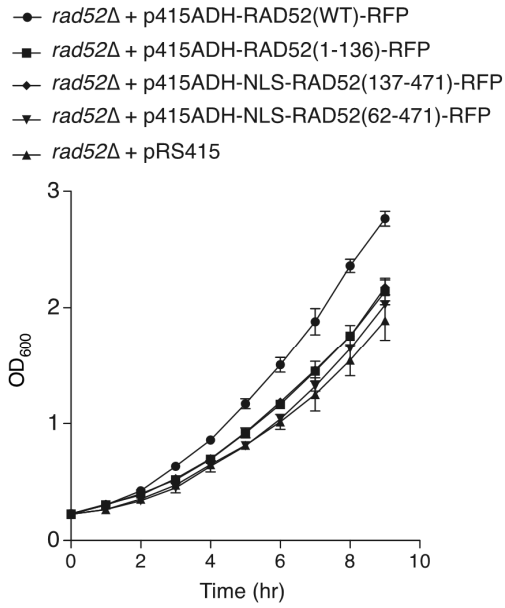
rad52Δ + p415ADH-RAD52(WT)-RFP
rad52Δ + p415ADH-RAD52(1-136)-RFP
rad52Δ + p415ADH-NLS-RAD52(137-471)-RFP
rad52Δ + p415ADH-NLS-RAD52(62-471)-RFP
rad52Δ + pRS415
OD600
0
1
2
3
0
2
4
6
8
10
Time (hr)

Fig. 5 Domains for DNA damage repair and growth-related function are separated in Rad52.

(A) Brief scheme of truncated mutants of Rad52. NLS indicates nuclear localization signal, and SV40 NLS (PKKKRKV) was used for these mutations. (B) Most N-terminus- and M-region-truncated mutants of Rad52, except 137-272Δ and 137-294Δ, were well expressed in cells and localized to the nucleus. *rad52*Δ cells containing indicated vectors were imaged during asynchronous log phase in SC-Leu media. Scale bars are 4 μm. (C) Only 1-61Δ mutant was functionally active under DNA damage condition. *rad52*Δ cells containing indicated vectors were serially diluted on SC-Leu agar plates with or without exposure to 100 J/m2 ultraviolet light. Plates were incubated at 30°C for 3 days. (D) All N-terminus- and M-region-truncated mutants of Rad52 could not recover growth defect of *rad52*Δ cells. *rad52*Δ cells containing indicated vectors were grown in SC-Leu media. Optical density was measured every 1 hr. Data represent the mean±SD of triplicate cultures.

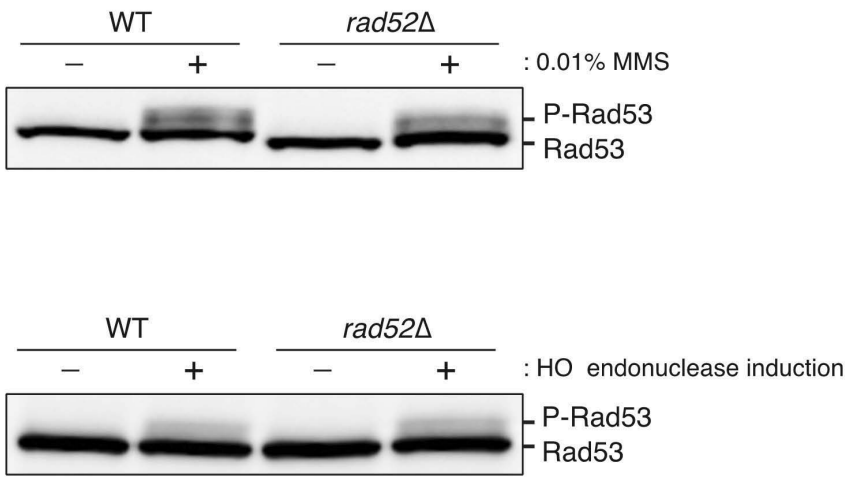

Fig. 6 DNA damage does not spontaneously occur in *rad52*Δ cells

Rad53 in *rad52*Δ cells was not phosphorylated without DNA damage induction by MMS treatment or HO endonuclease. 0.01% MMS was treated for 3 hr. HO endonuclease was expressed under GAL promoter for 7 hr using 2% galactose including YP media.

suggesting that DNA damage occurrence in *rad52*Δ cells is not sufficient to active DNA damage checkpoint. To confirm that the pathway for Rad53 phosphorylation is normal in *rad52*Δ cells, MMS was treated to wild-type and *rad52*Δ cells. As previously reported, Rad53 in wild-type cells was highly phosphorylated to response DNA damage stress. Moreover, the phosphorylation of Rad53 in *rad52*Δ cells was not different with that in wild-type cells, suggesting that deletion of *RAD52* does not affect to the pathway of Rad53 phosphorylation. Taken together, I concluded that Deletion of *RAD52* does not cause enough DNA damage for activation of Rad53 phosphorylation without induction of DNA damage stress.

Because MMS is a strong agent for DNA damage induction, sensitivity of Rad53 phosphorylation was investigated to exclude possibility that mild DNA damage was not detected by this method. HO endonuclease is a sequence-specific double-strand nuclease of yeast for mating type exchange. Although HO has three target sequences in yeast genomic DNA, HMRa, HMLα and MAT, HMRa and HMLα are protected by chromosome structure and only unprotected MAT loci is digested by HO. Thus, unlike MMS, expression of HO results single DNA double-strand break, which is repaired by Rad53 mediated DNA repair pathway (Janke et al., 2010). Interestingly, although single DNA damage by HO expression was clearly monitored by Rad53 phosphorylation, Rad53 in *rad52*Δ cells was not phosphorylated without HO expression (**Fig. 6; lower panel**). These data indicate that spontaneous DNA damage occurrence and accumulation is not the reason of cell cycle delay, which is observed in *rad52*Δ cells.

SUMOylation does not regulate the novel function of Rad52 for growth regulation

It is known that Rad52 is SUMOylated on three residues (K10, K11, and K220) (Altmannova et al., 2010). Thus, I examined whether SUMOylation of Rad52 is involved in cell growth regulation. To check this, I made a non-SUMOylable Rad52 mutant with three SUMOylated residues changed to arginine. I checked the expression of non-SUMOylable

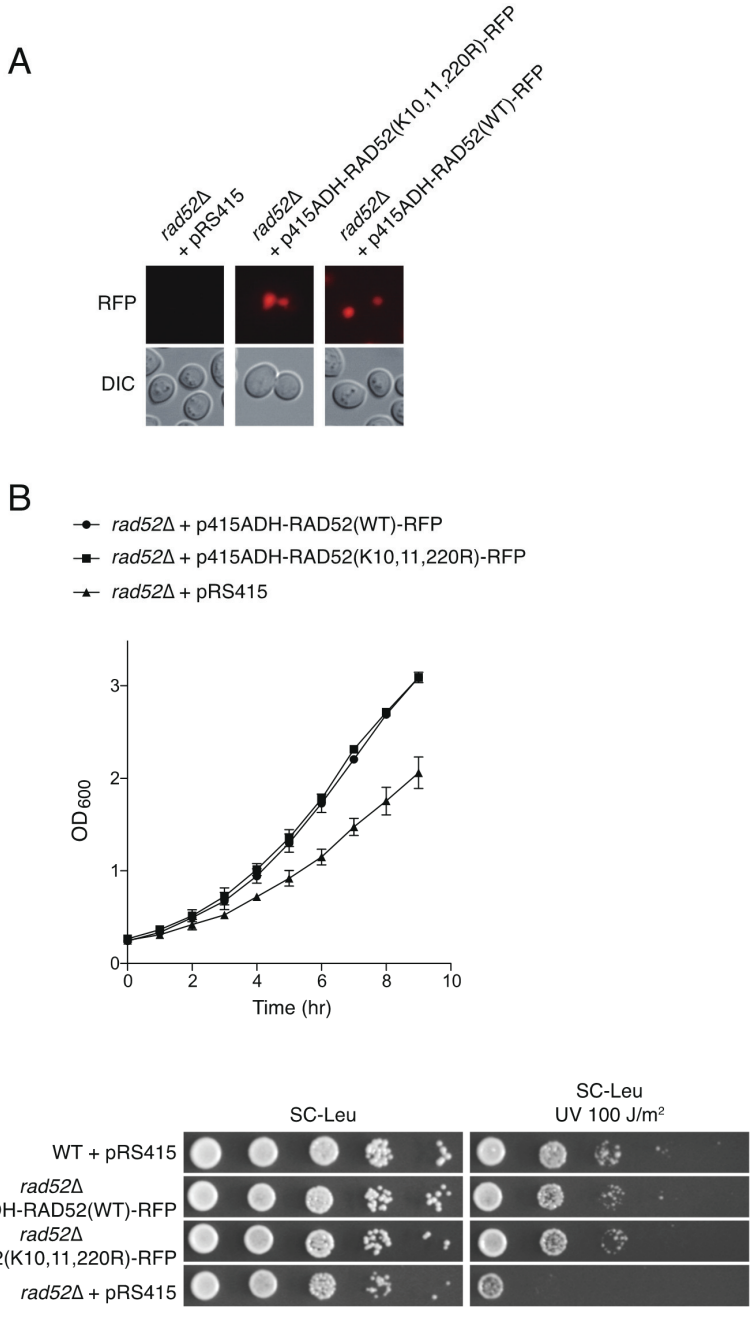
A
rad52Δ + pRS415
rad52Δ + p415ADH-RAD52(K10,11,220R)-RFP
rad52Δ + p415ADH-RAD52(WT)-RFP
RFP
DIC
B
rad52Δ + p415ADH-RAD52(WT)-RFP
rad52Δ + p415ADH-RAD52(K10,11,220R)-RFP
rad52Δ + pRS415
OD600
Time (hr)
C
SC-Leu
SC-Leu UV 100 J/m2
WT + pRS415
rad52Δ + p415ADH-RAD52(WT)-RFP
rad52Δ + p415ADH-RAD52(K10,11,220R)-RFP
rad52Δ + pRS415

Fig. 7 SUMOylation does not regulate growth-related function of Rad52.

(A) Non-SUMOylable Rad52 was well expressed in cells and localized to the nucleus. *rad52*Δ cells containing indicated vectors were imaged during asynchronous log phase in SC-Ura media. Scale bars are 4 μm. (B) Non-SUMOylable Rad52 recovered growth defect of *rad52*Δ cells similarly to wild-type Rad52. *rad52*Δ cells containing indicated vectors were grown in SC-Leu media. Optical density was measured every 1 hr. Data represent the mean±SD of triplicate cultures. (C) Non-SUMOylable Rad52 repaired DNA damage similarly to wild-type Rad52. *rad52*Δ cells containing indicated vectors were serially diluted on SC-Leu agar plates with or without exposure to 100 J/m2 ultraviolet light. Plates were incubated at 30°C for 3 days.

Rad52 mutant by fluorescence intensity of C-terminally tagged RFP and confirmed that non-SUMOylable Rad52 mutant were normally expressed and localized to nucleus (**Fig. 7A**). To check whether non-SUMOylable mutation affects to growth regulation, the optical density from lag phase to late log phase was measured using *rad52*Δ cells expressing non-SUMOylable Rad52 mutant. As shown in **Fig. 7B**, non-SUMOylable Rad52 mutant perfectly restored growth defect of *rad52*Δ cells compared to *rad52*Δ cells expressing wild-type Rad52. These results demonstrate that the novel function of Rad52 for cell growth regulation is not mediated by SUMOylation. To confirm the effect of non-SUMOylable mutation on DNA damage repair activity, I checked the viability under stress condition by UV radiation. Compared to *rad52*Δ cell expressing wild-type Rad52, *rad52*Δ cells expressing non-SUMOylable Rad52 mutant efficiently repaired DNA damages (**Fig. 7C**). These results demonstrate that the novel function of Rad52 for cell growth regulation is not mediated by SUMOylation.

Dephosphorylation of Kar9 is delayed in *rad52*Δ strain

While *rad52*Δ cells stayed in G2/M phase, prolonged spindle oscillation was also observed. Compared to wild-type cells, the spindle poles in *rad52*Δ cells oscillated vigorously and took more time to division (**Fig. 8A**). Especially, both spindle poles of *rad52*Δ cells were in the same side from bud neck at 30 min and 44 min, suggesting that spindle orientation is not precisely regulated in *rad52*Δ cells.

Cytoplasmic dynein, kinesin (Kip3) and other microtubule binding proteins, such as Kar9 and Bud6, are involved to spindle oscillation (Cottingham and Hoyt, 1997; Miller et al., 1999). When Kar9, which is a putative microtubule plus-end capturing protein, is deleted, spindle oscillation is significantly increased similarly to that in *rad52*Δ cells (Yeh et al., 2000). It has been reported that phospho-regulation of Kar9 makes asymmetric binding to the spindle pole destined to the bud, and spindle pole bound Kar9 subsequently moves to emerged mitotic spindles to guide them toward bud (Liakopoulos et al., 2003). To confirm whether prolonged

spindle oscillation in *rad52*Δ cells is related to mis-regulated Kar9, intercellular localization of Kar9 was examined in mitosis. Whereas more than 70% of wild-type cells showed asymmetric binding of Kar9, asymmetric binding of Kar9 was decreased and partially and completely symmetric binding of Kar9 was increased to nearly 60% in *rad52*Δ cells (**Fig. 8B**). Because both spindle poles were in the same side from bud neck, I checked the direction of spindles, which are emerged from both spindle poles, to examine the regulation of pulling forces for accurate mitosis. According to the previous report (Liakopoulos et al., 2003), Kar9 is accumulated to the spindle pole and moves toward the direction of microtubule plus end. As shown in **Fig. 8C**, one end of Kar9-GFP signal was attached to spindle pole. Thus, I could estimate that opposite direction from spindle pole of Kar9-GFP signal is the direction of emerged microtubule. Interestingly, both microtubules emerged from the spindle poles were headed to the bud by the guiding of Kar9 in *rad52*Δ cells (**Fig. 8C**), suggesting that non-selective binding of Kar9 causes unregulated spindle orientation in *rad52*Δ cells.

It has been reported that Cdc28/Clb4 controls spindle pole binding affinity of Kar9 by the phosphorylation (Liakopoulos et al., 2003). During the mitosis, Clb4 localizes to one spindle pole that is destined to the mother cell and phosphorylates Kar9 in a distance-dependent manner. Because phosphorylated Kar9 loses binding affinity to spindle pole, Kar9 binds to only one spindle pole that is destined to the bud. Thus, cell cycle-dependent Kar9 phosphorylation was checked in wild-type and *rad52*Δ cells. In wild-type cells, Kar9 was highly phosphorylated until 60 min and was dephosphorylated at 75 min (**Fig. 8E**). To identify the exact cell phase, DNA contents analysis was also performed using the samples for Kar9 phosphorylation analysis. Based on result of DNA contents analysis, I presumed that 75 min is the time after anaphase onset (**Fig. 8D**). In contrast, in *rad52*Δ cells, cell cycle progression was delayed in G2/M phase (**Fig. 8D**) and Kar9 was not dephosphorylated until 120 min (**Fig. 8E**). Interestingly, although Kar9 in *rad52*Δ cells was highly phosphorylated, spindle binding of Kar9 is not disrupted and Kar9 improperly localized to both spindle poles. To confirm that hyper-phosphorylation of Kar9

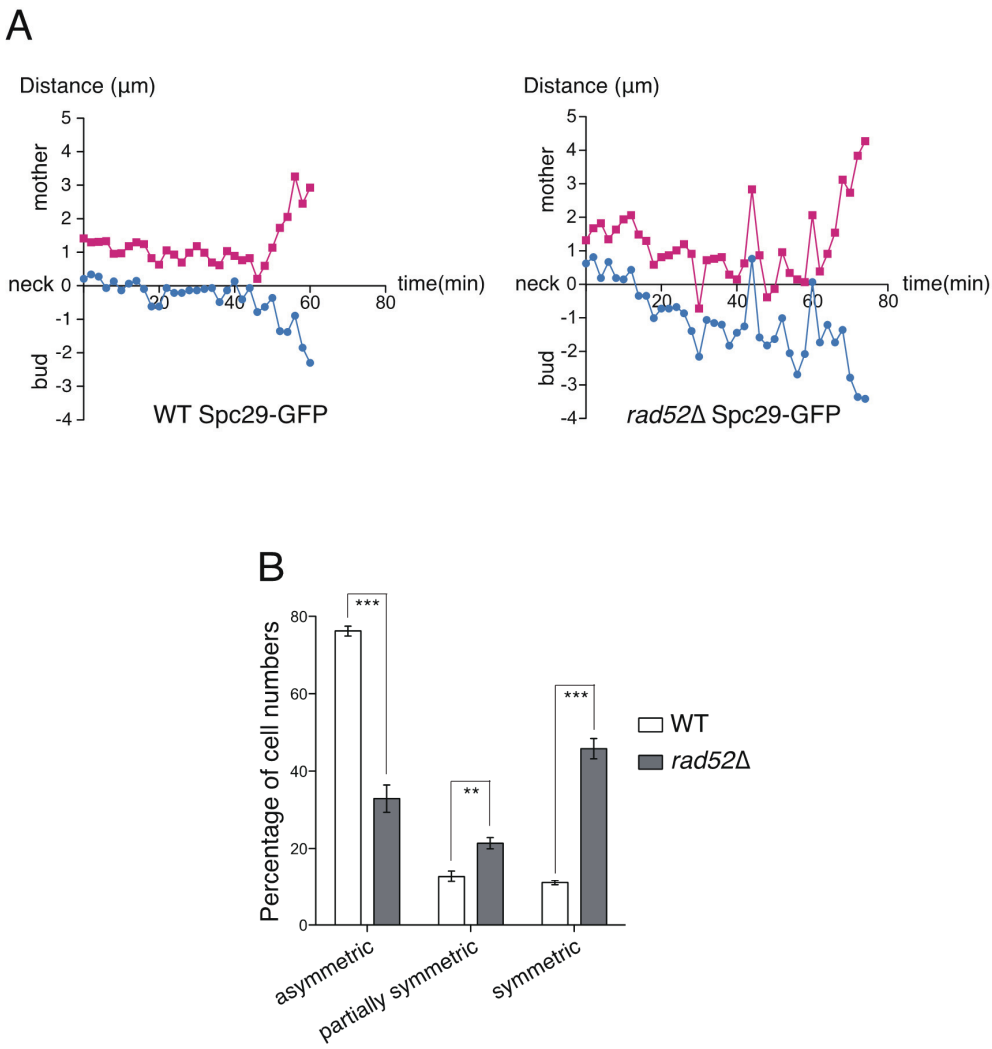
A
Distance (μm)
mother
neck
bud
time(min)
WT Spc29-GFP
rad52Δ Spc29-GFP
B
Percentage of cell numbers
WT
rad52Δ
asymmetric
partially symmetric
symmetric
C
Kar9-GFP
Spc29-RFP
merge
WT
rad52Δ

1

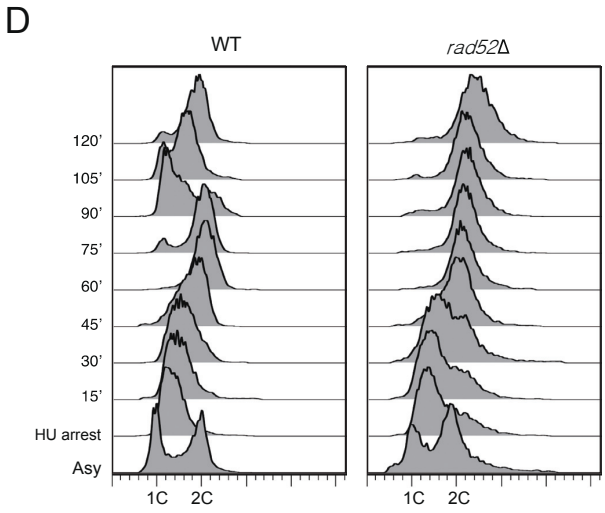
D
WT
rad52Δ
120'
105'
90'
75'
60'
45'
30'
15'
HU arrest
Asy
1C
2C
1C
2C

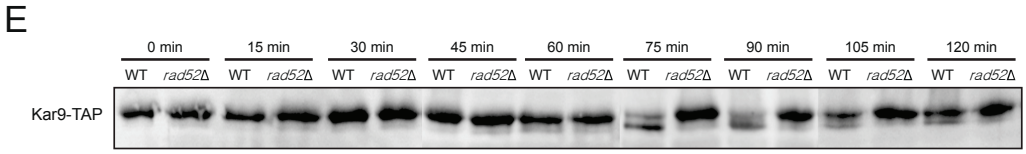
E
0 min
15 min
30 min
45 min
60 min
75 min
90 min
105 min
120 min
WT
rad52Δ
Kar9-TAP

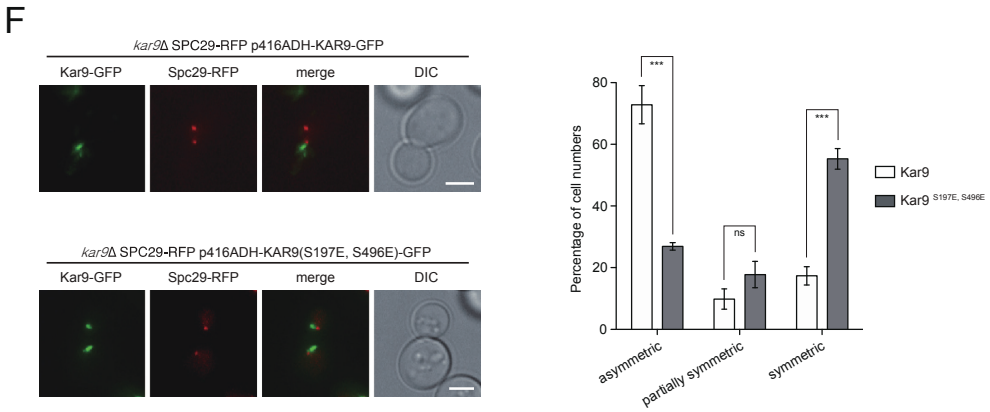
F
kar9Δ SPC29-RFP p416ADH-KAR9-GFP
Kar9-GFP
Spc29-RFP
merge
DIC
kar9Δ SPC29-RFP p416ADH-KAR9(S197E, S496E)-GFP
Kar9-GFP
Spc29-RFP
merge
DIC
Percentage of cell numbers
80
60
40
20
0
***
ns
***
asymmetric
partially symmetric
symmetric
Kar9
Kar9 S197E, S496E

Fig. 8 Dephosphorylation of Kar9 is delayed in *rad52*Δ strain.

(A) *rad52*Δ cells showed prolonged spindle oscillation. Wild-type and *rad52*Δ cells endogenously expressing GFP-tagged Spc29 were imaged every 2 min during asynchronous log phase. Spc29-GFP was used as a spindle pole marker, and the distance of Spc29-GFP was measured from the bud neck to indicate the location of spindle poles. (B) Non-selective binding of Kar9 was exacerbated in *rad52*Δ cells. Wild-type and *rad52*Δ cells expressing GFP-tagged Kar9 and RFP-tagged Spc29 were synchronized by α-factor treatment for 3 hr. Synchronized cells were released to fresh YPD media and fixed with formaldehyde at 75min after release from α-factor. When signal intensities of Kar9-GFP on both spindle poles were not equal, it was counted as partially symmetric binding. Data represent the mean±SD of triplicate cultures. P-values were determined by the Student's t test (**$p < 0.01$ and ***$p < 0.005$). (C) Microtubules emerged from both spindle poles in *rad52*Δ cells were headed to the bud. White arrows indicate direction of the bud. Scale bars are 2 μm. (D) Cell cycle of *rad52*Δ cells was delayed in G2/M phase. Cell cycle stages are indicated by DNA contents analysis. Wild-type and *rad52*Δ cells expressing TAP-tagged Kar9 were synchronized by 0.2 M hydroxyurea treatment for 3 hr, and samples were taken every 15 min after release to fresh YPD. 1C and 2C indicate single and double DNA haploid content. (E) Dephosphorylation of Kar9 was delayed in rad52Δ cells. The phosphorylation state of Kar9-TAP was examined by SDS–PAGE and rabbit anti-mouse IgG immunoblot assay. (F) Phospho-mimicking mutant of Kar9 binds to both spindle poles. *kar9*Δ cells expressing GFP-tagged wild-type Kar9 or GFP-tagged phospho-mimicking Kar9 (Kar9S197E,S496E) were synchronized by α-factor treatment for 3hr. Synchronized cells were released to fresh YPD media and fixed with formaldehyde at 75min after release from α-factor. When signal intensities of Kar9-GFP on both spindle poles were not equal, it was counted as partially symmetric binding. Data represent the mean±SD of triplicate cultures. P-values were determined by the Student's t test (***$p < 0.005$). Scale bars are 2 μm .

can result improper binding to both spindle poles similarly to non-phosphorylable Kar9 mutant, I constructed Kar9^{S197E,S496E} mutant, which is the phospho-mimicking Kar9 mutant for Cdc28/Clb4 target residues (Liakopoulos et al., 2003). As shown in **Fig. 8F**, Kar9^{S197E,S496E} mutant exhibited increased symmetric binding in wild-type cells, similarly to Kar9 in *rad52*Δ cells. It can be interpreted that asymmetric binding of Kar9 is regulated by the different affinity between dephosphorylated and phosphorylated Kar9. Taken together, these results suggest that delayed dephosphorylation of Kar9 in *rad52*Δ cells provides symmetric pulling force that results in mis-orientation of the spindles.

Mitotic arrest occurs in *rad52*Δ strain

To properly regulate asymmetric binding of Kar9, phosphorylation by Cdc28/Clb4 is removed by anaphase promoting phosphatase Cdc14 after anaphase onset (Bloom et al., 2011). Thus, I hypothesized that delayed dephosphorylation of Kar9 and prolonged spindle oscillation are caused by the delay in Cdc14 release, which is a hallmark of mitotic arrest. Nop56 was visualized by RFP conjugation to mark the nucleous and chased localization of Cdc14-GFP. As shown in **Fig. 9 (upper panel)**, Cdc14 is trapped in nucleolus before the anaphase onset to be separated from its substrate. In wild-type cells, Cdc14 was released to nucleus at 62 min and diffused to cytoplasm at 64 min. In contrast, Cdc14 in *rad52*Δcells was released to nucleus at 126 min and diffused to cytoplasm at 128 min. By checking Cdc14 release time using 150 cells of each strain, it was confirmed that Cdc14 release in *rad52*Δ cells was significantly delayed compared to wild-type cells (**Fig. 9; lower panel**). This observation suggests that the absence of Rad52 causes mitotic arrest that suppresses Cdc14 release and anaphase promotion.

Rad52 is in the same pathway with Mad1-mediated SAC

When mitosis is not properly regulated, Cdc14 release is suppressed by mitotic checkpoint to prevent mis-segregation of sister chromatids. Because mitotic checkpoint is

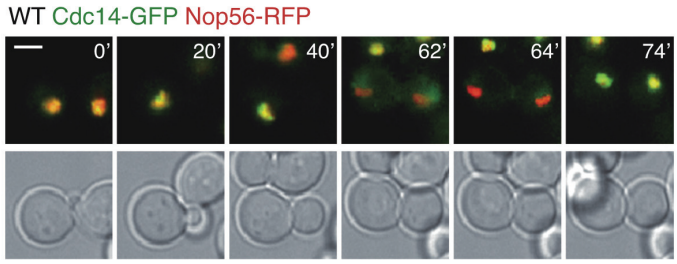
WT Cdc14-GFP Nop56-RFP
0'
20'
40'
62'
64'
74'

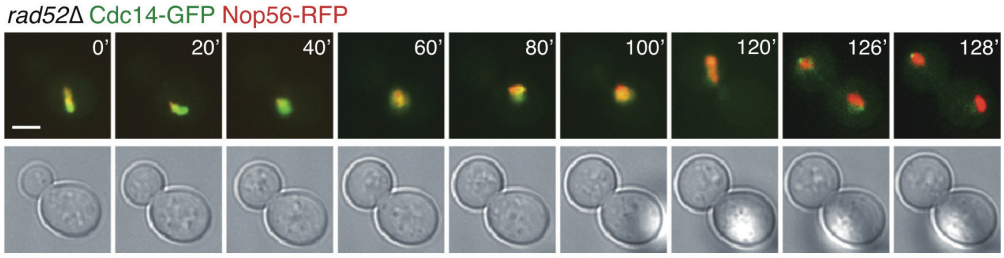
rad52Δ Cdc14-GFP Nop56-RFP
0'
20'
40'
60'
80'
100'
120'
126'
128'

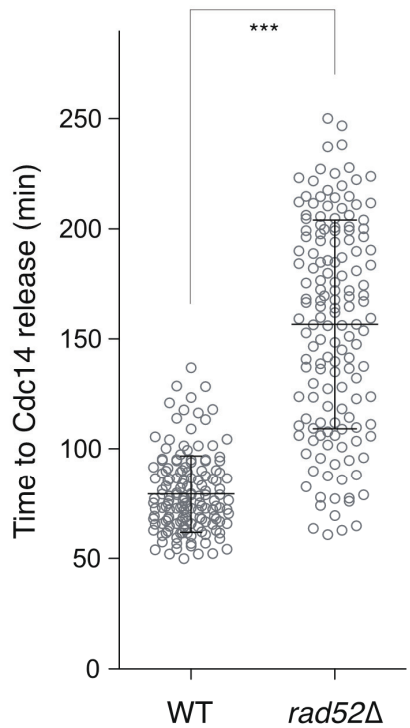
***
Time to Cdc14 release (min)
250
200
150
100
50
0
WT
rad52Δ

Fig. 9 Mitotic arrest is the cause of growth defect in *rad52*Δ cells.

Cdc14 release was significantly delayed in *rad52Δ* cells. Wild-type and *rad52*Δ cells expressing GFP-tagged Cdc14 and RFP-tagged Nop56 were imaged in asynchronous cells (Upper panel) and in α-factor-synchronized cells (lower panel). Nop56-RFP was used as a nucleolus marker. Each circle on the right graph indicates Cdc14 release time of individual cell. The mean±SD of all cells in each strain is also indicated in the graph. P-value was determined by the Mann-Whitney U test (***$p < 0.005$).

comprised of two pathways, which are Mad1-mediated SAC and Bub2-dependent checkpoint, I examined which pathway has responsibility to the mitotic delay of *rad52*Δ cells. To check epistatic effect between *RAD52* and mitotic checkpoint pathways, the colony formation assay was performed. A previous study has reported that double deletion of a mitotic checkpoint gene and a mitosis regulatory gene represents mitotic dysregulation. Mitotic dysregulation results various mitotic problems including mis-segregation of sister chromatids and some of cells having irregular number of chromosomes is not viable. Viability of cells can be confirmed by colony formation (Lee and Spencer, 2004). Thus, I made double deletion mutants with deletion of *RAD52* and each of two major mitotic checkpoint genes, *MAD1* and *BUB2*, to analyze the fidelity of mitosis and cell division. In contrast to control strains such as wild-type, *mad1*Δ, and *bub2*Δ cells, nearly 40% of *rad52*Δ cells could not make colony (**Fig. 10A**), indicating that deletion of *RAD52* caused mitotic stress that activates mitotic checkpoint, but this stress was not perfectly repaired by mitotic checkpoint in *rad52*Δ cells. Thus, I presumed that Rad52 has the roles in not only regulation of mitosis but also recovery of mitotic damages. Next, epistatic effect on colony formation was tested using double deletion strains. Interestingly, colony formation of *bub2*Δ *rad52*Δ cells was even more decreased than *rad52*Δ cells, whereas that of *mad1*Δ *rad52*Δ cells was not. It suggests that, when mitotic stress occurred by deletion of *RAD52*, additional deletion of *BUB2* synergistically intensified deficiency of repair process by mitotic checkpoint. However, defect of Mad1-dependent SAC by deletion of *MAD1* did not represent additive effect on deletion of *RAD52*. Thus, it can be interpreted that *RAD52* and *BUB2* are in parallel pathways, but *RAD52* and *MAD1* are in same pathway for regulation of accurate mitosis.

Interestingly, although division defect was severely intensified, *bub2*Δ *rad52*Δ cells showed phenotypes that represent passing through the mitotic arrest compared to *rad52*Δ cells. Because nucleus diffusion of Ipl1-GFP signal is the major phenotype of *rad52*Δ cells, which is resulted by mitotic arrest (**Fig. 3B, D**), nucleus diffusion of Ipl1-GFP signal was examined in

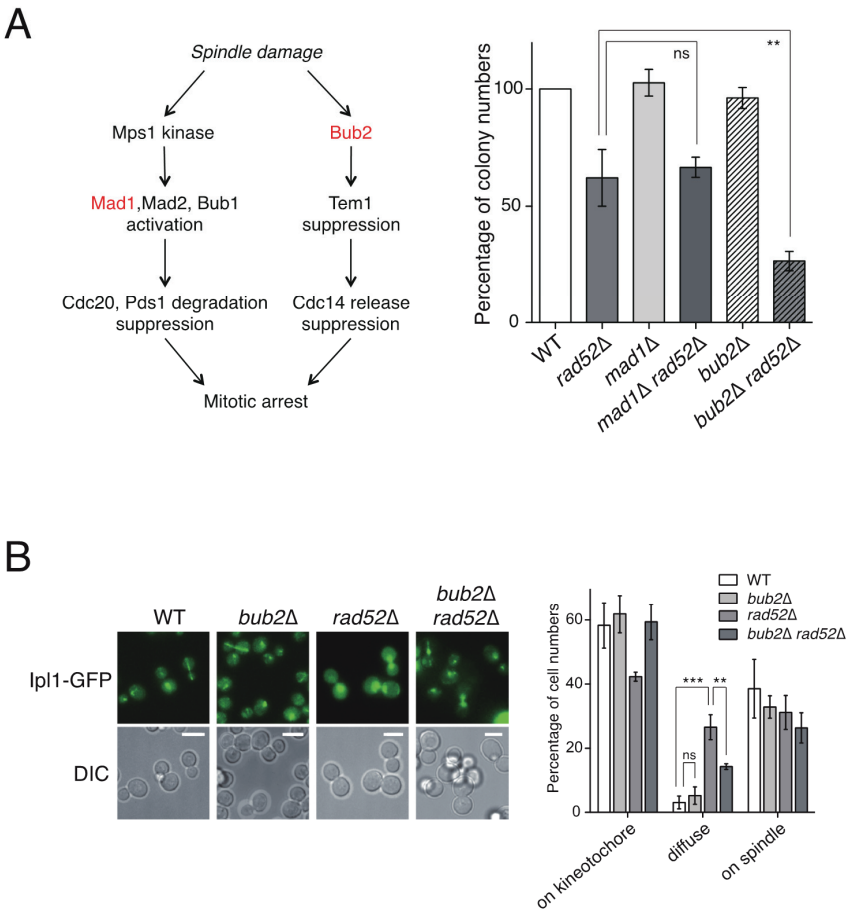
A
Spindle damage
Mps1 kinase
Bub2
Mad1,Mad2, Bub1 activation
Tem1 suppression
Cdc20, Pds1 degradation suppression
Cdc14 release suppression
Mitotic arrest
Percentage of colony numbers
100
50
0
ns
**
WT
rad52Δ
mad1Δ
mad1Δ rad52Δ
bub2Δ
bub2Δ rad52Δ
B
WT
bub2Δ
rad52Δ
bub2Δ rad52Δ
Ipl1-GFP
DIC
Percentage of cell numbers
60
40
20
0
***
**
ns
on kineotochore
diffuse
on spindle
C
Time to anaphase onset (min)
300
250
200
150
100
50
0
***
***
ns
WT
bub2Δ
rad52Δ
bub2Δ rad52Δ

Fig. 10 Rad52 is in the same pathway with Mad1-mediated SAC.

(A) *rad52*Δ cells showed mitotic division defect, which was exacerbated in *bub2*Δ *rad52*Δ cells. A schematic diagram showing two parallel pathways of SAC is shown on the left. Efficiency of colony formation was calculated by normalizing the colony numbers of each strain to those of wild-type strain. Data represent the mean±SD of triplicate cultures. P-values were determined by the Student's *t* test (***p* < 0.01). (B) Ipl1 diffusion ratio of *bub2*Δ *rad52*Δ cells was decreased to approximately half of that of *rad52*Δ cells. Indicated strains expressing GFP-tagged Ipl1 were imaged during asynchronous log phase (left panel). Data represent the mean±SD of triplicate cultures (right panel). P-values were determined by the Student's *t* test (***p* < 0.01 and ****p* < 0.005). (C) Anaphase onset time in *bub2*Δ *rad52*Δ cells was decreased compared to *rad52*Δ cells. Anaphase onset times were measured from washout of α-factor to spindle localization of Ipl1. Each circle indicates anaphase onset time of individual cell. The mean±SD of all cells in each strain was also indicated in the graph. P-values were determined by the Mann-Whitney *U* test (****p* < 0.005).

*bub2*Δ *rad52*Δ cells. As shown in **Fig. 10B**, nucleus diffusion of Ipl1-GFP signal was rarely observed in wild-type and *bub2*Δ cells during normal cell growth. Consistent with my previous data, ratio of nucleus diffusion of Ipl1-GFP signal was significantly increased in *rad52*Δ cells. However, the ratio of *bub2*Δ *rad52*Δ cells with diffused Ipl1-GFP signal was almost half of that of *rad52*Δ cells (**Fig. 10B**). Anaphase onset time of *bub2*Δ *rad52*Δ cells was also checked to examine the effect of *BUB2* deletion on mitotic arrest of *rad52*Δ cells. The timing of anaphase onset was significantly decreased in *bub2*Δ *rad52*Δ cells compared to *rad52*Δ cells (**Fig. 10C**). These findings indicate that *bub2*Δ *rad52*Δ cells cannot activate mitotic arrest that is generated by either Mad1-mediated SAC or Bub2-dependent checkpoint, when chromosome segregation is not properly regulated. Thus, I hypothesized that Rad52 is needed to activate SAC.

Rad52 is needed for SAC activation

To test whether Rad52 is needed to activate SAC, the degradation of Cdc20 under spindle damage condition was examined. According to the previous report (Ge et al., 2008), Cdc20, which is the activator of anaphase promoting complex APC/C, is degraded by SAC under spindle damage condition to suppress the anaphase transition and repair damaged kinetochore-spindle attachment. Thus, the amount of Cdc20 under spindle damage condition, which was generated by spindle-depolymerizing agent nocodazole, was examined to determine the activation of SAC. Whereas Cdc20 was degraded in wild-type cells in nocodazole-treated media, the protein level of Cdc20 in *rad52*Δ cells under nocodazole treatment was similar to that in wild-type cells and *rad52*Δ cells in normal media (**Fig. 11A**). It suggests that SAC was not properly activated to degrade Cdc20 in *rad52*Δ cells under spindle damage condition. To further confirm the disruption of SAC activation in *rad52*Δ cells, Pds1 degradation kinetics under nocodazole treatment was analyzed. Pds1 is the suppressor of separase, which is the protease responsible for anaphase promotion, and the direct substrate of APC/C^{Cdc20} complex. When spindle is damaged, SAC suppresses APC/C complex by degradation of Cdc20 to prevent

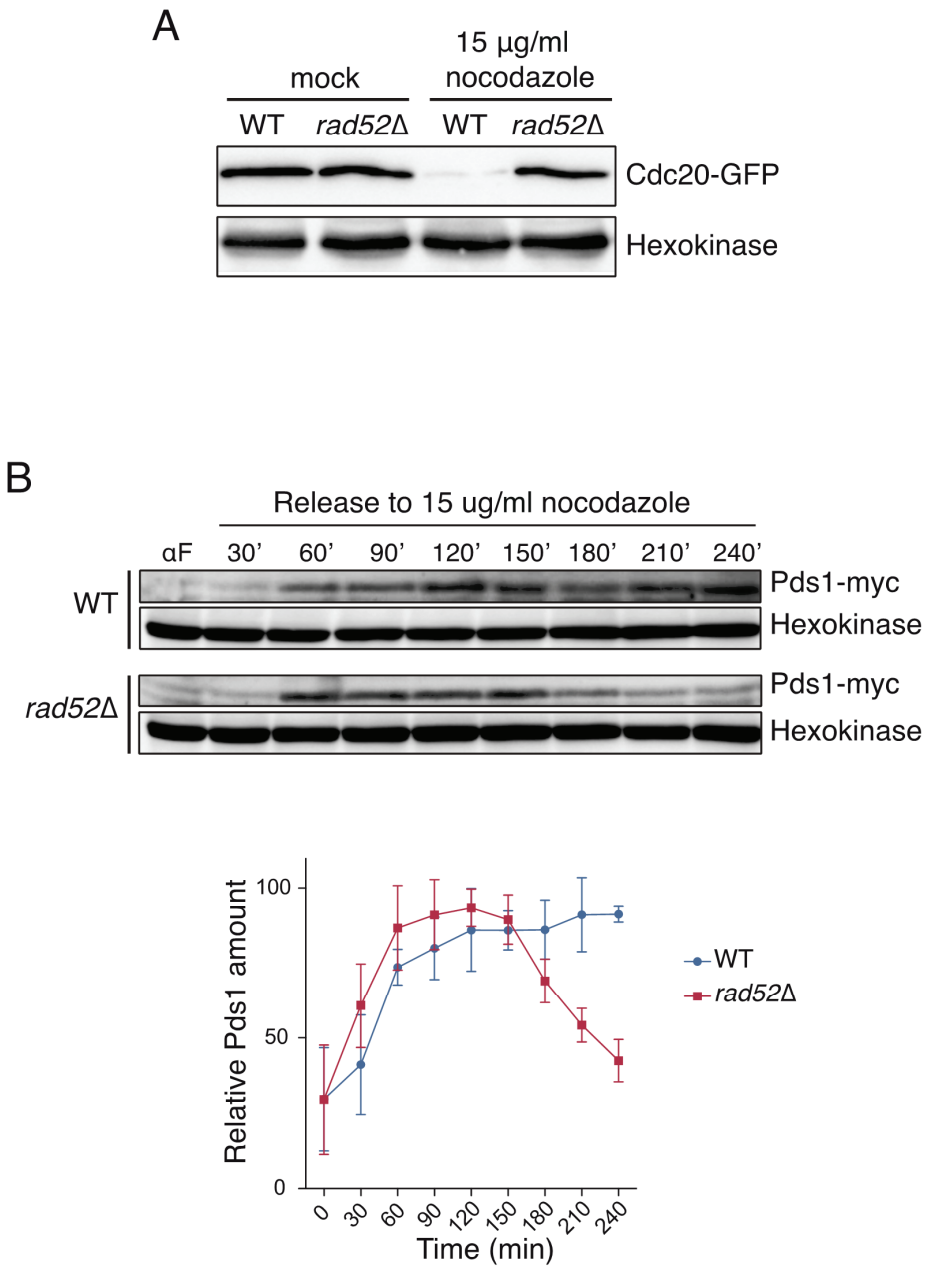
A
mock
15 µg/ml nocodazole
WT
rad52Δ
WT
rad52Δ
Cdc20-GFP
Hexokinase
B
Release to 15 ug/ml nocodazole
αF
30'
60'
90'
120'
150'
180'
210'
240'
WT
Pds1-myc
Hexokinase
rad52Δ
Pds1-myc
Hexokinase
Relative Pds1 amount
100
50
0
0
30
60
90
120
150
180
210
240
Time (min)
WT
rad52Δ

Fig. 11 Rad52 is needed for SAC activation.

(A) Cdc20 in *rad52*Δ cells was not degraded under spindle damage condition. 15 μg/ml nocodazole was treated for 3 hr. Hexokinase was used as a loading control. (B) *rad52*Δ cells could not block the degradation of Pds1 under spindle damage condition. Immunoblot assay was performed using an anti-myc antibody. Highest value in each trial was used as 100% standard to normalize the relative amounts of Pds1 (lower panel). Data represent the mean±SD of triplicate cultures.

degradation of Pds1. Thus, Pds1 is mainly used as indicator of SAC activation. Whereas wild-type cells maintained high levels of Pds1 until 240 min under nocodazole treated condition, the Pds1 level in *rad52*Δ cells remarkably decreased after 120 min (**Fig. 11B**). It strongly demonstrates that SAC was not efficiently activated in *rad52*Δ cells. Taken together, these data suggest that Rad52 is essential to activate SAC.

Rad52 is also required for accurate chromosome segregation during unperturbed cell cycle

Although SAC and Bub2-dependent checkpoint are closely related to spindle-kinetochore interaction and chromosome segregation, most mitotic checkpoint proteins such as Mad2 and Bub2 are unnecessary for cell growth under normal condition (Fraschini et al., 1999). In contrast, some upstream regulators of SAC such as Ipl1 and Mps1 have functions to control ordinary mitosis (Maure et al., 2007; Nakajima et al., 2011). It was clearly confirmed that Rad52 is essential for SAC activation under spindle damage condition. In addition, it was also found that *rad52*Δ cells showed growth defect, which is caused by cell cycle delay in G2/M phase, even without treatment of spindle damage agent (**Fig. 1A, 8D, and 10C**). Furthermore, in contrast to *mad1*Δ and *bub2*Δ cells, *rad52*Δ cells exhibited division defect, which is caused by mitotic stress, during unperturbed mitosis (**Fig. 10A**). Thus, I hypothesized that Rad52 regulates not only SAC activation but also accurate chromosome segregation during unperturbed cell cycle.

To examine the accuracy of chromosome segregation during unperturbed cell cycle, vector loss assay was performed using yeast minichromosome. Yeast minichromosomes with yeast centromere sequence are transmitted with high fidelity by chromosome segregation machinery, and bi-orientation of minichromosomes is impaired by the inactivation of the regulatory system for chromosome inheritance (Dewar et al., 2004; Schleiffer et al., 2012). Chromosome inheritance fidelity was measured during unperturbed cell cycle by using pRS415,

which has yeast *CEN6* sequence. Because loss of vector does not affect to the viability in non-selectable media, cells were continuously lost vector during repeated mitosis. Thus, I compared the ratio change of vector containing cells at regular interval of cell division. As shown in **Fig. 12A**, *rad52*Δ cells lost vectors dramatically faster than other control cells, suggesting that the regulatory system for chromosome inheritance is not efficiently controlled in *rad52*Δ cells.

Next, the kinetochore morphology was checked using GFP-conjugated Ndc80 during mitosis. Ndc80 is a major component of outer kinetochore and binds to microtubule for formation of kinetochore-microtubule attachment (Kalantzaki et al., 2015). To properly progress chromosome segregation, all kinetochores on sister chromatids should be attached to microtubules and pulled toward to each spindle pole. In the case of budding yeast, because nuclear envelope is not disrupted during the entire cell cycle, kinetochores are always localized close to spindle pole. Consistent with this, it was confirmed that all kinetochores in wild-type cells were accumulated to both spindle poles (**Fig. 12B; left panel**). In *rad52*Δ cells, however, I observed lagging chromosomes, which are the hallmark of incorrect microtubule attachment and improper chromosomes segregation, during mitosis (Cimini et al., 2001; Huang and Huffaker, 2006; Tytell and Sorger, 2006). Compared to other control strains such as wild-type, *mad1*Δ, and *bub2*Δ cells, Ratio of cells with lagging chromosomes was significantly increased in *rad52*Δ cells (**Fig. 12B; right panel**). It suggests that chromosome segregation was not properly regulated in *rad52*Δ cells during unperturbed cell cycle.

According to previous report (Mitra et al., 2014), absence of Rad52 reduces the level of kinetochore protein CENP-A^{CaCse4}, resulting in disruption of kinetochore structure in *Candida albicans*. Because disruption of kinetochore structure makes abnormal interaction between kinetochores and microtubules, chromosomes are not fully accumulated to spindle poles. To confirm whether improper chromosome segregation of *rad52*Δ cells is caused by disruption of kinetochore structure, I performed major experiments reported in Mitra et al. by using Cse4, *Saccharomyces cerevisiae* homolog of CENP-A^{CaCse4}. In *Candida albicans*, the fluorescence

intensity of GFP-conjugated CENP-A^{CaCse4} is severely decreased by deletion of *RAD52*. However, the fluorescence intensity of centromere-localized Cse4 was not different between wild-type cells and *rad52*Δ cells in *Saccharomyces cerevisiae* (**Fig. 13A**). Protein expression of CENP-A^{CaCse4} is also remarkably decreased in RAD52-deleted *Candida albicans*. In contrast, protein expression of Cse4 in *RAD52*-deleted *Saccharomyces cerevisiae* was also similar to that in wild-type cells (**Fig. 13B**). Strikingly, *RAD52* deleted *Candida albicans* shows decreased centromere-binding affinity of CENP-A^{CaCse4}, which is the major evidence for disruption of kinetochore structure. However, centromere-binding affinity of Cse4, which was measured by ChIP assay, was not changed by deletion of *RAD52* in *Saccharomyces cerevisiae* (**Fig. 13C**), suggesting that improper chromosome segregation in *rad52*Δ cells is caused by aberrant connections between spindles and kinetochores, but not by disruption of kinetochore structure.

Next, the fidelity of chromosome alignment was checked during mitosis to find direct evidence of chromosome mis-segregation. To visualize the location of single centromere, *CEN5*-GFP strain was used. *CEN5*-GFP strain contains $(tetO2)_{112}$ sequence, which is originated from tetracycline system, on nearby centromere sequence of chromosome V and expresses tetR-GFP, which has binding affinity to *tetO* sequence, to detect the location of $(tetO2)_{112}$ sequence. As described in previous report (Akiyoshi et al., 2009), Nuclear DNA was visualized by DAPI staining to evaluate the location of *CEN5*-GFP signals in nucleus. Because all centromeres are closely localized to spindle pole during accurate chromosome segregation, most of wild-type cell properly aligned sister chromatids to each site of nucleus (**Fig. 14; upper panel, proper alignment**). Consistent with results from vector loss assay and lagging chromosome analysis, *mad1*Δ and *bub2*Δ cells showed similar phenotypes to wild-type cells. This result is also consistent with previous reports (Fraschini et al., 1999; Jin et al., 2012) that confirm the non-functionality of Mad1 and Bub2 on the regulation of unperturbed cell cycle. In *rad52*Δ cells, however, cells containing both *CEN5*-GFP signals in the same side from bud neck were frequently observed (**Fig. 14; upper panel, mis-alignment**) and the ratio of cells containing

mis-aligned *CEN5*-GFP was remarkably increased compared to other control strains (**Fig. 14; lower panel**). It suggests that deletion of *RAD52* causes mis-regulation in chromosome segregation that activates mitotic checkpoints.

In total, these data indicate that Rad52 not only activates SAC under spindle damage condition, but also regulates the attachment of spindles and kinetochores for accurate chromosome segregation.

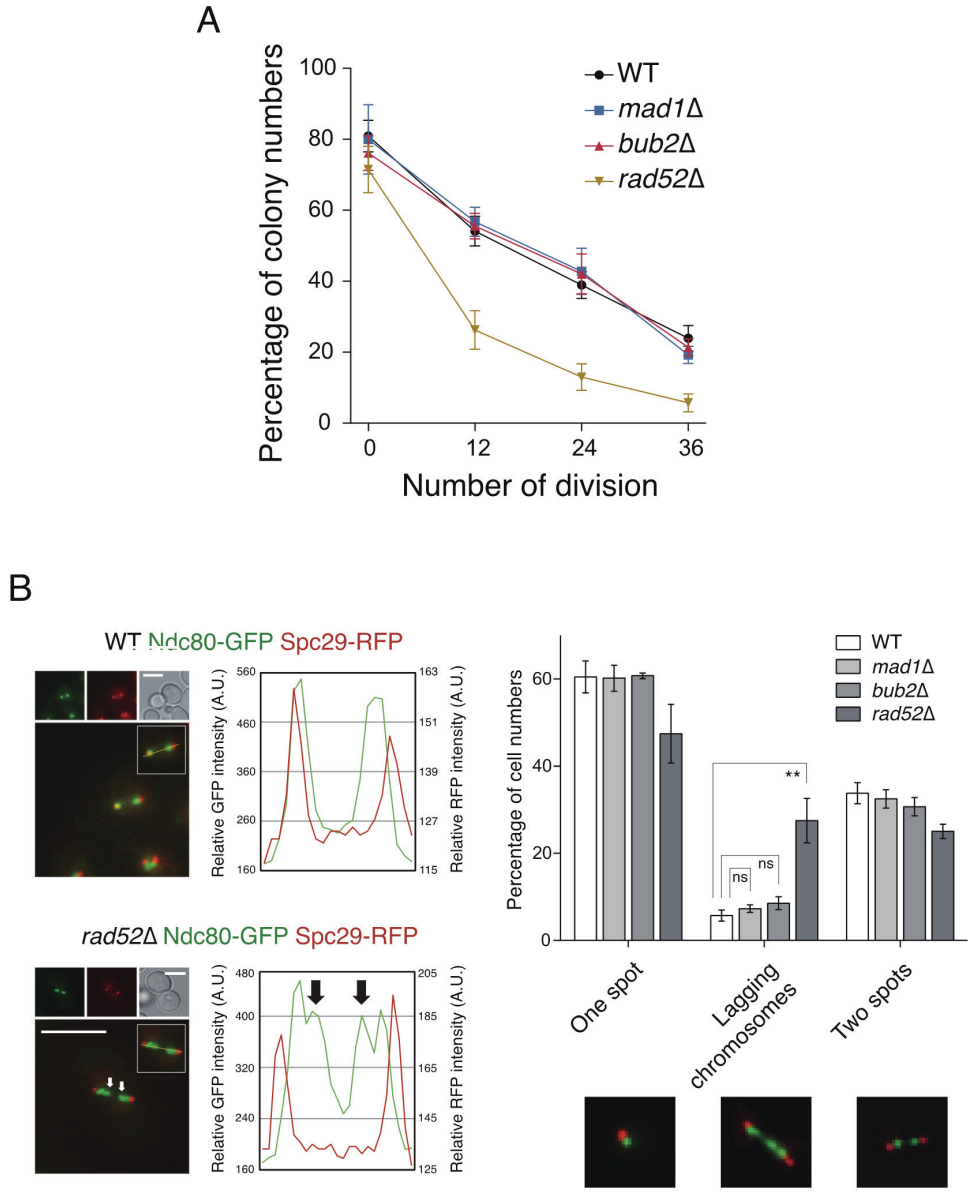
A
Percentage of colony numbers
100
80
60
40
20
0
0
12
24
36
Number of division
WT
mad1Δ
bub2Δ
rad52Δ
B
WT Ndc80-GFP Spc29-RFP
Relative GFP intensity (A.U.)
560
460
360
260
160
Relative RFP intensity (A.U.)
163
151
139
127
115
rad52Δ Ndc80-GFP Spc29-RFP
Relative GFP intensity (A.U.)
480
400
320
240
160
Relative RFP intensity (A.U.)
205
185
165
145
125
Percentage of cell numbers
60
40
20
0
WT
mad1Δ
bub2Δ
rad52Δ
**
ns
ns
One spot
Lagging chromosomes
Two spots

Fig. 12 *rad52*Δ cells show the phenotypes that represent inaccurate regulation of chromosome segregation.

(A) *rad52*Δ cells showed lower fidelity of vector inheritance than other control cells. Data represent the mean±SD of triplicate cultures. (B) Ratio of cells with lagging chromosomes was increased in *rad52*Δ cells. Fluorescence images were taken in asynchronous log phase. Fluorescence intensity was measured along the yellow lines on images. White arrows on the image and black arrows on the relative fluorescence intensity graph indicate lagging chromosomes that were not accumulated to the spindle poles properly. Scale bars are 4 μm. Right panel represents the mean±SD of triplicate cultures using indicated strains. P-values were determined by the Student's *t* test (**$p < 0.01$).

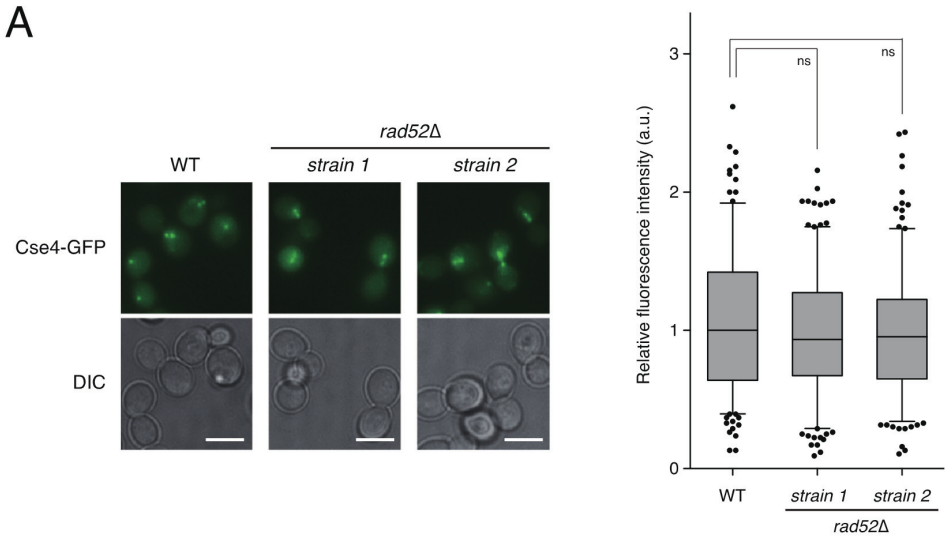
A
rad52Δ
WT
strain 1
strain 2
Cse4-GFP
DIC
Relative fluorescence intensity (a.u.)
ns
ns
0
1
2
3
WT
strain 1
strain 2
rad52Δ

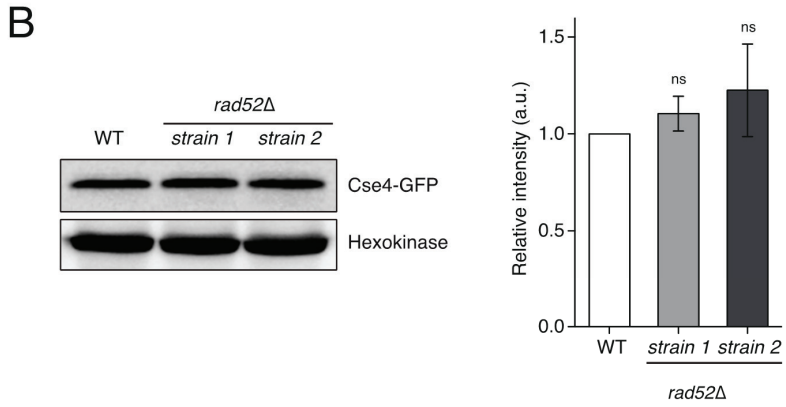
B
rad52Δ
WT
strain 1
strain 2
Cse4-GFP
Hexokinase
Relative intensity (a.u.)
ns
ns
0.0
0.5
1.0
1.5
WT
strain 1
strain 2
rad52Δ

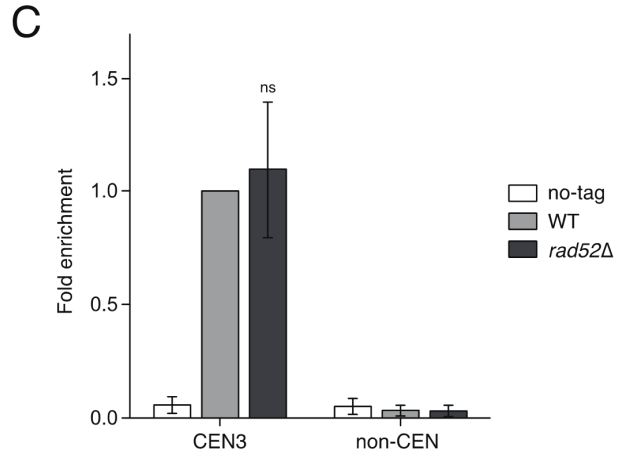
C
Fold enrichment
ns
0.0
0.5
1.0
1.5
CEN3
non-CEN
no-tag
WT
rad52Δ

Fig. 13 Absent of Rad52 does not affect to kinetochore structure in *Saccharomyces cerevisiae*.

(A) Fluorescence intensity of Cse4-GFP was not different between *rad52*Δ cells and wild-type cells. Fluorescence images were taken in asynchronous log phase (left panel). The relative fluorescence intensity was calculated by subtracting background intensity from Mps1-GFP signal intensity (right panel). Box plot was represented with whiskers from 5th to 95th percentile, and data was normalized to the median of *RAD52* cells (N > 200). P-values were determined by the Mann-Whitney *U* test. (B) Protein amount of Cse4 was not different between *rad52*Δ cells and wild-type cells. Amount of Cse4 in wild-type cells was used as standard to normalize the relative amounts of Cse4 in *rad52*Δ cells (right panel). Hexokinase was used as a loading control. Data represent the mean±SD of triplicate cultures. P-values were determined by the one sample *t* test, and WT column was used as a hypothetical mean. (C) Centromere binding of Cse4 was not different between *rad52*Δ cells and wild-type cells. ChIP assays were performed in wild-type cells and *rad52*Δ cells for CEN3 and non-centromeric DNA (non-CEN). Quantification of ChIP assasy was measured by quantitative real time PCR (qPCR). WT column of CEN3 was used for standard to calculate relative fold enrichment of each column. Data represent the mean±SD of triplicate cultures. P-values were determined by the one sample *t* test, and WT column of CEN3 was used as a hypothetical mean.

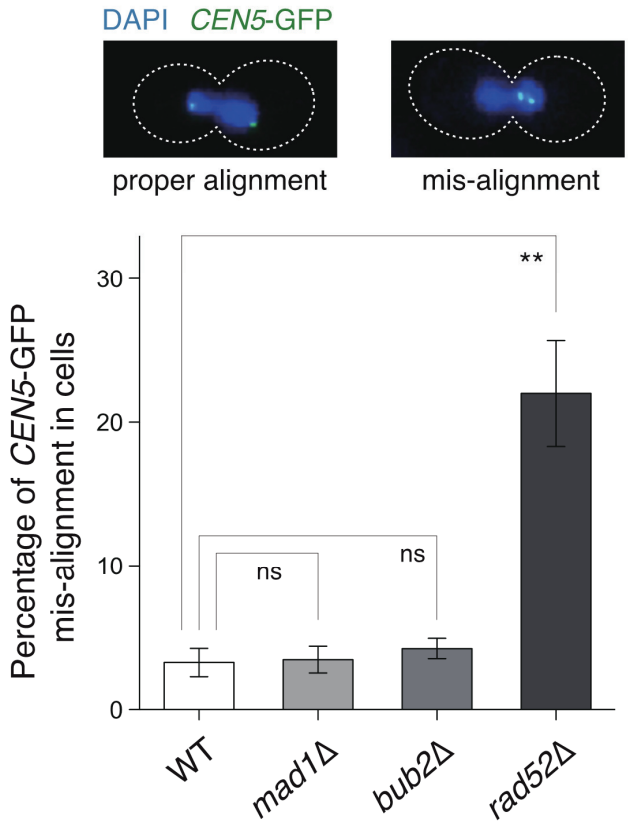

Fig. 14 Rad52 is also required for accurate chromosome segregation during unperturbed cell cycle.

Chromosome mis-alignment was significantly increased in *rad52*Δ cells. Wild-type and *rad52*Δ cells containing *CEN5-(tetO2)*$_{112}$ and tetR-GFP were synchronized by α-factor treatment for 3hr. Synchronized cells were released to fresh YPD media and fixed with formaldehyde at 75min after release from α-factor. DAPI staining was used for visualization of Nuclear DNA. Data represent the mean±SD of triplicate cultures. P-values were determined by the Student's *t* test (**$p < 0.01$).

3. Discussion

In present study, I demonstrate that Rad52 regulates Mad1-dependent SAC activation and accurate chromosome segregation in different manner to homologous recombination. By the truncation assay, it was clearly confirmed that the domains for mitotic regulation and homologous recombination are completely separated on Rad52. Ultimately, it was defined that Rad52 is crucial factor for SAC activation and it also regulates appropriate chromosome segregation to maintain genome inheritance.

According to the finding by Liakopoulos et al. (2003), dephophorylated form of Kar9 has the affinity to the spindle pole. However, I found that hyper-phosphorylated Kar9 in *rad52*Δ strain was bound to both spindle poles. In addition, phospho-mimicking Kar9 was also bound to both spindle poles. It suggests that the previous report by Liakopoulos et al. (2003) is needed additional explanation to understand precise mechanism of Kar9 regulation. Although I did not examine the detailed mechanism of asymmetric regulation of Kar9, it is presumable that asymmetric loading of Kar9 onto spindle pole is depends on the difference of binding affinity between dephosphorylated form and phosphorylated form. Thus, defining the precise mechanism that regulates asymmetric binding of Kar9 will be interesting subject for future work.

As shown in my data, Rad52 is related to Mad1-dependent SAC pathway. By the Pds1 degradation assay, it was confirmed that deletion of *RAD52* disrupts SAC activation under spindle damage condition. Interestingly, despite checkpoint is not functional in *rad52*Δ strain, cell cycle progression is arrested at G2/M phase. This phenomenon can be addressed by epistatic assay using double deletion strains. Deletion of *RAD52* spontaneously causes chromosome mis-alignment, which should be repaired by mitotic checkpoint, and disrupts Mad1-dependent SAC activation. Thus, *mad1*Δ *rad52*Δ strain did not show additive effect on mitotic dysregulation. In contrast, *bub2*Δ *rad52*Δ strain showed synergistic effect on mitotic dysergulation and passed through the mitotic checkpoint. It suggests that Bub2-dependent

mitotic arrest stops the cell cycle progression in *rad52*Δ cells. Based on these findings, I can presume that growth delay of *rad52*Δ occurs as following steps; (1) When *RAD52* is deleted, incorrect microtubule attachment spontaneously occurs. (2) Because SAC is abolished by deletion of *RAD52*, incorrect microtubule attachments are not repaired by SAC. (3) Unrepaired spindle stress activates Bub2-dependent mitotic arrest to stop the cell cycle progression before chromosome segregation.

In total, this study demonstrates that Rad52 controls SAC activation and appropriate chromosome segregation in different manner to DNA damage repair function. Because detailed mechanism of mitotic regulation is not completely investigated, defining Rad52 as a novel mitotic regulator will provide further insight into the regulatory mechanism of mitosis.

4. Material and Methods

4.1. Yeast Growth Condition

Yeast cells were grown at 30°C in YPD or SC medium lacking amino acids as required. For all chemical treatments, cells were grown to mid-log phase (OD_{600} = 0.7-1.0) and diluted to OD_{600} = 0.5. Chemical-treated cells were incubated in 30°C for 3 hr.

4.2. Construction of Plasmid

Full-length Rad52 expression vectors (p415ADH-RAD52-RFP, p416ADH-RAD52-RFP, p416ADH-RAD52-HA) were constructed as follows: XbaI and XmaI sites-inserted RAD52 ORF sequence was amplified from yeast genomic DNA, digested with XbaI and XmaI, and ligated with p415ADH-RFP plasmid and p416ADH-RFP plasmid that were digested by XbaI and XmaI. For constructing p416ADH-RAD52-HA, HA sequence was substituted for RFP sequence by XmaI and XhoI digestion and ligation.

Truncated Rad52 expression vectors [p415ADH-RAD52 (1-294)-RFP, p415ADH-RAD52 (1-136)-RFP, p415ADH-NLS-RAD52 (136-471)-RFP, p415ADH-NLS-RAD52 (61-471)-RFP, p416ADH-RAD52 (1-294)-HA] were constructed as follows: Truncated RAD52 sequences were amplified from yeast genomic DNA. For the N-terminus truncation, DNA sequence for SV40 NLS peptide was inserted by the forward primer. Digestion, ligation, and HA sequence cloning were performed as described above.

Especially, middle part-truncated Rad52 expression vectors [p415ADH-RAD52 (1-136, 273-471)-RFP, p415ADH-RAD52 (1-136, 294-471)-RFP] were constructed by one-step sequence- and ligation-independent cloning (SLIC) method (Jeong et al., 2012).

Sequence-mutated Rad52 expression vector [p415ADH-RAD52 (K10,11,220R)-RFP] was constructed by SLIC-based sequence substitution cloning.

p416ADH-NOP56-RFP and p416ADH-KAR9-GFP were constructed by PCR-based cloning. XbaI and XmaI sites-inserted ORF sequences were amplified from yeast genomic DNA. Amplified ORFs were digested by XbaI and XmaI, ligated with p416ADH-RFP or p416ADH-GFP. p416ADH-KAR9 (S197,496E)-GFP was constructed by SLIC-based sequence substitution cloning.

4.3. Measurement of Growth Curve

All growth curves were measured by using yeast strains carrying vectors, which are indicated in figures. Cells were grown at 30°C in SC media lacking amino acids as required and diluted to OD_{600} = 0.2-0.25. OD_{600} was measured every 1 hr during incubation at 30°C.

4.4. Measurement of DNA Contents

DNA contents measurement by flow cytometry was performed as previously described (Haase and Reed, 2002). Approximately 1x107 cells were harvested and fixed with 5 ml of 70% ethanol for 1 hr at room temperature. Fixed cells were collected and washed once with 1 ml of distilled water and transferred to microfuge tube. 0.5 ml of 2 mM RNase solution (2 mg/ml RNase A in 50 mM Tris, pH 8.0, 15 mM NaCl, boiled for 15 min) was treated to harvested cells for 2-3 hr at 37°C. After removing RNase solution, 0.2 ml of pepsin solution (5 mg/ml pepsin in 1 ml distilled water, 4.5 μl HCl) was directly treated to collected cells for 0.5-1 hr at 37°C. Cells were collected by centrifugation and re-suspended to 0.5 ml of 50 mM Tris, pH 7.5. This sample can be analyzed immediately or stored at 4°C for few days. To analyze DNA contents, 50 μl of sample solution was added to 1 ml of SYTOX green solution (1 mM SYTOX green (Invitrogen) in 50 mM Tris, pH 7.5) and this mixture was sonicated for few minutes at low power. DNA contents were measured by FACS Canto cytometer (BD Biosciences) using 488 nm excitation filter and 510 nm emission filter.

4.5. Fluorescence and Time-lapse Microscopy

Fluorescence microscopy was performed on a Nikon Eclipse Ti inverted microscope and DeltaVision microscope (Applied Precision). Cells were grown to OD_{600} = 0.7-1.0 in SC media at 30°C. For sample fixation, 1x107 cells were harvested and treated with 1 ml of paraformaldehyde solution (4% paraformaldehyde, 3.4% sucrose in distilled water) for 15 min at room temperature. Fixed cells were collected by centrifugation and washed twice with PBS. Washed cells were resuspended to 0.5 ml PBS. Fixed samples can be analyze immediately or stored at 4°C for few days. To visualize Nuclear DNA, Fixed samples were directly treated with 2 μg/ml DAPI (Invitrogen). To attach cells on plates, 96-well glass bottom plate (Metrical Bioscience) for Nikon Eclipse Ti inverted microscope and coverglass bottom dish (SPL) for DeltaVision microscope were pre-treated with 5 μg/ml concanavalin A (Sigma-Aldrich).

Time-lapse microscopy of living cells was performed using DeltaVision microscope. Cells grown to OD_{600} = 0.7-1.0 were used for asynchronous time-lapse microscopy immediately or cell cycle synchronization. 150 μM α-factor was treated for 3 hr to synchronize cell cycle to G1 phase and washed twice with fresh media. Washed cells were resuspended to fresh media, and fluorescence images were acquired in environmental chamber of DeltaVision microscope. To maintain cell growth, environmental chamber was heated to 30°C while time-lapse images were acquired.

4.6. Serial Dilution Assay

Cells carrying indicated vectors were grown to OD_{600} = 1.0-2.0 in SC media lacking amino acid as required and adjusted to OD_{600} = 0.75 with distilled water for the first dilution. Four 10-fold serial dilutions were prepared by using the first dilution sample. For MMS sensitivity test, 3 μl of five serial dilution samples were subsequently spotted on media plates in the absence or presence of 0.01% MMS and incubated at 30°C for 3 days. For UV sensitivity test, 3 μl of five serial dilution samples were subsequently spotted on two media plates, and one

of them was exposed to 100 J/m2 UV light by using UV crosslinker (UVP HL-2000 Hybrilinker). Both plates were incubated at 30°C for 3 days.

4.7. Colony Formation Assay

Cells were grown to OD_{600} = 1.0-2.0 in YPD media and adjusted to OD_{600} = 0.75 with distilled water for the first dilution. Four 10-fold serial dilutions were prepared by using the first dilution sample, and 200 µl of last serial dilution sample was plated onto YPD plate. YPD plates were incubated at 30°C for 3 days. Percentage of colony formation cells was calculated by normalizing the colony numbers of each strain to the colony numbers of wild-type strain.

4.8. Vector Loss Assay

Vector loss assay was modified from a previous method (Schleiffer et al., 2012). Cells carrying pRS415 vector were grown to OD_{600} = 0.7-1.0 in SC-Leu media and collected by centrifugation. Collected cells were resuspended to YPD media, and OD_{600} was adjusted to 1.0. Four 10-fold serial dilutions were prepared, and 200 µl of the last dilution was plated onto YPD and SC-Leu plates for the zero point of cell division. Resuspended cells were continuously incubated at 30°C and diluted to fresh YPD before OD_{600} reaches 3.0. The numbers of division were calculated by doubling time of each strain, and cultures were plated at 12, 24, and 36 division as described above. Percentage of vector-containing cells was calculated by normalizing the number of colonies formed on SC-Leu plate to the number of colonies formed on YPD plate.

4.9. Western Blot Assay

To measure cell cycle-dependent Pds1-myc amount, cells were cultured in 25 ml YPD to OD_{600} = 1.0 and mixed with 25 ml fresh YPD to dilute cell density. 150 µM α-factor was treated for 3 hr to synchronize cell cycle to G1 phase and washed twice with YPD. Washed cells were

resuspended to 100 ml YPD, and 1x108 cells were harvested for the zero time point. Remaining cultures were incubated at 30°C, and 1x108 cells were harvested every 30 min from the zero time point. Harvested cells were washed twice with PBS and resuspended to 100 µl lysis buffer (150 mM NaCl, 50 mM Tris, pH 7.5, 0.15% NP-40, 1 mM phenylmethylsulfonyl fluoride, 1 mM benzamidine, 1 µg/ml leupeptin, 1 µg/ml pepstatin). Cells were disrupted by bead-beating using a cell pellet volume equivalent of 0.5 mm glass beads. Lysates were clarified by centrifugation at 14,000 RPM for 10 min on 4°C pre-cooled microcentrifuge. Protein concentration was determined by Bradford assay.

4.10. Chromatin Immunoprecipitation Assay

Cells were grown in 100 ml YPD to OD_{600} = 1 and 3 ml of paraformaldehyde solution (37.5% paraformaldehyde, 20 mM NaOH in PBS) was treated to cell culture for 15 min. 6 ml of 2.5 M glycine was treated for stopping paraformaldehyde fixation and cultures were incubated at 30°C for 5 min. Cells were harvested and washed twice with pre-cooled PBS. Harvested cells were divided to two microfuge tubes and resuspended with 400 µl ChIP lysis buffer (50 mM HEPES/KOH pH 7.5, 500 mM NaCl, 1 mM EDTA, 1% Triton X-100, 0.1% deoxychlate, 0.1% SDS, 1 mM phenylmethylsulfonyl fluoride, 1 mM benzamidine, 1 µg/ml leupeptin, 1 µg/ml pepstatin) for each tube. Cell lysis was performed as described in Western Blot Assay. Lysates were collected to a microfuge tube, and sonication was performed with Sonicator-XL2020 (Misonix) to get sheared chromatin fragments of an average size of 500–1000 bp. After clearance of cell debris by centrifugation at 14,000 RPM, 50 µl aliquot was set aside to make INPUT sample. 750 ul aliquot was incubated with 30 µl of IgG-sepharose beads (GE Healthcare). After 3 hr incubation at 4°C, the beads in microfuge tube were collected by centrifugation at 2,000 RPM and lysate was removed. The beads were washed twice with 1 ml of ChIP lysis buffer, once with 1 ml of DOC buffer (10 mM Tris-Cl pH 8.0, 250 mM LiCl, 0.5% NP-40, 0.5% deoxycholate, 1 mM EDTA) and once with 1 ml of TE buffer (10 mM Tris-Cl pH

7.5, 1 mM EDTA). Washed beads were mixed with 50 µl TES buffer (50 mM Tris-Cll pH 8.0, 10 mM EDTA, 1% SDS) and incubated at 65°C for 10 min. By centrifugation at 14,000 RPM, supernatant was collected and transferred to microfuge tube. Precipitated beads were mixed again with 150 µl TES buffer and centrifuged to collect supernatant. 150 µl of supernatant was transferred to microfuge tube with first 50 ul of supernatant. Cell lysate for INPUT sample was also mixed with 150 µl of TES buffer. INPUT sample and IP sample were incubated at 65°C for over-night. Over-night incubated samples were mixted with 200 µl of TE buffer and 12.5 µl of 20 mg/ml Proteinase K and incubated at 37°C for 2 hr. After Proteinase K incubation, 400 µl of PCI was added to each microfuge tube and mixtures were centrifuged at 14,000 RPM. 350 µl of supernatant was transferred to new microfuge tube and mixed with 44 µl of 3 M NaOAc and 20 µl of 1 mg/ml glycogen. This mixture was mixed with 1 ml of -20°C pre-cooled EtOH and incubated at -20°C for 10 min. To collect DNA, mixture was centrifuged at 14,000 RPM for 5min and precipitated DNA was washed with -20°C pre-cooled 70% EtOH. Precipitated DNA was resolved to 40 µl of TE buffer including 200 µg/ml RNase A and DNA solution was incubated at 37°C for 1 hr. qPCR was performed on 7300 real time PCR system (Applied Biosystems) with SensiFAST SYBR Hi-ROX Mix (Bioline). Primer pair of CUP1 was used for amplifying non-centromeric DNA.

Table 2 Yeast strains used in this study

Strain	Genotype	Source
BY4741	*MATa his3Δ1 leu2Δ0 met15Δ0 ura3Δ0*	EUROSCARF
Y00540	*MATa his3Δ1 leu2Δ0 met15Δ0 ura3Δ0 rad52Δ::kanMX4*	EUROSCARF
GL21E08	*MATa his3Δ1 leu2Δ0 met15Δ0 ura3Δ0 IPL1-GFP:HIS3*	Huh et al. (2003)
HY1578	*MATa his3Δ1 leu2Δ0 met15Δ0 ura3Δ0 rad52Δ::kanMX4 IPL1-GFP:LEU2*	This study
GL08D10	*MATa his3Δ1 leu2Δ0 met15Δ0 ura3Δ0 SLI15-GFP:HIS3*	Huh et al. (2003)
HY1579	*MATa his3Δ1 leu2Δ0 met15Δ0 ura3Δ0 rad52Δ::kanMX4 SLI15-GFP:HIS3*	This study
HY1580	*MATa his3Δ1 leu2Δ0 met15Δ0 ura3Δ0 [pRS415]*	This study
HY1581	*MATa his3Δ1 leu2Δ0 met15Δ0 ura3Δ0 rad52Δ::kanMX4 [pRS415]*	This study
HY1582	*MATa his3Δ1 leu2Δ0 met15Δ0 ura3Δ0 rad52Δ::kanMX4 [p415ADH-RAD52-RFP]*	This study

HY1583	*MATa his3Δ1 leu2Δ0 met15Δ0 ura3Δ0 rad52Δ::kanMX4 [p415ADH-RAD52(1-294)-RFP]*	This study
HY1584	*MATa his3Δ1 leu2Δ0 met15Δ0 ura3Δ0 rad52Δ::kanMX4 [p415ADH-RAD52(1-136)-RFP]*	This study
HY1585	*MATa his3Δ1 leu2Δ0 met15Δ0 ura3Δ0 rad52Δ::kanMX4 [p415ADH-RAD52(1-136, 273-471)-RFP]*	This study
HY1586	*MATa his3Δ1 leu2Δ0 met15Δ0 ura3Δ0 rad52Δ::kanMX4 [p415ADH-RAD52(1-136, 294-471)-RFP]*	This study
HY1587	*MATa his3Δ1 leu2Δ0 met15Δ0 ura3Δ0 rad52Δ::kanMX4 [p415ADH-NLS-RAD52(136-471)-RFP]*	This study
HY1588	*MATa his3Δ1 leu2Δ0 met15Δ0 ura3Δ0 rad52Δ::kanMX4 [p415ADH-NLS-RAD52(61-471)-RFP]*	This study
HY1589	*MATa his3Δ1 leu2Δ0 met15Δ0 ura3Δ0 rad52Δ::kanMX4 [p415ADH-RAD52(K10,11,220R)-RFP]*	This study
GL28G03	*MATa his3Δ1 leu2Δ0 met15Δ0 ura3Δ0 SPC29-GFP:HIS3*	Huh et al. (2003)
HY1590	*MATa his3Δ1 leu2Δ0 met15Δ0 ura3Δ0 rad52Δ::kanMX4 SPC29-GFP:LEU2*	This study
HY1591	*MATa his3Δ1 leu2Δ0 met15Δ0 ura3Δ0 KAR9-GFP:HIS3 SPC29-RFP:LEU2*	This study
HY1592	*MATa his3Δ1 leu2Δ0 met15Δ0 ura3Δ0 rad52Δ::kanMX4 KAR9-GFP:HIS3 SPC29-RFP:LEU2*	This study

TL12F02	*MATa his3Δ1 leu2Δ0 met15Δ0 ura3Δ0 KAR9-TAP:HIS3*	Ghaemmaghami et al. (2003)
HY1593	*MATa his3Δ1 leu2Δ0 met15Δ0 ura3Δ0 rad52Δ::kanMX4 KAR9-TAP:LEU2*	This study
HY1594	*MATa his3Δ1 leu2Δ0 met15Δ0 ura3Δ0 kar9Δ::kanMX4 SPC29-RFP:LEU2 [p416ADH-KAR9-GFP]*	This study
HY1595	*MATa his3Δ1 leu2Δ0 met15Δ0 ura3Δ0 kar9Δ::kanMX4 SPC29-RFP:LEU2 [p416ADH-KAR9(S197,496E)-GFP]*	This study
HY1596	*MATa his3Δ1 leu2Δ0 met15Δ0 ura3Δ0 CDC14-GFP:LEU2 [p416ADH-NOP56-RFP]*	This study
HY1597	*MATa his3Δ1 leu2Δ0 met15Δ0 ura3Δ0 rad52Δ::kanMX4 CDC14-GFP:LEU2 [p416ADH-NOP56-RFP]*	This study
Y04453	*MATa his3Δ1 leu2Δ0 met15Δ0 ura3Δ0 mad1Δ::kanMX4*	EUROSCARF
Y06189	*MATa his3Δ1 leu2Δ0 met15Δ0 ura3Δ0 bub2Δ::kanMX4*	EUROSCARF
HY1598	*MATa his3Δ1 leu2Δ0 met15Δ0 ura3Δ0 rad52Δ::kanMX4 mad1Δ::HIS3*	This study
HY1599	*MATa his3Δ1 leu2Δ0 met15Δ0 ura3Δ0 rad52Δ::kanMX4 bub2Δ::HIS3*	This study
HY1600	*MATa his3Δ1 leu2Δ0 met15Δ0 ura3Δ0 bub2Δ::kanMX4 IPL1-GFP:LEU2*	This study

HY1601	*MATa his3Δ1 leu2Δ0 met15Δ0 ura3Δ0 rad52Δ::kanMX4 bub2Δ::HIS3 IPL1-GFP:LEU2*	This study
GL11E03	*MATa his3Δ1 leu2Δ0 met15Δ0 ura3Δ0 CDC20-GFP:HIS3*	Huh et al. (2003)
HY1602	*MATa his3Δ1 leu2Δ0 met15Δ0 ura3Δ0 rad52Δ::kanMX4 CDC20-GFP:HIS3*	This study
HY1603	*MATa his3Δ1 leu2Δ0 met15Δ0 ura3Δ0 PDS1-myc:LEU2*	This study
HY1604	*MATa his3Δ1 leu2Δ0 met15Δ0 ura3Δ0 rad52Δ::kanMX4 PDS1-myc:LEU2*	This study
HY1605	*MATa his3Δ1 leu2Δ0 met15Δ0 ura3Δ0 rad52Δ::kanMX4 [p416ADH-RAD52-HA]*	This study
HY1607	*MATa his3Δ1 leu2Δ0 met15Δ0 ura3Δ0 rad52Δ::kanMX4 [p416ADH-RAD52(S86A, T96A, S136A, T349A, S374A)-HA]*	This study
HY1608	*MATa his3Δ1 leu2Δ0 met15Δ0 ura3Δ0 rad52Δ::kanMX4 [p416ADH-RAD52(S136A, T349A, S374A)-HA]*	This study
HY1609	*MATa his3Δ1 leu2Δ0 met15Δ0 ura3Δ0 rad52Δ::kanMX4 [p416ADH-RAD52(S86A, T96A, T349A, S374A)-HA]*	This study
HY1610	*MATa his3Δ1 leu2Δ0 met15Δ0 ura3Δ0 rad52Δ::kanMX4 [p416ADH-RAD52(S86A, T96A, S136A, S374A)-HA]*	This study
HY1611	*MATa his3Δ1 leu2Δ0 met15Δ0 ura3Δ0 rad52Δ::kanMX4 [p416ADH-RAD52(S86A, T96A, S136A, T349A)-HA]*	This study

HY1612	*MATa his3Δ1 leu2Δ0 met15Δ0 ura3Δ0 mad1Δ::kanMX4 [pRS415]*	This study
HY1613	*MATa his3Δ1 leu2Δ0 met15Δ0 ura3Δ0 bub2Δ::kanMX4 [pRS415]*	This study
HY1614	*MATa his3Δ1 leu2Δ0 met15Δ0 ura3Δ0 NDC80-GFP:HIS3 SPC29-RFP:LEU2*	This study
HY1615	*MATa his3Δ1 leu2Δ0 met15Δ0 ura3Δ0 rad52Δ::kanMX4 NDC80-GFP:HIS3 SPC29-RFP:LEU2*	This study
HY1616	*MATa his3Δ1 leu2Δ0 met15Δ0 ura3Δ0 mad1Δ::kanMX4 NDC80-GFP:LEU2 SPC29-RFP:URA3*	This study
HY1617	*MATa his3Δ1 leu2Δ0 met15Δ0 ura3Δ0 bub2Δ::kanMX4 NDC80-GFP:LUE2 SPC29-RFP:URA3*	This study
TL07G06	*MATa his3Δ1 leu2Δ0 met15Δ0 ura3Δ0 RAD53-TAP:HIS3*	Ghaemmaghami et al. (2003)
HY1657	*MATa his3Δ1 leu2Δ0 met15Δ0 ura3Δ0 rad52Δ::kanMX4 RAD53-TAP:LEU2*	This study
HY1658	*MATa his3Δ1 leu2Δ0 met15Δ0 ura3Δ0 RAD53-TAP:HIS3 [pJH132 (GAL1-HO URA3)]*	This study
HY1659	*MATa his3Δ1 leu2Δ0 met15Δ0 ura3Δ0 rad52Δ::kanMX4 RAD53-TAP:LEU2 [pJH132 (GAL1-HO URA3)]*	This study
GL34A07	*MATa his3Δ1 leu2Δ0 met15Δ0 ura3Δ0 CSE4-GFP:HIS3*	Huh et al. (2003)

HY1660	*MATa his3Δ1 leu2Δ0 met15Δ0 ura3Δ0 rad52Δ::kanMX4 CSE4-GFP:LEU2 (strain 1)*	This study
HY1661	*MATa his3Δ1 leu2Δ0 met15Δ0 ura3Δ0 rad52Δ::kanMX4 CSE4-GFP:LUE2 (strain 2)*	This study
TL46E12	*MATa his3Δ1 leu2Δ0 met15Δ0 ura3Δ0 CSE4-TAP:HIS3*	Ghaemmaghami et al. (2003)
HY1662	*MATa his3Δ1 leu2Δ0 met15Δ0 ura3Δ0 rad52Δ::kanMX4 CSE4-TAP:LEU2*	This study
T8567	*MATa ade2- 1 ura3-1 his3-11,15 trp1-1 leu2-3,112 can1-100 leu2::tetR-GFP:LEU2 CEN5::tetO2X112:HIS3*	T. U. Tanaka
HY1664	*MATa ade2- 1 ura3-1 his3-11,15 trp1-1 leu2-3,112 can1-100 leu2::tetR-GFP:LEU2 CEN5::tetO2X112:HIS3 mad1Δ::TRP1*	This study
HY1665	*MATa ade2- 1 ura3-1 his3-11,15 trp1-1 leu2-3,112 can1-100 leu2::tetR-GFP:LEU2 CEN5::tetO2X112:HIS3 bub2Δ::TRP1*	This study
HY1666	*MATa ade2- 1 ura3-1 his3-11,15 trp1-1 leu2-3,112 can1-100 leu2::tetR-GFP:LEU2 CEN5::tetO2X112:HIS3 rad52Δ::TRP1*	This study
HY1671	*MATa his3Δ1 leu2Δ0 met15Δ0 ura3Δ0 IPL1-GFP:HIS3 BIM1-RFP-URA*	This study
HY1672	*MATa his3Δ1 leu2Δ0 met15Δ0 ura3Δ0 rad52Δ::kanMX4 IPL1-GFP:LEU2 BIM1-RFP-URA*	This study

Table 3 Oligonucleotide primers used in this study

Primer name	Sequence (5' to 3')
SLI15-F2	AAACAGGTTGAAACCGCGTCAAATTGTGCCCAAAAGGTCTGGTCGACGGATCCCCGGGTT
SLI15-R1	GTTAACCAGTTTGAATTTTTCTTTTCTGGGGTAATCGAATTCGATGAATTCGAGCTCGTT
SLI15-CHK	CTTCAATTACTT CCACCAGC
BIM1-F2	TGGCGTGAGCAACAACTTGATCATCGACGAGGAAACTTTTGGTCGACGGATCCCCGGGTT
BIM1-R1	AATACATATTCGAAAACAATACTGCTTTTTAGTTCTCAACTCGATGAATTCGAGCTCGTT
BIM1-CHK	TGTTACCCAAGGTCAGTTGG
KAR9-F2	TTCACCAAGAGAAGGGCGTTTAGATAAAACCCCAACTTATGGTCGACGGATCCCCGGGTT
KAR9-R1	GATATATAAAAATGTATAAGTATACAGTTTTAGGTTAGTATCGATGAATTCGAGCTCGTT
KAR9-CHK	CTGATACTAAGTAGTGTTCC
KAR9-F(SLIC)	GCTATACCAAGCATACAATCAACTTCTAGAATTTCAGTAGCACTGCCATGGATAATGATG
KAR9-R(SLIC)	TGAAAAGTTCTTCTCCTTTACTGTTAATTAACCCGGGGATCCGTCGACCATAAGTTGGGG
KAR9(S197E)-F	GGTTCGCGGAGCCGATACGGCATACTCC

KAR9(S197E)-R	GGAGTATGCCGTATCGGCTCCGCGAACC
KAR9(S496E)-F	GATCCGGAGGAGCCAAACAAAGGAAAAC
KAR9(S496E)-R	GTTTTCCTTTGTTTGGCTCCTCCGGATC
MAD1-F	TCGAGAGGTAATAGTAAATAATGGATGTGAGAGCGGCATTCACAGGAAACAGCTATGACC
MAD1-R	TGGCTTGTCGCTGTTCCCATAGACGCAATGTTATTGTTGCGTTGTAAAACGAGGCCAGT
MAD1-400	GTTAATATCGTCGCTATCAG
BUB2-F	CAACAGACTTTTAAACTTGTTAACTTTTGCATGACCTCAACACAGGAAACAGCTATGACC
BUB2-R	TCACATAGTTTACGGTATATATATGTCTGGGTCGGTCAAGGTTGTAAAACGACGGCCAGT
BUB2-400	TGGTGTCATCTCATTGTACG
RAD52+NLS184(XbaI)	ACTGTCTAGAAATGGGTGGTCCAAAGAAGAAGAGAAAGGTTGGTGGATATAATGGCTGGTCTACG
RAD52+NLS409(XbaI)	ACTGTCTAGAATGGGTGGTCCAAAGAAGAAGAGAAAGGTTGGTTTGAGATTGTTTGGTAATGC
RAD52+1F(SLIC)	GCTATACCAAGCATACAATCAACTTCTAGAATGAATGAAATTATGGATATGG
RAD52+408R	AGATCTTTTCAAGGCATCCGTAACG
RAD52-M-F2(SLIC)	TCTGCCGTTACGGATGCCTTGAAAAGATCT GATCCCGTTGTAGCTAAGCAAAGC

RAD52-M-F3(SLIC)	TCTGCCGTTACGGATGCCTTGAAAAGATCTGATTTTCAAGACGACGACTTG
RAD52+1413R(SLIC)	CTCGGAGGAGGCCATGTTAATTAACCCGGGGATCCGTCGACCAGTAGGCTTGC
CSE4-F2	AGACATGCAACTAGCAAGAAGAATCAGGGGACAGTTTATTGGTCGACGGATCCCCGGGTT
CSE4-R1	AAAGGGAAAAATCGGCTCCAGCCCTGAAGCACAAATATCATCGATGAATTCGAGCTCGTT
CSE4-CHK	GAAACTGAAGTACCTGCACC

CHAPTER 2

Phosphorylation of Rad52 by Ipl1/Aurora and Mps1 contributes to Mps1 kinetochore localization and spindle assembly checkpoint activation

1. Introduction

Protein post-translational modifications act as switches that regulate protein activity, concentration and subcellular localization. To control cellular processes after protein translation, cells attach post-translational modifier such as phosphate, ubiquitin, and small-ubiquitin like modifier (SUMO) to the target proteins. Mitosis is also regulated by phosphorylation and ubiquitylation. Phosphorylation is major signal factor to accurately regulate mitosis progression. During the mitosis, mitotic kinases assist proper spindle attachment to kinetochore and finally regulate activity of APC/C for accurate mitosis. APC/C is an E3 ubiquitin ligase and it regulates mitosis progression by ubiquitin-dependent degradation of target proteins. APC/C binds to Cdc20, which is the activator of APC/C, and this complex degrades Securin (Pds1 in *S. cerevisiae*) and cyclin B by ubiquitylation to activate seperase (Cohen-Fix et al., 1996; Glotzer et al., 1991; Visintin et al., 1997).

To maintain the number of chromosomes after cell division, many mitotic kinases regulate spindle-kinetochore attachment and repair abnormal attachment. Among them, Ipl1 (Aurora B kinase in *Homo sapiens*) is known as a major regulator for monitoring spindle-kinetochore attachment and activating spindle assembly checkpoint (SAC) (Yamagishi et al., 2014). Ipl1 composes Ipl1 complex with Sli15 (INCENP in *Homo sapiens*) and Bir1 (Survivin in *Homo sapiens*) (Carmena et al., 2012). Sli15 acts as a scaffold for other subunits and also assists kinase activity of Ipl1. Bir1 provides binding affinity to the centromeres but is not necessary for kinase activity of Ipl1 complex. Because, Ipl1 complex is tightly bound to centromere by Bir1, most target proteins of Ipl1 complex are localized close to centromere.

The mechanism of monitoring accurate spindle attachment by Ipl1 complex is well characterized in many eukaryotic organisms. Ipl1 complex localizes between sister kinetochores during metaphase (Ruchaud et al., 2007) and phosphorylates target proteins in a distance-dependent manner (Wang et al., 2011). Ipl1 dependent phosphorylation of substrates at

kinetochore destabilizes spindle-kinetochore interaction (Kalantzaki et al., 2015; Liu et al., 2009). When tension is generated by bi-directional attachment of spindles, the distance between Ipl1 and its substrates increases. Increasing distance from Ipl1 complex helps that substrates are dephosphorylated by PP1 phosphatase, resulting in stabilization of spindle-kinetochore interaction (Emanuele et al., 2008; Liu et al., 2010). All spindle-kinetochore attachment are stabilized by bi-directional tension, the cell cycle progresses to anaphase to separate sister chromatids. By contrast, when kinetochores are not connected properly to spindles, substrates in kinetochore are stayed close to centromere and continuously phosphorylated by Ipl1 complex. The kinetochore including phosphorylated substrates loses the stability of spindle attachment and it is sequentially detached from mitotic spindle. Because unattached kinetochore acts as a signal for SAC activation, anaphase transition is suppressed to recover accurate attachment between spindle and unattached kinetochore.

Mps1 was identified originally in *Saccharomyces cerevisiae* as a gene required for duplication of the spindle pole body. Subsequently, kinase activity for SAC regulation was also defined. When unattached kinetochores are generated by kinase activity of Ipl1 complex, Mps1 is accumulated to unattached kinetochores to activate SAC. Kinetochore-accumulated Mps1 recruits SAC proteins such as Mad1, Mad2, and Bub1 to kinetochore and phosphorylates substrates in SAC pathway such as Knl1 and Bub1 (London and Biggins, 2014; London et al., 2012). SAC protein complex suppresses APC/C activator Cdc20 by proteasome-dependent proteolysis and prevents metaphase to anaphase transition. By the recent report, it is clearly confirmed that kinase activity of Ipl1 and outer kinetochore component Ndc80 are required for Mps1 localization to kinetochore (Heinrich et al., 2012). However, how localization of Mps1 can be regulated by kinase activity of centromere bound Ipl1 is not yet discovered.

In this study, it was confirmed that Rad52 is a novel substrate of Ipl1 and Mps1. Mps1-dependent Rad52 phosphorylation is needed for SAC activation under spindle damage condition. Ipl1-dependent Rad52 phosphorylation acts as a signal for Mps1 recruitment to the kinetochore.

It was also confirmed that Ipl1 regulates mitosis by multi target phosphorylation. In addition, human Rad52 is phosphorylated by Aurora B and human Mps1, suggesting that Rad52 may also play a role as a regulator of mitosis in human cells. Finally, present study provides further insight for understanding of signal transduction between Ipl1 and Mps1 in mitotic regulatory pathway.

2. Results

Rad52 is a substrate of Ipl1

SAC-related proteins and chromosome segregation proteins are regulated by mitotic kinases such as Ipl1 and Mps1 (Malvezzi et al., 2013; Maure et al., 2007; Yamagishi et al., 2014). Among the mitotic kinases, Ipl1 is a major kinase for regulation of mitosis. It recognizes improper attachment between kinetochore and microtubule (Yamagishi et al., 2014) and recruits SAC activating kinase Mps1 to unattached kinetochores (Heinrich et al., 2012). Because Rad52 regulates accurate mitosis and activates SAC under spindle damage condition, I tested whether Rad52 is regulated by mitotic kinases. Phosphorylation of Rad52 was detected in normal SDS-page gel and it was more clearly detected in SDS-page gel including phos-tag, which binds to the phosphate of protein to reduce the mobility in SDS-page gel. Furthermore, slow migration band of Rad52 was totally removed by λ phosphatase treatment, suggesting that Rad52 is a phospho-protein (**Fig. 15B**). Next, I checked whether Ipl1 is a kinase for Rad52. Rad52 has five Ipl1 consensus residues, which are serine or threonine in (R/K)X(S/T)(I/L/V) (**Fig. 15A**) (Cheeseman et al., 2002), and all Ipl1 consensus residues were substituted to alanine by sequence substitution to examine the effect of non-phosphorylable mutation. Compared to wild-type Rad52, non-Ipl1-phosphorylatable mutant ($Rad52^{S86A,T96A,S136A,T349A,S374A}$) exhibited significantly decreased phosphorylation (**Fig. 15B**). To check whether disruption of Ipl1-dependent phosphorylation results growth defect similarly to *rad52*Δ cells, the optical density from lag phase to late log phase was measured using *rad52*Δ cells expressing wild-type Rad52 or non-Ipl1-phosphorylable Rad52. As shown in **Fig. 15C**, Cells expressing non-Ipl1-phosphorylable Rad52 showed growth defect. To further confirm the effect of Ipl1-dependent phosphorylation on cell cycle progression, DNA contents analysis was performed. Compared to cells expressing wild-type Rad52, cells expressing non-Ipl1-phosphorylable Rad52 showed cell cycle accumulation in G2/M phase similarly to *rad52*Δ cells (**Fig. 15D**). These data suggests

that non-Ipl1-phosphorylable mutation results similar mitotic phenotypes to deletion of *RAD52*. Because residue substitution has potential to cause unexpected problem such as mis-folding of protein structure or function lost, I checked whether non-Ipl1-phosphorylable mutation disturbs only the regulation by Ipl1 or causes non-functional protein mis-folding. To prove that non-Ipl1-phosphorylable Rad52 is specific mutant to disturb mitotic regulation, DNA repair activity was examined. The DNA repair activity was measured by serial dilute assay under stress condition using cells expressing wild-type Rad52 or non-Ipl1-phosphorylable Rad52. Compared to *rad52*Δ cells expressing wild-type Rad52, cells expressing non-Ipl1-phosphorylable Rad52 efficiently repaired DNA damage generated by MMS (**Fig. 15E**). These results suggest that only Rad52 functions for SAC activation and chromosome segregation regulation are defected in non-Ipl1-phosphorylable Rad52.

The substrates of Ipl1 usually show cell cycle-dependent phosphorylation change (Bock et al., 2012; Keating et al., 2009), because kinase activity of Ipl1 is changed according to mitotic phases. Thus, cell cycle-dependent change of Rad52 phosphorylation was examined. The phosphorylation of Rad52 was highly increased during metaphase and decreased at 90 min after release from cell cycle synchronization (**Fig. 15F**), which is considered as cell phase after anaphase onset. However, the phosphorylation of non-Ipl1-phosphorylable Rad52 was not changed by cell cycle. From these results, I hypothesized that Ipl1 phosphorylates Rad52 on five Ipl1 consensus residues. To check this hypothesis, *in vitro* phosphorylation of Rad52 by Ipl1 was examined. Ipl1 phosphorylated Rad52 on Ipl1 consensus residues, whereas kinase-dead Ipl1 with K133R (Nakajima et al., 2011) could not phosphorylate Rad52 (**Fig. 16A**). To determine the exact phosphorylation site, *in vitro* kinase assay using four revertants of non-Ipl1-phosphorylable Rad52, which was reverted each mutated residue of non-Ipl1-phosphorylable Rad52 to the original residue, was performed. Among the revertants, only $Rad52^{S86A,T96A,S136A,T349A}$ was phosphorylated by Ipl1 (**Fig. 16B**), indicating that Ipl1 is a kinase for Rad52 and the target residue is S374.

A

```
  1 MNEIMDMDEK  KPVFGNHSED  IQTKLDKKLG  PEYISKRVGF  GTSRIAYIEG  WRVINLANQI  FGYNGWSTE\
 71 KSVVIDFLDE  RQGKFSIGCT  AIVRVTLTSG  TYREDIGYGT  VENERRKPAA  FERAKKSAVT  DALKRSLRGI
141 GNALGNCLYD  KDFLAKIDKV  KFDPPDFDEN  NLFRPTDEIS  ESSRTNTLHE  NQEQQQYPNK  RRQLTKVTNT
211 NPDSTKNLVK  IENTVSRGTP  MMAAPAEANS  KNSSNKDTDL  KSLDASKQDQ  DDLLDDSLMF  SDDFQDDDLI
281 NMGNTNSNVL  TTEKDPVVAK  QSPTASSNPE  AEQITFVTAK  AATSVQNERY  IGEESIFDPK  YQAQSIRHT\
351 DQTTSKHIPA  SVLKDKTMTT  ARDSVYEKFA  PKGKQLSMKN  NDKELGPHML  EGAGNQVPRE  TTPIKTNAT/
421 FPPAAAPRFA  PPSKVVHPNG  NGAVPAVPQQ  RSTRREVGRP  KINPLHARKP  T*
```

[R/K],X,[S/T],[I/L/V] : Ipl1 consensus sequence

B

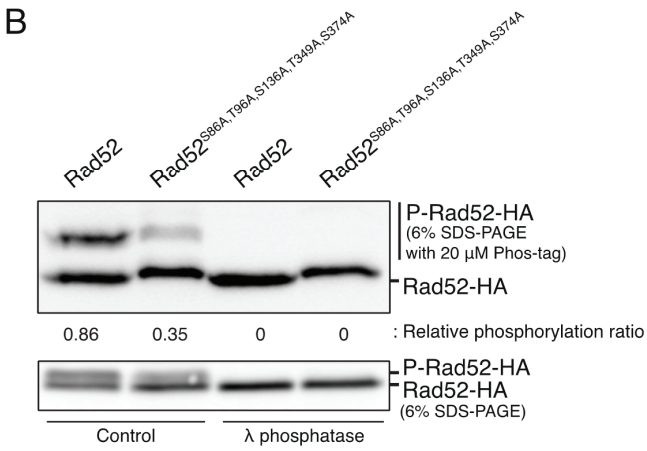

C

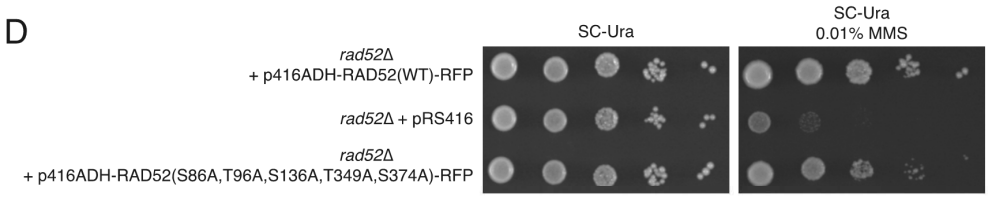
D
SC-Ura
SC-Ura
0.01% MMS
rad52Δ
+ p416ADH-RAD52(WT)-RFP
rad52Δ + pRS416
rad52Δ
+ p416ADH-RAD52(S86A,T96A,S136A,T349A,S374A)-RFP

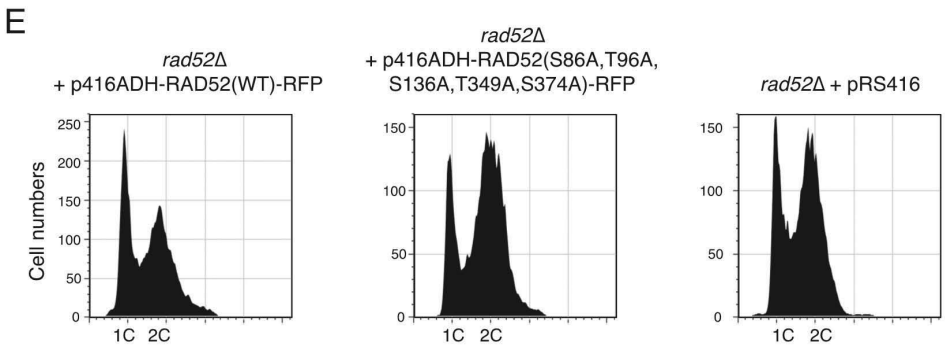
E
rad52Δ
+ p416ADH-RAD52(WT)-RFP
rad52Δ
+ p416ADH-RAD52(S86A,T96A,
S136A,T349A,S374A)-RFP
rad52Δ + pRS416
Cell numbers
250
200
150
100
50
0
1C 2C

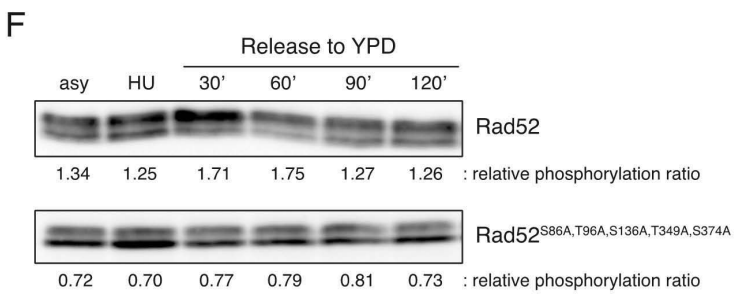
F
Release to YPD
asy
HU
30'
60'
90'
120'
Rad52
1.34 1.25 1.71 1.75 1.27 1.26 : relative phosphorylation ratio
Rad52S86A,T96A,S136A,T349A,S374A
0.72 0.70 0.77 0.79 0.81 0.73 : relative phosphorylation ratio

Fig. 15 Rad52 functions involved in cell growth regulation are related to the phosphorylation on Ipl1 consensus residues.

(A) Rad52 has five Ipl1 consensus residues. Ipl1 consensus sequences are marked with yellow and red on full-length amino acid sequence of Rad52 (Uniprot-P06778). (B) Phosphorylation of Rad52 was highly reduced in Rad52^{S86A,T96A,S136A,T349A,S374A}. The phosphorylation state of wild-type Rad52 and Rad52^{S86A,T96A,S136A,T349A,S374A} was examined by 20 μM Phos-tag SDS–PAGE, and λ phosphatase was treated at 30°C for 2 hr. To calculate the relative phosphorylation ratio, the intensity of major phosphorylated band was divided by that of dephosphorylated band on 20 μM Phos-tag SDS–PAGE. (C) The expression of Rad52^{S86A,T96A,S136A,T349A,S374A} did not recover growth defect of *rad52*Δ cells. *rad52*Δ cells containing indicated vectors were grown in SC-Ura media. Optical density was measured every 1 hr. Data represent the mean ±SD of triplicate cultures. (D) *rad52*Δ cells expressing Rad52^{S86A,T96A,S136A,T349A,S374A} repaired DNA damage. *rad52*Δ cells containing indicated vectors were serially diluted on SC-Ura agar plates in the absence or presence of 0.01% MMS. Plates were incubated at 30°C for 3 days. (E) Large numbers of *rad52*Δ cells expressing Rad52^{S86A,T96A,S136A,T349A,S374A} were accumulated in G2/M phase. *rad52*Δ cells containing indicated vectors were grown in SC-Ura media. Although wild-type cells in SC-Ura media exhibited different cell cycle distribution to wild-type cells in SC-Leu media that was used in Supplementary Fig. S2, *rad52*Δ cells with empty vector or expression vector for Rad52^{S86A,T96A,S136A,T349A,S374A} showed G2/M accumulated phenotype compared to wild-type cells. DNA contents of indicated strains were analyzed by FACS. 1C and 2C indicate single and double DNA haploid content. (F) Rad52^{S86A,T96A,S136A,T349A,S374A} did not exhibit cell cycle-dependent phosphorylation. *rad52*Δ cells expressing Rad52 or Rad52^{S86A,T96A,S136A,T349A,S374A} were synchronized by 0.2 M hydroxyurea treatment for 3 hr, and samples were taken every 30 min after release to fresh SC-Ura medium. To calculate the relative phosphorylation ratio, the intensity of phosphorylated band was divided by that of dephosphorylated band.

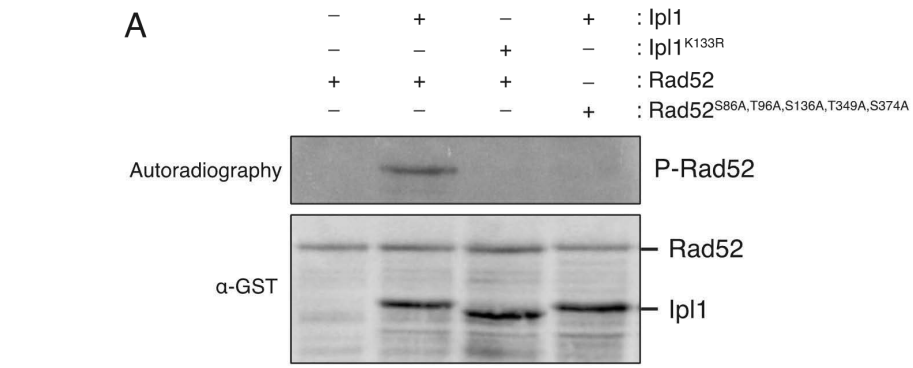
A
– + – + : Ipl1
– – + – : Ipl1K133R
+ + + – : Rad52
– – – + : Rad52S86A,T96A,S136A,T349A,S374A
Autoradiography
P-Rad52
α-GST
Rad52
Ipl1

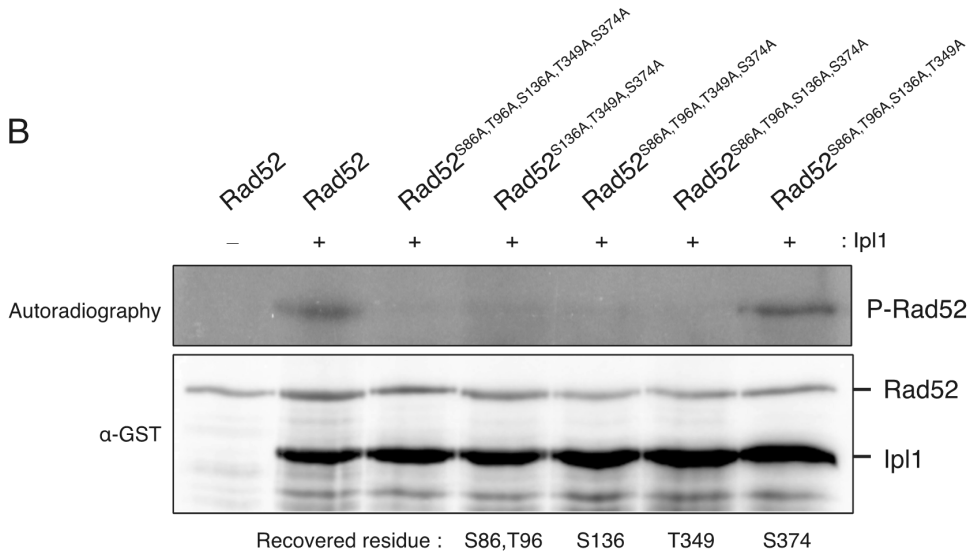
B
Rad52
Rad52
Rad52S86A,T96A,S136A,T349A,S374A
Rad52S136A,T349A,S374A
Rad52S86A,T96A,T349A,S374A
Rad52S86A,T96A,S136A,S374A
Rad52S86A,T96A,S136A,T349A
– + + + + + + : Ipl1
Autoradiography
P-Rad52
α-GST
Rad52
Ipl1
Recovered residue : S86,T96 S136 T349 S374

Fig. 16 Ipl1 phosphorylates Rad52 at serine 374.

(A) Ipl1 phosphorylated Rad52. *In vitro* kinase assay was performed with purified proteins from *E. coli*. Immunoblot assay was conducted with an anti-GST antibody. (B) $Rad52^{S86A,T96A,S136A,T349A}$ was phosphorylated by Ipl1. $Rad52^{S136A,T349A,S374A}$, $Rad52^{S86A,T96A,T349A,S374A}$, $Rad52^{S86A,T96A,S136A,S374A}$, and $Rad52^{S86A,T96A,S136A,T349A}$ were made by reverting mutated residues from $Rad52^{S86A,T96A,S136A,T349A,S374A}$.

Rad52 is a substrate of Mps1

Although Ipl1 is a major kinase for mitotic regulation during unperturbed mitosis, SAC is activated by another mitotic kinase Mps1 under spindle damage condition. Because Rad52 is essential for activation of SAC, I examined whether Rad52 is a substrate of Mps1 by *in vitro* kinase assay. In contrary to Ipl1, because Mps1 was not synthesized in *E. coli*, active Mps1 and kinase-dead Mps1 were purified in yeast cells. As shown in **Fig. 17A**, Mps1 phosphorylated Rad52, but kinase-dead Mps1 with D580A (Araki et al., 2010) could not. Interestingly, non-Ipl1-phosphorylable Rad52 was not phosphorylated by Mps1, suggesting that the target residue of Mps1 is within five Ipl1 consensus residues. Because the C-terminus-truncated Rad52 was phosphorylated by Mps1 (**Fig. 17B**), I concluded that T349 and S374 are not the target residues of Mps1. As expected, S86 or T96 was strongly phosphorylated and S136 was weakly phosphorylated by Mps1 (**Fig. 17C**).

By *in vivo* phosphorylation assay using four revertants from non-Ipl1-phosphorylable Rad52, it was also confirmed that $Rad52^{S136A,T349A,S374A}$ and $Rad52^{S86A,T96A,T349A,S374A}$ recover phosphorylation pattern similar to that of wild-type Rad52 (**Fig. 17D**). Taken together, these results demonstrate that Rad52 is a novel substrate of Mps1.

Human Rad52 is also phosphorylated by Aurora B kinase and Human Mps1

Human Rad52 has similar amino acid sequence and protein structure to yeast Rad52 (Kagawa et al., 2002). Thus, I checked whether human Rad52 is a substrate of Aurora B kinase and human Mps1. Human Rad52 was efficiently phosphorylated by Aurora B kinase (**Fig. 18A**). Interestingly, yeast Rad52 was also phosphorylated by Aurora B kinase, and Ipl1 could phosphorylate human Rad52, suggesting that kinase-substrate interface for phosphorylation event is well conserved to human system.

Similarly to Aurora B kinase, human Mps1 phosphorylated human Rad52 and yeast Rad52 (**Fig. 18B**). These data indicate that Rad52 phosphorylation by Mps1 is also conserved

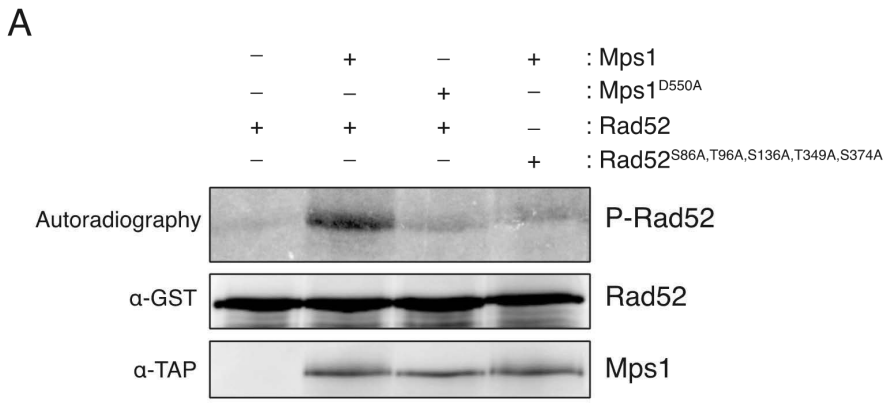
A
– + – + : Mps1
– – + – : Mps1D550A
+ + + – : Rad52
– – – + : Rad52S86A,T96A,S136A,T349A,S374A
Autoradiography
P-Rad52
α-GST
Rad52
α-TAP
Mps1

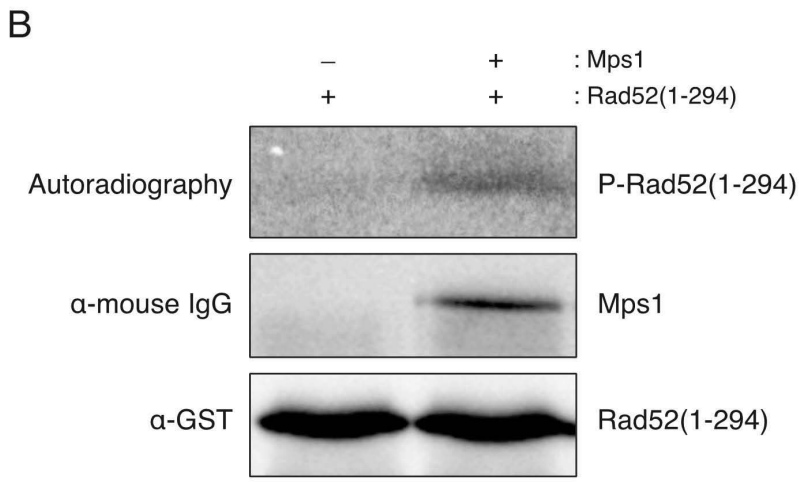
B
– + : Mps1
+ + : Rad52(1-294)
Autoradiography
P-Rad52(1-294)
α-mouse IgG
Mps1
α-GST
Rad52(1-294)

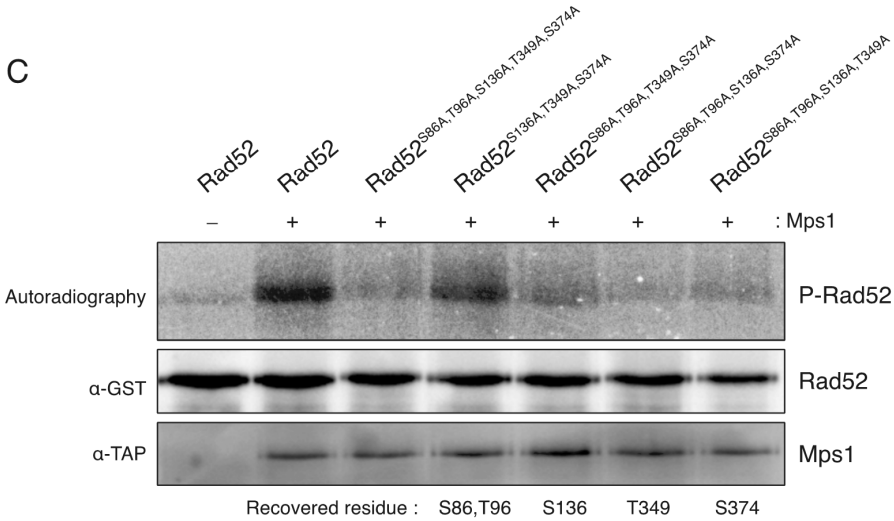
C
Rad52
Rad52
Rad52S86A,T96A,S136A,T349A,S374A
Rad52S136A,T349A,S374A
Rad52S86A,T96A,T349A,S374A
Rad52S86A,T96A,S136A,S374A
Rad52S86A,T96A,S136A,T349A
– + + + + + + : Mps1
Autoradiography
P-Rad52
α-GST
Rad52
α-TAP
Mps1
Recovered residue : S86,T96 S136 T349 S374

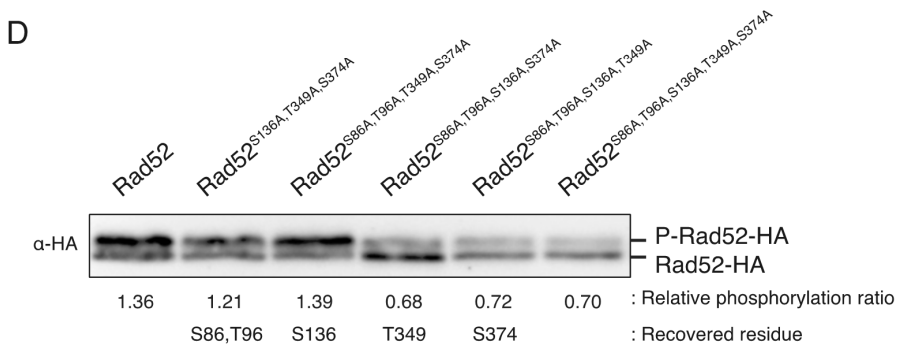
D
Rad52
Rad52S136A,T349A,S374A
Rad52S86A,T96A,T349A,S374A
Rad52S86A,T96A,S136A,S374A
Rad52S86A,T96A,S136A,T349A
Rad52S86A,T96A,S136A,T349A,S374A
α-HA
P-Rad52-HA
Rad52-HA
1.36 1.21 1.39 0.68 0.72 0.70 : Relative phosphorylation ratio
S86,T96 S136 T349 S374 : Recovered residue

Fig. 17 Mps1 phosphorylates Rad52 at serine serine 86, threonine 96, and serine 136.

(A) Mps1 phosphorylated Rad52. *In vitro* kinase assay was performed with purified Rad52 from *E. coli* and immunoprecipitated Mps1 from *S. cerevisiae*. (B) The C-terminus-truncated Rad52 was phosphorylated by Mps1. *In vitro* kinase assay was performed with purified Rad52 from *E. coli* and immunoprecipitated Mps1 from *S. cerevisiae*. Immunoblot assay was conducted with an anti-GST antibody for the C-terminus-truncated Rad52 and an anti-mouse IgG for Mps1. (C) $Rad52^{S136A,T349A,S374A}$ and $Rad52^{S86A,T96A,T349A,S374A}$ were phosphorylated by Mps1. Immunoblot assay was conducted with an anti-GST antibody for Rad52 and a rabbit anti-mouse IgG antibody for Mps1. (D) $Rad52^{S136A,T349A,S374A}$ and $Rad52^{S86A,T96A,T349A,S374A}$ recovered similar phosphorylation pattern to wild-type Rad52. The phosphorylation state of *rad52*Δ cells expressing indicated Rad52 mutants was examined by SDS-PAGE and anti-HA immunoblot assay. To calculate the relative phosphorylation ratio, the intensity of phosphorylated band was divided by that of dephosphorylated band.

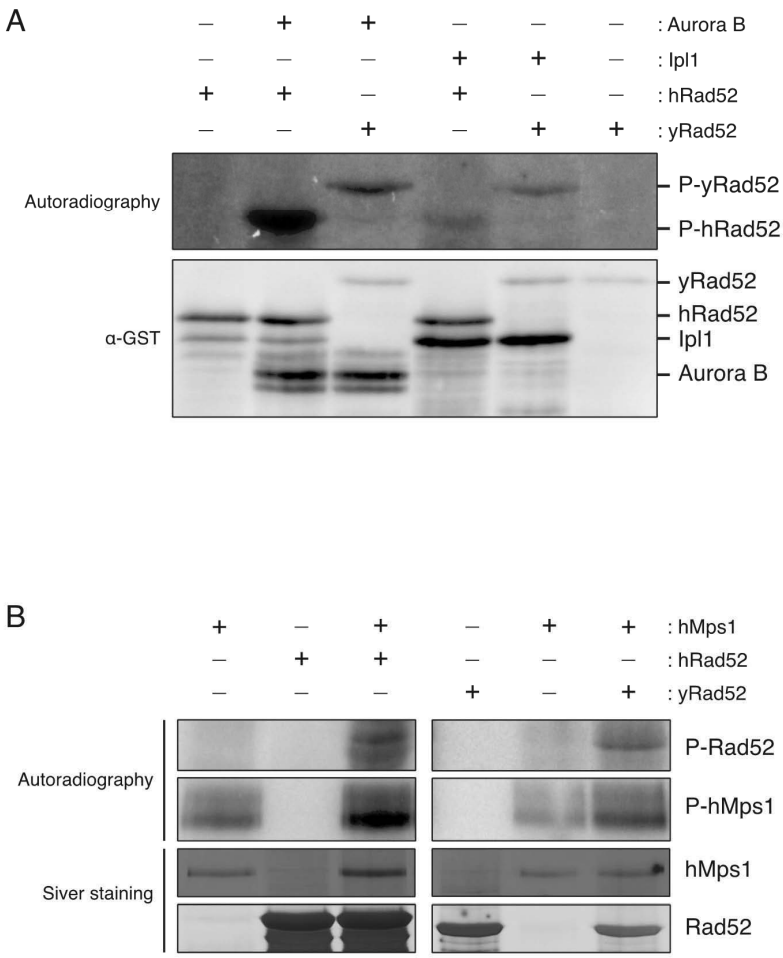

Fig. 18 Human Rad52 is also phosphorylated by Aurora B kinase and Human Mps1.

(A) Aurora B kinase phosphorylated human Rad52. hRad52 and yRad52 indicate human Rad52 and yeast Rad52. Human Rad52 and Aurora B kinase were purified from *E. coli*. Immunoblot assay was conducted with an anti-GST antibody. (B) Human Mps1 phosphorylated human Rad52. hMps1 indicates human Mps1. Proteins were visualized by

in human cells. Hence, it is presumable that novel functions of Rad52, which are regulated by Ipl1- and Mps1-dependent phosphorylation, are conserved from yeast to human.

Mps1-dependent phosphorylation of Rad52 is required to activate SAC

Next, I tested whether SAC activation is regulated by Mps1-dependent phosphorylation of Rad52. To make stable cells for expression of Rad52 mutants, DNA sequence of Rad52 mutant was integrated to genome of *rad52*Δ cells. Using Rad52 mutant-integrated strains, Pds1 degradation kinetics was analyzed to examine SAC activation under nocodazole-treated condition. Cells with wild-type Rad52 maintained high levels of Pds1 in nocodazole-treated media. However, *rad52-3A* cells with Rad52^{S86A,T96A,S136A}, which is not phosphorylated by Mps1, and *rad52-5A* cells with Rad52^{S86A,T96A,S136A,T349A,S374A}, which is not phosphorylated by either Mps1 or Ipl1, showed a rapid decrease in Pds1 level after 120 min of nocodazole treatment (**Fig. 19A**). This observation suggests that Rad52 is phosphorylated by Mps1 to activate SAC under spindle damage condition.

Because nocodazole depolymerizes microtubules, chromosomes in nocodazole-treated cell cannot maintain the localization and scatters to the nucleoplasm. Unattached kinetochores, which are generated by depolymerization effect of nocodazole, are detected by distance-dependent phosphorylation of Ipl1 and SAC related proteins are accumulated to unattached kinetochores by Ipl1 to prevent cell cycle progression (Yamagishi et al., 2014). After nocodazole washout, microtubules are regenerated and connected to adjacent kinetochores. During restoration of connection between microtubule and kinetochore, incorrect connections such as merotelic attachment are formed (Cimini et al., 2001). For proper sister-chromosome separation, Ipl1 and SAC pathway also repair incorrect connection between kinetochore and microtubule (Musacchio and Salmon, 2007). Thus, I observed kinetochore morphology and chromosome separation after depolymerizing microtubules by nocodazole treatment to check the restoration ability of incorrect attachment in cells expressing Rad52 mutants. Nocodazole-

A

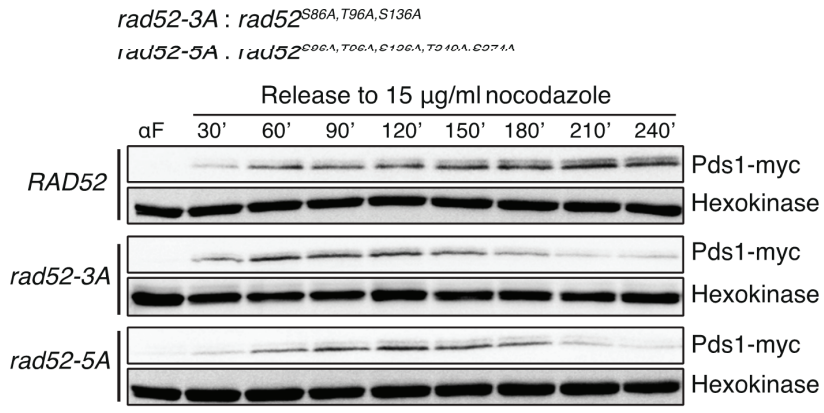
rad52-3A : rad52S86A,T96A,S136A
rad52-5A : rad52S86A,T96A,S136A,T340A,S374A
Release to 15 µg/ml nocodazole
αF
30'
60'
90'
120'
150'
180'
210'
240'
RAD52
rad52-3A
rad52-5A
Pds1-myc
Hexokinase

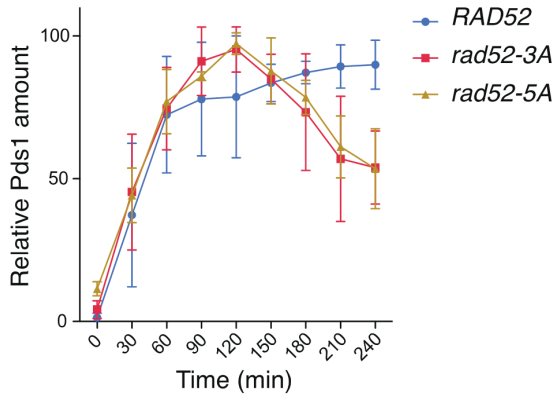
Relative Pds1 amount
100
50
0
0
30
60
90
120
150
180
210
240
Time (min)
RAD52
rad52-3A
rad52-5A

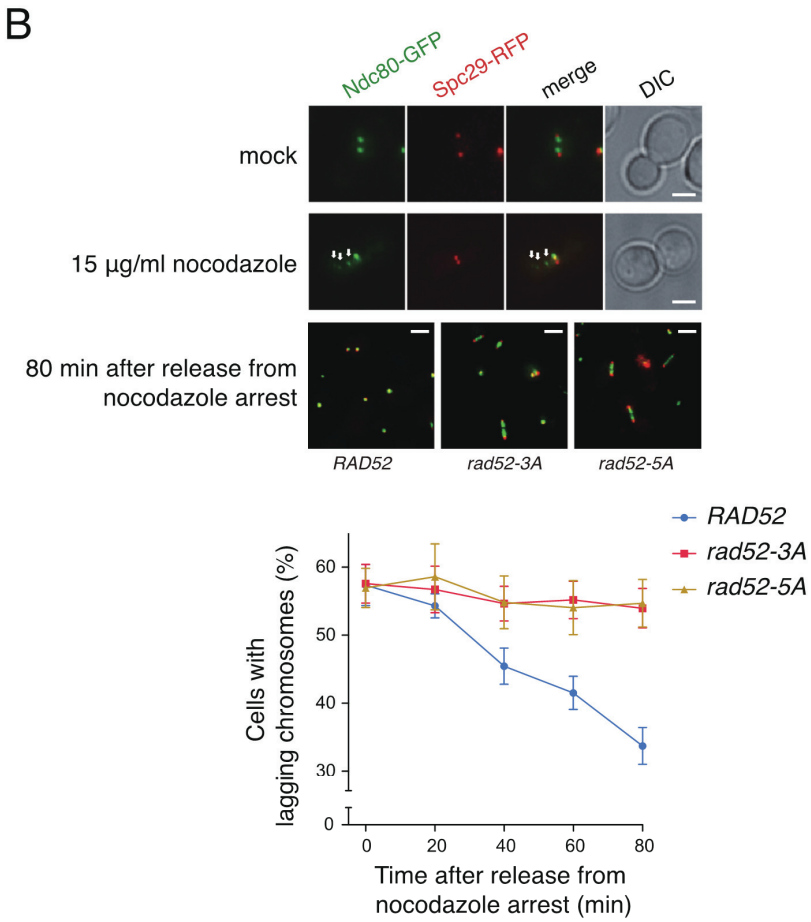
B
Ndc80-GFP
Spc29-RFP
merge
DIC
mock
15 µg/ml nocodazole
80 min after release from nocodazole arrest
RAD52
rad52-3A
rad52-5A
RAD52
rad52-3A
rad52-5A
Cells with lagging chromosomes (%)
60
50
40
30
0
0
20
40
60
80
Time after release from nocodazole arrest (min)

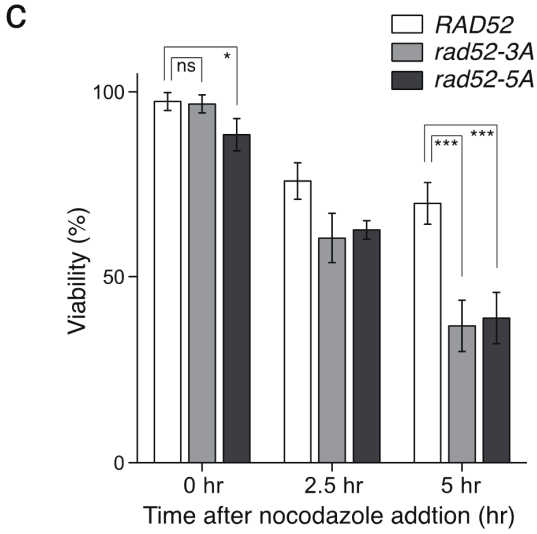
C
RAD52
rad52-3A
rad52-5A
ns
*
***
***
Viability (%)
100
50
0
0 hr
2.5 hr
5 hr
Time after nocodazole addtion (hr)

Fig. 19 Mps1-dependent phosphorylation of Rad52 is required to activate SAC.

(A) *rad52-3A* and *rad52-5A* cells could not block the degradation of Pds1. *RAD52*, *rad52-3A*, and *rad52-5A* indicate *rad52*Δ cells with integrated DNA sequence encoding each Rad52 variant. Immunoblot assay was conducted with an anti-myc antibody. Highest value in each trial was used as 100% standard to normalize the relative amount of Pds1 (lower panel). Data represent the mean±SD of triplicate cultures. (B) *rad52-3A* and *rad52-5A* cells could not recover aberrant spindle-kinetochore interaction caused by nocodazole treatment. White arrows on images indicate scattered kinetochores (upper panel). Scale bars are 2 μm. Cells were sampled every 20 min after nocodazole washout and fixed with paraformaldehyde (lower panel). Data represent the mean±SD of triplicate cultures. (C) *rad52-3A* and *rad52-5A* cells showed decreased viability under spindle damage condition. *RAD52*, *rad52-3A*, and *rad52-5A* cells were incubated in 15 μg/ml nocodazole-treated media for indicated times. Nocodazole-treated cells were aligned on YPD plate using a tetrad dissection microscope. Viability was calculated by normalizing the number of colonies to total number of aligned cells. Data represent the mean±SD of triplicate cultures. P-values were determined by the Student's t test (*$p < 0.05$ and ***$p < 0.005$).

treated cells showed scattered kinetochores. After 80 min release from nocodazole-treated condition, cells with wild-type Rad52 accumulated the chromosomes to the spindle poles accurately. In contrast, scattered chromosomes in *rad52-3A* and *rad52-5A* cells predominantly formed lagging chromosomes (**Fig. 19B**). I measured incorrect localization of kinetochores by counting cells containing lagging chromosomes at regular interval of time after release from nocodazole-treated condition. Approximately 60% of nocodazole-treated cells showed scattered chromosomes in the nucleoplasm at 0 min and cells with wild-type Rad52 continuously recovered proper localization of kinetochores. In contrast, the ratio of cells with lagging chromosomes was not decreased until 80 min in *rad52-3A* and *rad52-5A* cells, suggesting that the spindle-kinetochore interaction is not efficiently recovered in these mutants.

The nocodazole sensitivity was also examined to check the repair ability of SAC pathway. When incubated with nocodazole, the viabilities of *rad52-3A* and *rad52-5A* cells were significantly decreased compared to *RAD52* cells (**Fig. 19C**). These data indicate that Mps1-dependent phosphorylation of Rad52 regulates recovery of accurate spindle-kinetochore interaction when spindle damage occurs. Taken together, Mps1-dependent phosphorylation of Rad52 is crucial to activate SAC under spindle damage condition.

Mps1-dependent phosphorylation leads to the proteasome-dependent degradation of Rad52

To investigate the direct effect of Mps1-dependnet phosphorylation, I examined whether Mps1-dependent phospho-mimicking mutant of Rad52 stimulates SAC protein complex without spindle damage. All Mps1 target residues were mutated to glutamate by sequence substitution to make Mps1-dependent phospho-mimicking Rad52 ($Rad52^{S86E,T96E,S136E}$). Unfortunately, Mps1-dependent phospho-mimicking Rad52 was rapidly degraded in the cells. By using proteasome inhibitor MG-132, it was confirmed that Mps1-dependent phospho-mimicking Rad52 is degraeded in the proteasome-dependent manner (**Fig. 20A**). In addition, the expression of

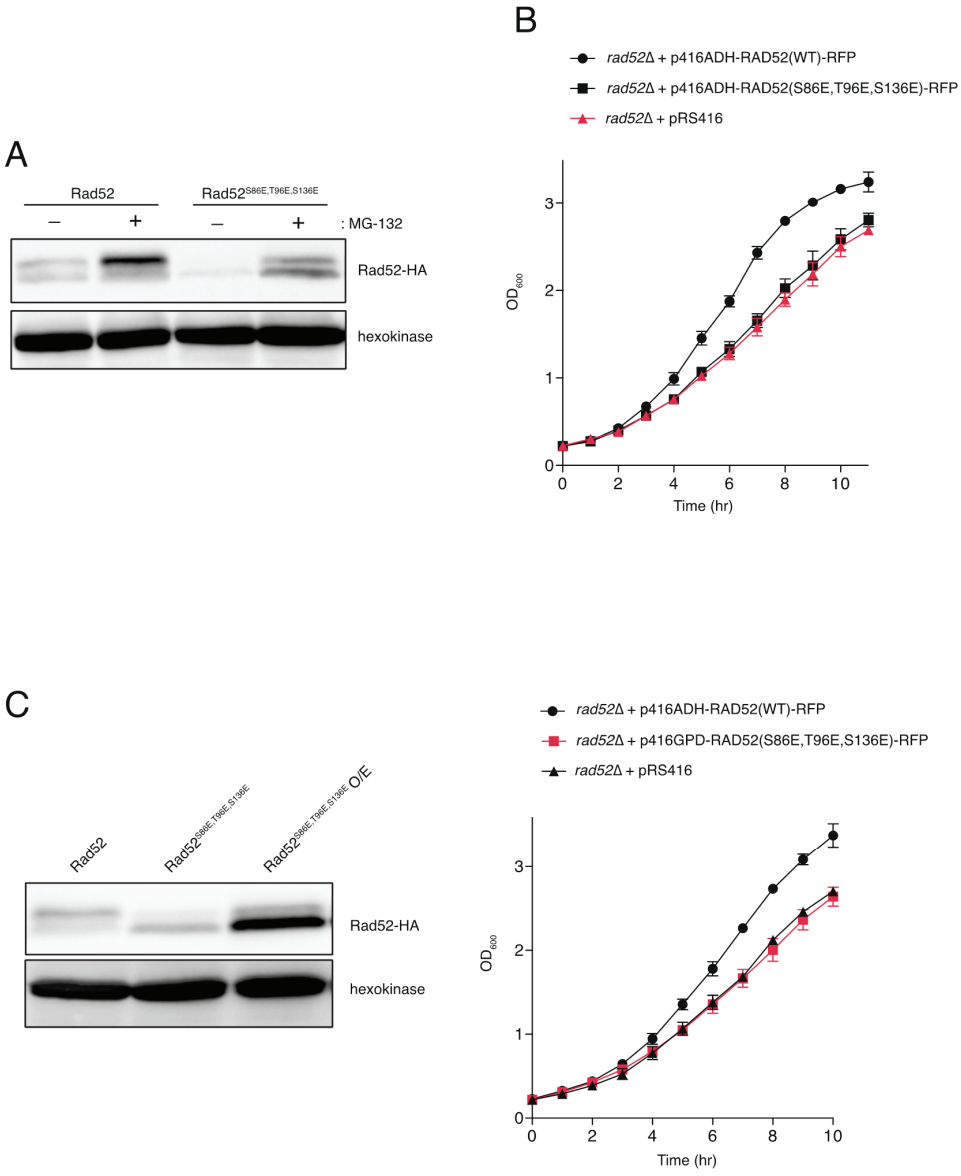
A
Rad52
Rad52S86E,T96E,S136E
–
+
–
+
: MG-132
Rad52-HA
hexokinase
B
rad52Δ + p416ADH-RAD52(WT)-RFP
rad52Δ + p416ADH-RAD52(S86E,T96E,S136E)-RFP
rad52Δ + pRS416
OD600
Time (hr)
C
Rad52
Rad52S86E,T96E,S136E
Rad52S86E,T96E,S136E O/E
Rad52-HA
hexokinase
rad52Δ + p416ADH-RAD52(WT)-RFP
rad52Δ + p416GPD-RAD52(S86E,T96E,S136E)-RFP
rad52Δ + pRS416
OD600
Time (hr)

Fig. 20 Mps1-dependent phospho-mimicking mutant of Rad52 is degraded in the proteasome-dependent manner.

(A) Rad52^{S86E,T96E,S136E} was rapidly degraded in the proteasome-dependent manner. Phosphorylation-dependent mobility shift of Rad52-HA was analyzed by 8% SDS-PAGE, and immunoblot assay was conducted with an anti-HA antibody. 50 μM MG-132 was treated for 3 hr to suppress proteasome-dependent protein degradation. (B) Expression of Rad52^{S86E,T96E,S136E} did not affect cell growth. *rad52*Δ cells containing indicated vectors were grown in SC-Ura medium. Optical density was measured every 1 hr. Data represent the mean±SD of triplicate cultures. (C) Over-expression of Rad52^{S86E,T96E,S136E} did not affect cell growth. Phosphorylation-dependent mobility shift of Rad52-HA was analyzed by 8% SDS-PAGE, and immunoblot assay was conducted with an anti-HA antibody (left panel). Rad52^{S86E,T96E,S136E} was over-expressed under the *GPD1* promoter. *rad52*Δ cells containing indicated vectors were grown in SC-Ura medium. Optical density was measured every 1 hr. Data represent the mean±SD of triplicate cultures (right panel).

Mps1-dependent phospho-mimicking Rad52 did not exert any effect on the growth of *rad52*Δ cells (**Fig. 20B**).

To remain enough Mps1-dependent phospho-mimicking Rad52 for SAC activation in cells, Mps1-dependent phospho-mimicking Rad52 was over-expressed under GPD promoter. As shown in **Fig. 20C**, although the amount of Mps1-dependent phospho-mimicking Rad52 exceeded the expression of wild-type Rad52, over-expression of Mps1-dependent phospho-mimicking Rad52 did not affect the growth of *rad52*Δ cells (**Fig. 20C**). As such, I could not confirm the effect of Mps1-dependent phosphorylation of Rad52. Interestingly, however, I found that the phosphorylated form of wild-type Rad52 is also degraded in the proteasome-dependent manner (**Fig. 20A**), suggesting that the function of Rad52 phosphorylated by Mps1 may be related to the ubiquitin/proteasome-dependent protein degradation. Consistent with this, E3 ubiquitin ligase APC/C-mediated degradation of Cdc20 in MCC is necessary for SAC activation (Ge et al., 2008; Hwang et al., 1998; Sudakin et al., 2001). Hence, it is presumable that Rad52 phosphorylated by Mps1 can assist the function of Mps1 for the MCC formation and Cdc20 degradation in APC/C-dependent manner to activate SAC.

Mps1-dependent phosphorylation is not related to the function of Rad52 for regulation of accurate mitosis

Because evidences about mitosis regulatory functions of Rad52 under normal condition were observed (**Fig. 12A, B and 14**), I hypothesized that Rad52 has dual functions for SAC activation and mitosis regulation. It is confirmed that the Rad52 function for SAC activation is retained to Mps1-dependent phosphorylation. Thus, by the measuring of increase rate of optical density from lag phase to late log phase, I tested whether Rad52 function for mitotic regulation under normal condition is retained to Mps1-dependent phosphorylation or Ipl1-dependent phosphorylation. Interestingly, the expression of *rad52-3A* mutant recovered growth defect of *rad52*Δ cells, whereas the expression of *rad52-5A* mutant could not (**Fig. 21A**). It

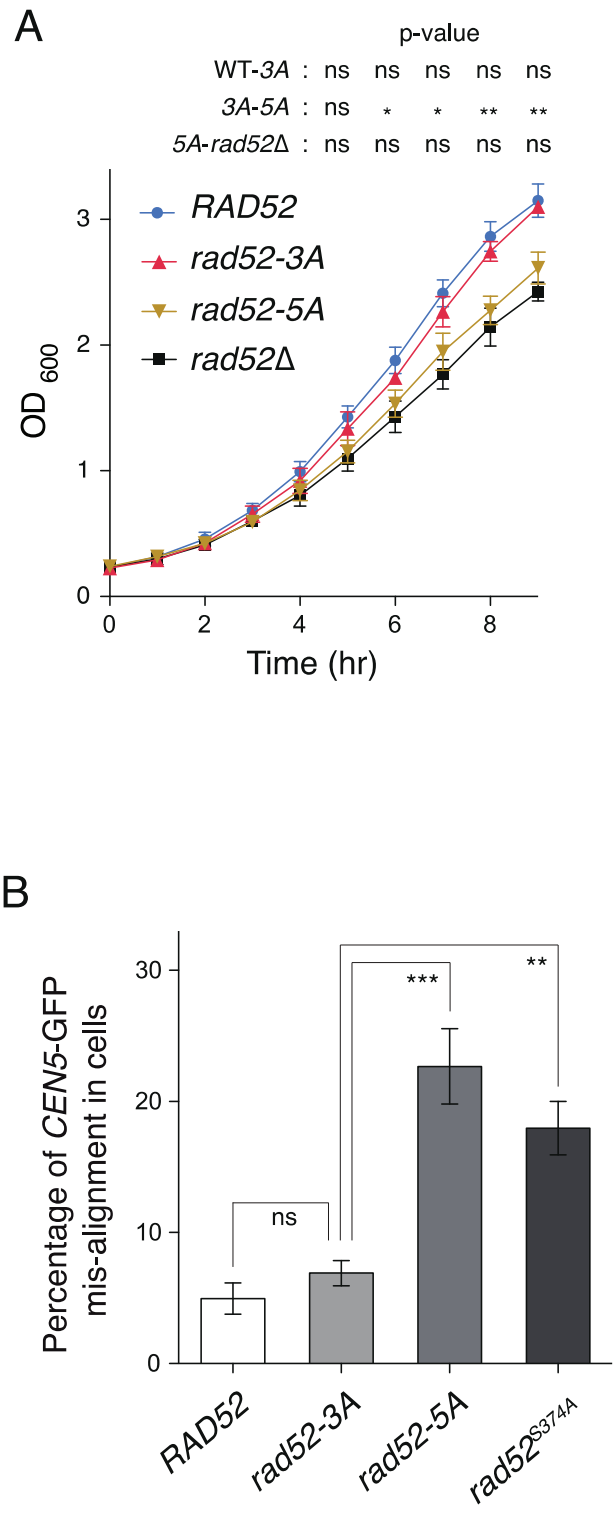
A
p-value
WT-3A : ns ns ns ns ns
3A-5A : ns * * ** **
5A-rad52Δ : ns ns ns ns ns
RAD52
rad52-3A
rad52-5A
rad52Δ
OD 600
Time (hr)
B
Percentage of CEN5-GFP mis-alignment in cells
ns
***
**
RAD52
rad52-3A
rad52-5A
rad52S374A

Fig. 21 Mps1-dependent phosphorylation is not related to the function of Rad52 for regulation of accurate mitosis.

(A) *rad52-3A* cells recovered growth, whereas *rad52-5A* cells could not. Data represent the mean±SD of triplicate cultures. P-values were determined by the Student's t test (*$p < 0.05$ and **$p < 0.01$). (B) Chromosome mis-alignment was significantly increased in *rad52-5A* and *rad52*^{S374A} strain, but not in *rad52-3A* strain. Rad52 mutant strains containing *CEN5-(tetO2)*$_{112}$ and tetR-GFP were synchronized by α-factor treatment for 3hr. Synchronized cells were released to fresh YPD media and fixed with formaldehyde at 75min after release from α-factor. DAPI staining was used for visualization of Nuclear DNA. Data represent the mean±SD of triplicate cultures. P-values were determined by the Student's t test (**$p < 0.01$ and ***$p < 0.005$).

suggests that disruption of Mps1-dependent phosphorylation does not affect to mitosis regulation. To further confirm the effect of Mps1-dependent phosphorylation on mitotic regulation, the fidelity of chromosome alignment during mitosis was checked to compare the difference of chromosome mis-segregation ratio between *rad52-3A* and *rad52-5A* cells. Consistent with optical density data, chromosome alignment was properly regulated in *rad52-3A* cells, whereas the ratio of chromosome mis-alignment was significantly increased in *rad52-5A* cells (**Fig. 21B**). These results indicate that Mps1-dependent phosphorylation is important only for SAC activation, but not for regulation of accurate mitosis.

Ipl1-dependent phosphorylation of Rad52 regulates Mps1 recruitment to the kinetochores

Although Mps1-dependent phosphorylation is not related to regulation of accurate mitosis, *rad52-5A* mutant, which contains both of non-Mps1-dephosphorylable mutation and non-Ipl1-dephosphorylable mutation, showed the phenotypes of improper regulation of mitosis. Thus, I anticipated that Ipl1-dependent phosphorylation of Rad52 is connected to the function for mitosis regulation.

Kinetochore localization of Ipl1 is essential for the function to regulate mitosis and spindle-kinetochore attachment (Shimogawa et al., 2009). Because substrates of Ipl1 in mitotic signaling are regulated by distance-dependent phosphorylation by kinetochore-bound Ipl1, most of substrates are kinetochore protein or move close to kinetochores before anaphase onset (Yamagishi et al., 2014). Consistent with previous report, it was confirmed that Rad52 was co-localized with Ipl1 complex before anaphase onset (**Fig. 22A**). In addition, *rad52-5A* cells could not accurately regulate chromosome alignment during mitosis, whereas *rad52-3A* could. To confirm whether chromosome mis-alignment in *rad52-5A* cells is due to the defect of Ipl1-dependent phosphorylation, the fidelity of chromosome alignment in cells expressing $rad52^{S374A}$ mutant, which is non-Ipl1-phosphorylable Rad52 mutant, was checked. As shown in **Fig. 21B**, the ratio of chromosome mis-alignment was remarkably increased in $rad52^{S374A}$ cells compared

to *RAD52* and *rad52-3A* cells. It demonstrates that Ipl1-dependent phosphorylation of Rad52 has a role for mitosis regulation under normal condition.

Before anaphase onset, kinetochore-bound Ipl1 recruits Mps1 to kinetochores and regulates Mps1 activity for chromosome bi-orientation even though mitosis is not perturbed by spindle damage (Heinrich et al., 2012; Maure et al., 2007; Nijenhuis et al., 2013). Because Ipl1 is bound to kinetochores to monitor the interaction between kinetochore and microtubule, regulator that transfers Ipl1 signal to nucleoplasmic soluble protein Mps1 is needed to regulate the localization of Mps1 (Yamagishi et al., 2014). However, regulator between Ipl1 and Mps1 is not clearly defined. As shown in **Fig. 16 and Fig. 17**, Rad52 was defined as a shared substrate between Ipl1 and Mps1. In addition, the functions of Rad52 were closely related to Mps1 (**Fig. 20**). Thus, I hypothesized that Rad52 acts as an Ipl1-dependent Mps1 regulator. To confirm this hypothesis, I tested whether non-phosphorylatable mutants of Rad52 affect the accumulation of Mps1 on the kinetochores. Although Mps1 is localized to kinetochores during unperturbed mitosis, intensity of Mps1-GFP signals is too weak to detect without induction of Mps1 accumulation (**Fig. 22B**). Thus, nocodazole was treated to induce Mps1 accumulation on the kinetochores. Interestingly, although *rad52-3A* cells cannot activate SAC (**Fig. 20A**), Mps1 was efficiently accumulated on the kinetochores similarly to in *RAD52* cells (**Fig. 22C**). It suggests that Mps1 accumulation to kinetochores and SAC activation are separately regulated. In contrast, Mps1 accumulation ratios of *rad52-5A* and *rad52*^{S374A} cells were decreased to approximate 50% of *RAD52* cells (**Fig. 22C**). Moreover, fluorescence intensity of Mps1-GFP spots on the kinetochores was also significantly decreased in *rad52-5A* and *rad52*^{S374A} cells compared to *RAD52* and *rad52-3A* cells (**Fig. 22D**). These data indicate that Rad52 regulates Mps1 accumulation on the kinetochores independently of its function for SAC activation, and Ipl1-dependent phosphorylation of Rad52 is required to regulate Mps1 localization.

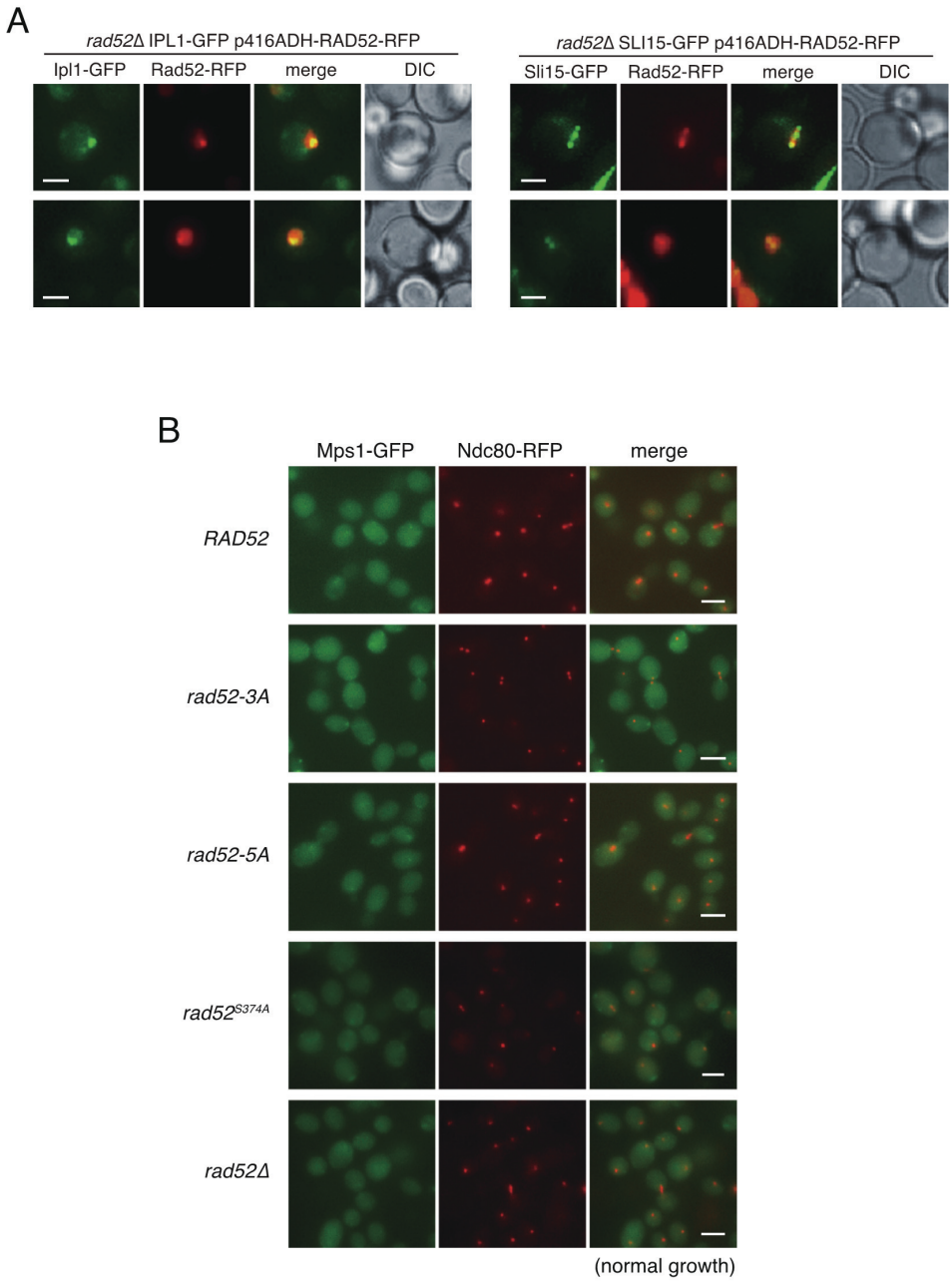
A
rad52Δ IPL1-GFP p416ADH-RAD52-RFP
Ipl1-GFP
Rad52-RFP
merge
DIC
rad52Δ SLI15-GFP p416ADH-RAD52-RFP
Sli15-GFP
Rad52-RFP
merge
DIC
B
Mps1-GFP
Ndc80-RFP
merge
RAD52
rad52-3A
rad52-5A
rad52S374A
rad52Δ
(normal growth)

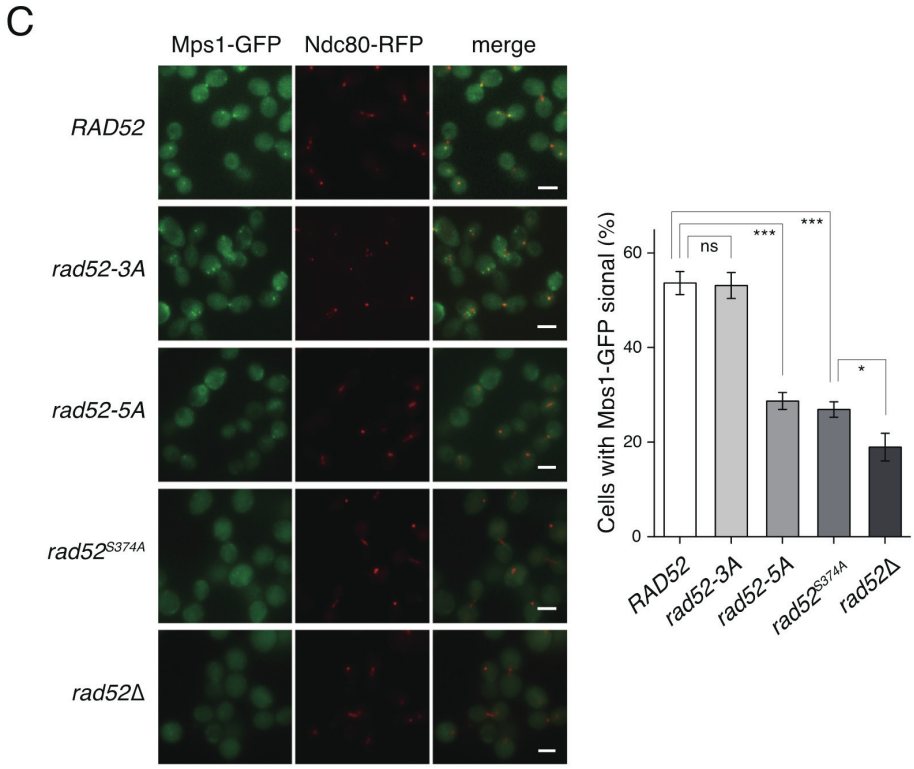
C
Mps1-GFP
Ndc80-RFP
merge
RAD52
rad52-3A
rad52-5A
rad52S374A
rad52Δ
Cells with Mps1-GFP signal (%)
ns
***
***
*
0
20
40
60
RAD52
rad52-3A
rad52-5A
rad52S374A
rad52Δ

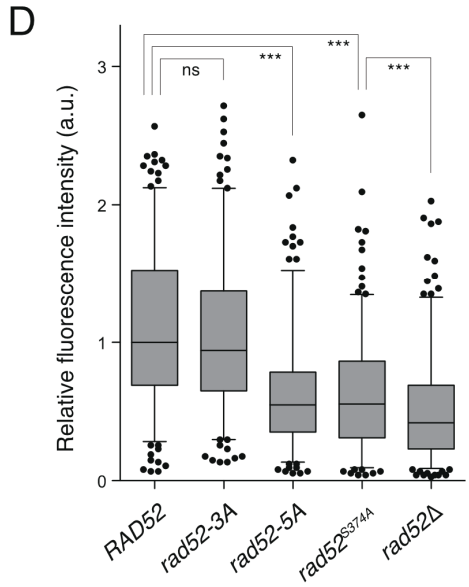
D
Relative fluorescence intensity (a.u.)
ns
***
***
***
0
1
2
3
RAD52
rad52-3A
rad52-5A
rad52S374A
rad52Δ

Fig. 22 Ipl1-dependent phosphorylation of Rad52 regulates Mps1 recruitment to the kinetochores.

(A) Rad52 was co-localized with Ipl1 complex. GFP-tagged Ipl1 and Sli15 were endogenously expressed in *rad52*Δ cells, and RFP-tagged Rad52 was expressed from pRS416ADH plasmid. Fluorescence images were taken during asynchronous log phase in SC-Ura media. Scale bars are 2 μm. (B) Mps1-GFP was rarely accumulated on the kinetochore under normal condition. Indicated strains were sampled during mid-log phase and fixed with paraformaldehyde, and GFP and RFP images were acquired. Scale bars are 4 μm. (C) Kinetochore accumulation of Mps1 was decreased in *rad52-5A* and $rad52^{S374A}$ cells. Indicated strains were fixed with paraformaldehyde. Scale bars are 4 μm. Data represent the mean±SD of triplicate cultures (right panel). P-values were determined by the Student's *t* test (*$p < 0.05$ and ***$p < 0.005$). (D) Fluorescence intensity of Mps1-GFP at the kinetochore was decreased in *rad52-5A* and $rad52^{S374A}$ cells. The relative fluorescence intensity was calculated by subtracting background intensity from Mps1-GFP signal intensity. Box plot was represented with whiskers from 5th to 95th percentile, and data was normalized to the median of *RAD52* cells (N > 200). P-values were determined by the Mann-Whitney *U* test (***$p < 0.005$).

Ipl1-dependent Phospho-mimicking mutant of Rad52 accumulates Mps1 under normal condition

I found the evidences that Ipl1-dependent phosphorylation of Rad52 is crucial for Mps1 localization and proper mitosis. Thus, the direct effect of Ipl1-dependent phosphorylation of Rad52 to the regulation of mitosis was examined. Because Ipl1 is bound to kinetochore at metaphase and phosphorylates substrates in a distance-dependent manner, the function of Ipl1-dependent phosphorylation for mitotic regulation is active at the kinetochore (Foley and Kapoor, 2012). To imitate Ipl1-dependent phosphorylation of Rad52 at kinetochores before anaphase onset, Ipl1-dependent phospho-mimicking mutant of Rad52 ($Rad52^{S374E}$) was tethered to kinetochore protein Ndc80. Using Ndc80 and Rad52 fusion proteins (Ndc80-$Rad52^{WT}$ and Ndc80-$Rad52^{S374E}$), I checked whether Rad52 phosphorylation by Ipl1 induces Mps1 accumulation to kinetochores and without induction of spindle damage. To check the expression and localization of Ndc80-Rad52 fusion proteins, RFP was inserted between Ndc80 and Rad52. Ndc80-Rad52 fusion proteins were well expressed under GAL promoter in galactose containing media and properly localized to kinetochores by Ndc80. When wild-type Rad52 was conjugated to the kinetochores, Mps1-GFP signal was not detected on the kinetochores. In contrast, conjugation of $Rad52^{S374E}$ to kinetochores efficiently stimulates accumulation of Mps1-GFP signal to the kinetochore without spindle damage agent treatment (**Fig. 23 ; upper panel**). Compared to the Mps1 accumulation ratio of Ndc80-$Rad52^{WT}$, Mps1 accumulation was significantly increased by expression of Ndc80-$Rad52^{S374E}$ (**Fig. 23**). These results strongly indicate that Ipl1-dependent phosphorylation of Rad52 at kinetochores is a signal for Mps1 accumulation.

Ipl1-dependent Phospho-mimicking mutant of Rad52 activates SAC under normal condition

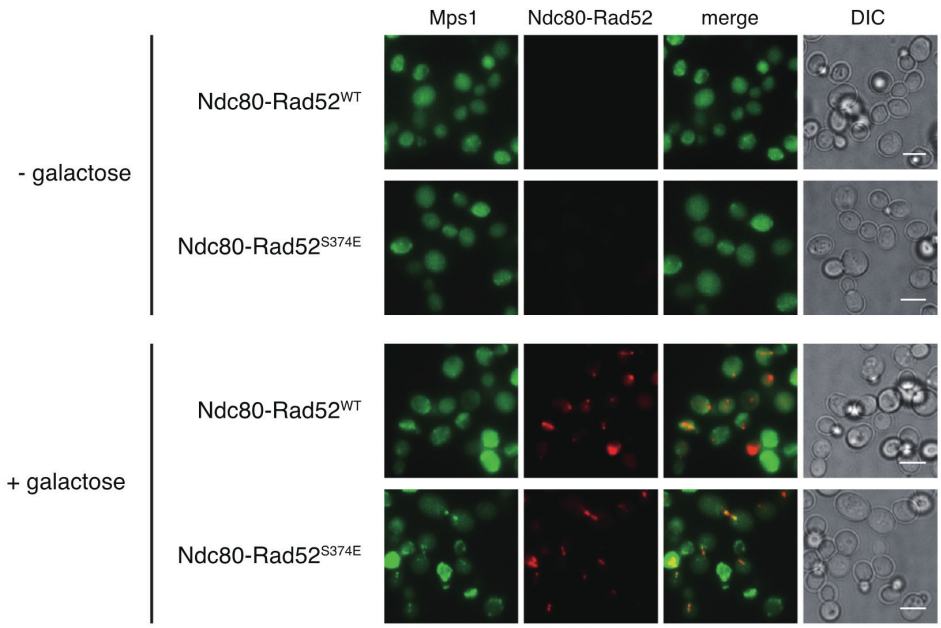
Mps1
Ndc80-Rad52
merge
DIC
- galactose
Ndc80-Rad52WT
Ndc80-Rad52S374E
+ galactose
Ndc80-Rad52WT
Ndc80-Rad52S374E

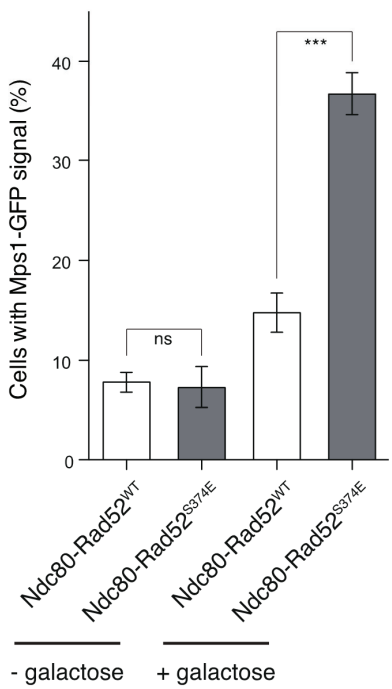
Cells with Mps1-GFP signal (%)
0
10
20
30
40
ns
***
Ndc80-Rad52WT
Ndc80-Rad52S374E
Ndc80-Rad52WT
Ndc80-Rad52S374E
- galactose
+ galactose

Fig. 23 Ipl1-dependent Phospho-mimicking mutant of Rad52 accumulates Mps1 under normal condition.

Tethering Ipl1-dependent phospho-mimicking mutant of Rad52 to kinetochores stimulates kinetochore accumulation of Mps1. Strains were grown in 2% raffinose containing YP media and 2% galactose was treated to the cell cultures for 3 hr at log phase. Indicated strains were fixed with paraformaldehyde. Scale bars are 4 μm. Data represent the mean±SD of triplicate cultures (lower panel). P-values were determined by the Student's *t* test (***$p < 0.005$).

Because expression of kinetochore conjugated Rad52^{S374E} stimulates accumulation of Mps1 without induction of spindle damage, I tested whether expression of Ndc80-Rad52^{S374E} activates SAC that causes mitotic arrest. To observe the effect of Ndc80-Rad52^{WT} and Ndc80-Rad52^{S374E} to the cell cycle progression, the budding index of cells expressing Ndc80-Rad52 fusion proteins was checked. Cells expressing Ndc80-Rad52^{WT} or Ndc80-Rad52^{S374E} were synchronized to G1 phase by using α-factor treated galactose-containing media. G1 arrested cells by α-factor treatment was released to galactose-containing media and cell cycle was classified to three phases, Unbudded, Budded, and Separated, according to the cell morphology detected by microscopy (Araki et al., 2010; Buvelot et al., 2003). The kinetics of Unbudded to Budded, which indicates the cell cycle progression from G1 to G2, was identical between cells expressing Ndc80-Rad52^{WT} and Ndc80-Rad52^{S374E} (**Fig. 24A, B; blue line, E**). However, the kinetics of Budded to Separated, which indicates the cell cycle progression from G2 to next G1, was delayed in cells expressing Ndc80-Rad52^{S374E} compared to cells expressing Ndc80-Rad52^{WT} (**Fig. 24A, B; yellow line, F**).

To address whether delayed kinetics of Budded to Separated is caused by cell cycle delay in mitosis, I confirmed Pds1 generation and degradation kinetics of cells expressing Ndc80-Rad52^{S374E}. Whereas Pds1 levels were similarly increased in cells expressing Ndc80-Rad52^{WT} and Ndc80-Rad52^{S374E} after release from α-factor arrest, Pds1 degradation was delayed in cells expressing Ndc80-Rad52^{S374E} compared to cells expressing Ndc80-Rad52^{WT} (**Fig. 24G**), suggesting that Ndc80-Rad52^{S374E} causes mitotic delay before anaphase onset. To confirm whether SAC activation is the reason of mitotic delay of cells expressing Ndc80-Rad52^{S374E}, SAC activator *MAD1* gene was deleted from cells expressing Ndc80-Rad52^{S374E}. Deletion of *MAD1* recovered delayed kinetics of Budded to Separated, which was shown in cells expressing Ndc80-Rad52^{S374E}, at a similar level to that of cells expressing Ndc80-Rad52^{WT} (**Fig. 24C, F**). Furthermore, Pds1 degradation kinetics of cells expressing Ndc80-Rad52^{S374E} was also

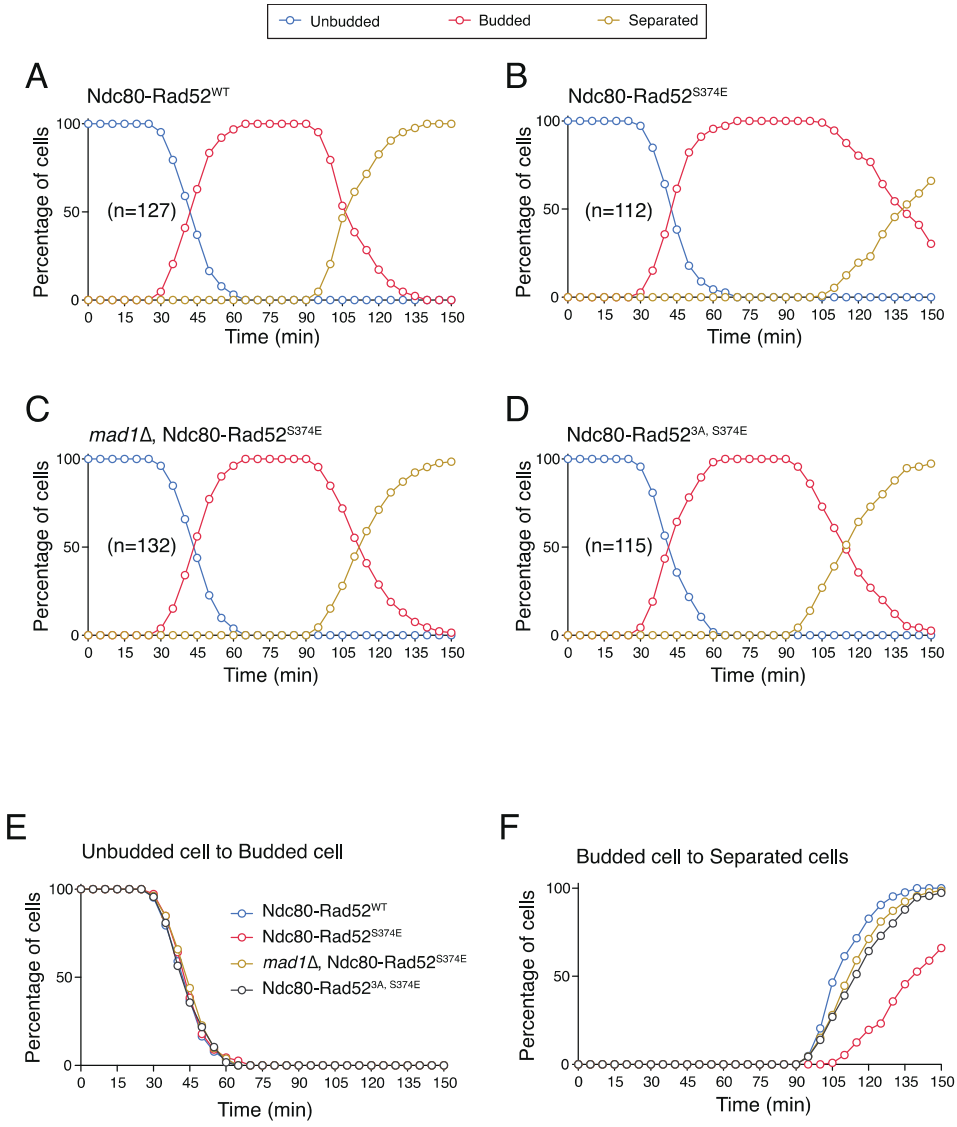
Unbudded
Budded
Separated
A
Ndc80-Rad52WT
(n=127)
B
Ndc80-Rad52S374E
(n=112)
C
mad1Δ, Ndc80-Rad52S374E
(n=132)
D
Ndc80-Rad52 3A, S374E
(n=115)
Percentage of cells
Time (min)
E
Unbudded cell to Budded cell
Ndc80-Rad52WT
Ndc80-Rad52S374E
mad1Δ, Ndc80-Rad52S374E
Ndc80-Rad52 3A, S374E
F
Budded cell to Separated cells

G

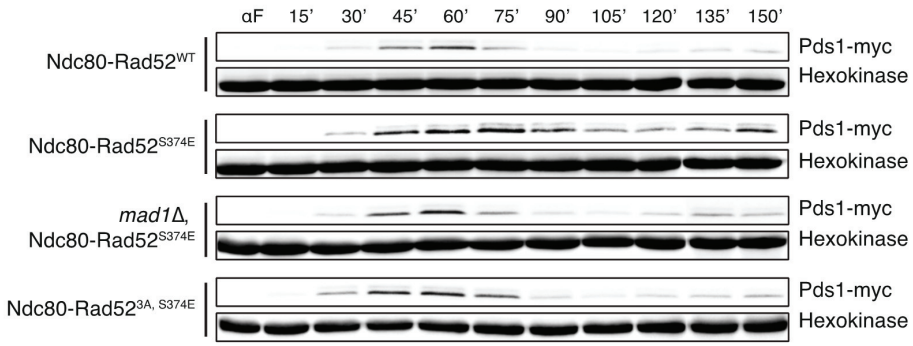
αF
15'
30'
45'
60'
75'
90'
105'
120'
135'
150'
Ndc80-Rad52WT
Ndc80-Rad52S374E
mad1Δ, Ndc80-Rad52S374E
Ndc80-Rad523A, S374E
Pds1-myc
Hexokinase

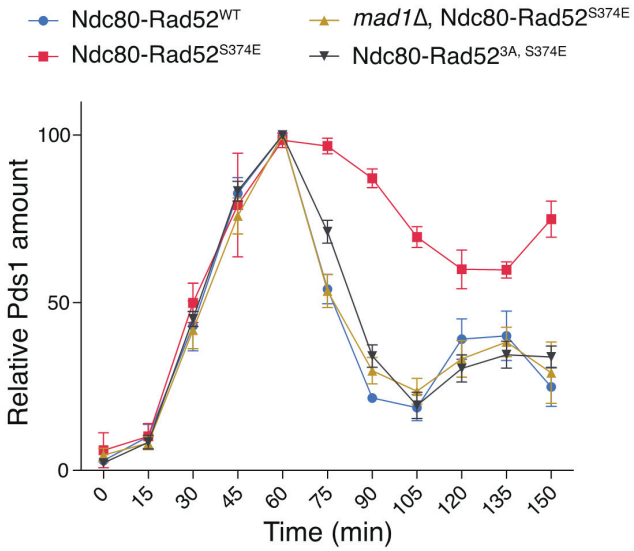
Ndc80-Rad52WT
Ndc80-Rad52S374E
mad1Δ, Ndc80-Rad52S374E
Ndc80-Rad523A, S374E
Relative Pds1 amount
100
50
0
0
15
30
45
60
75
90
105
120
135
150
Time (min)

Fig. 24 Ipl1-dependent phospho-mimicking mutant of Rad52 activates SAC under normal condition.

(A-G) Ndc80-Rad52^{S374E} cells showed mitotic delay, which is dependent on Mad1 and Mps1-dependent phosphorylation of Rad52. Ndc80-Rad52^{WT}, Ndc80-Rad52^{S374E}, *mad1*Δ Ndc80-Rad52^{S374E} and Ndc80-Rad52$^{3A, S374E}$ cells were grown in 2% raffinose containing YP media, treated with α-factor and 2% galactose for 3 hr at log phase and released to fresh 2% galactose containing YP media. (A-eD) Cell morphology images were taken every 5 min by microscopy. Indicated numbers mean counted cell numbers for each strain. (E,F) Kinetics of Unbudded to Budded and kinetics of Budded to Separated are compared in four strains. (G) Samples were taken every 15 min after release from α-factor arrest. Immunoblot assay was conducted with an anti-myc antibody. Highest value in each trial was used as 100% standard to normalize the relative amount of Pds1 (lower panel). Data represent the mean±SD of triplicate cultures.

recovered by deletion of *MAD1* (**Fig. 24G**). These results indicate that SAC is activated by Ipl1-dependent phosphorylation of Rad52 at kinetochores.

Mps1 also phosphorylates Rad52 and this phosphorylation is essential to activate SAC (**Fig. 17 and Fig. 19**). Interestingly, it was also clearly defined that Rad52 is an Ipl1-dependent Mps1 regulator of Mps1 re-localization at kinetochores (**Fig. 22C, D and Fig. 23**). According to the previous report, Ipl1 acts as an upstream regulator of Mps1 to repair incorrect interaction between kinetochore and microtubule that results improper chromosome inheritance (Heinrich et al., 2012; Yamagishi et al., 2014) and some substrates, which are related to the regulation of mitosis, are regulated by both of Ipl1 and Mps1 (Akiyoshi et al., 2009; Kemmler et al., 2009). Thus, I hypothesized that Ipl1-dependent phosphorylation of Rad52 is upstream signal of Mps1-dependent phosphorylation of Rad52 in same pathway for mitotic regulation. To test this, I checked whether SAC activation by Ipl1-dependent phosphorylation is blocked by non-phosphorylable mutation on Mps1 target sites of Rad52. Expression of Ndc80-Rad52$^{3A,\ S374E}$, which includes three non-Mps1-phosphorylable mutation with Ipl1-phospho-mimicking mutation, did not result delay on kinetics of Budded to Separated. Furthermore, delay of Pds1 degradation, which was shown in cells expressing Ndc80-Rad52^{S374E}, was not detected in cells expressing Ndc80-Rad52$^{3A,\ S374E}$ (**Fig. 24D, F, G**). It suggests that Rad52 is the crucial factor for both of Ipl1 signal transduction to Mps1 and Mps1 signal transduction to downstream of SAC in mitotic regulation.

Taken together, these results indicate that Ipl1 phosphorylates Rad52 at kinetochore to regulate Mps1 localization and proper mitosis.

Ipl1-dependent phospho-mimicking mutants of Ndc80 and Rad52 show synergetic effect on SAC activation.

Previous researches had reported that Ipl1 phosphorylates seven Ipl1 consensus residues of Ndc80 (Akiyoshi et al., 2009; Kalantzaki et al., 2015). According to the findings by Akiyoshi

et al. (2009), although Ipl1-dependent phosphorylation on Ndc80 is important for proper microtubule dynamics, non-Ipl1-phosphorylable mutant of Ndc80 ($Ndc80^{7A}$) cannot block the SAC activation under spindle damage condition. From these results, they insisted that Ipl1 has another target site on Ndc80 or other target proteins for SAC activation. Consistent with this, it was previously reported that Ipl1-phospho-mimicking mutant of Ndc80 ($Ndc80^{7D}$) did not represent dominant delay on sister chromatid separation (Kalantzaki et al., 2015), suggesting that only Ndc80 is not enough to regulate proper mitosis, although the function of Ipl1 is closely related to the seven-Ipl1-dependent phosphorylation sites of Ndc80 (Akiyoshi et al., 2009). Thus, I hypothesized that Ipl1 regulates mitosis by phosphorylation of multiple targets including Ndc80 and Rad52. To test this, Ipl1-dependent phosphorylation of multiple targets at kinetochores was imitated by tethering $Ndc80^{7D}$ and $Rad52^{S374E}$ ($Ndc80^{7D}$-$Rad52^{S374E}$). Similar to the findings by Kalantzaki et al. (2015), which report that $Ndc80^{7D}$ shows a slight delay on sister chromatid separation by weaken the end-on conversion between microtubule and kinetochore, the kinetics of Budded to Separated was delayed in cells expressing $Ndc80^{7D}$-$Rad52^{WT}$ (**Fig. 25A, B; yellow line**). To confirm whether expression of $Ndc80^{7D}$-$Rad52^{WT}$ results SAC activation similarly to $Ndc80^{WT}$-$Rad52^{S374E}$, Pds1 degradation kinetics was checked using cells expression $Ndc80^{7D}$-$Rad52^{WT}$. As shown in **Fig. 25H**, Pds1 degradation kinetics was also delayed in cells expressing $Ndc80^{7D}$-$Rad52^{WT}$ compared to cells expressing $Ndc80^{WT}$-$Rad52^{WT}$ (**Fig. 25G**), suggesting that $Ndc80^{7D}$-$Rad52^{WT}$ causes mitotic delay before anaphase onset similarly to $Ndc80^{WT}$-$Rad52^{S374E}$ (**Fig. 25B, C; yellow line, F, G**). Next, I checked physiological effect of Ipl1-dependent phosphorylation on multiple target proteins by using $Ndc80^{7D}$-$Rad52^{S374E}$. Interestingly, the kinetics of Budded to Separated was predominantly delayed by expression of $Ndc80^{7D}$-$Rad52^{S374E}$ (**Fig. 25D; yellow line, F**). In addition, Pds1 in cells expressing $Ndc80^{7D}$-$Rad52^{S374E}$ was highly preserved until 150min after release from α-factor arrest (**Fig. 25G**). This synergetic effect of $Ndc80^{7D}$ and $Rad52^{S374E}$ on mitosis progression was dramatically recovered to the level of $Ndc80^{WT}$-$Rad52^{WT}$ by deletion of SAC

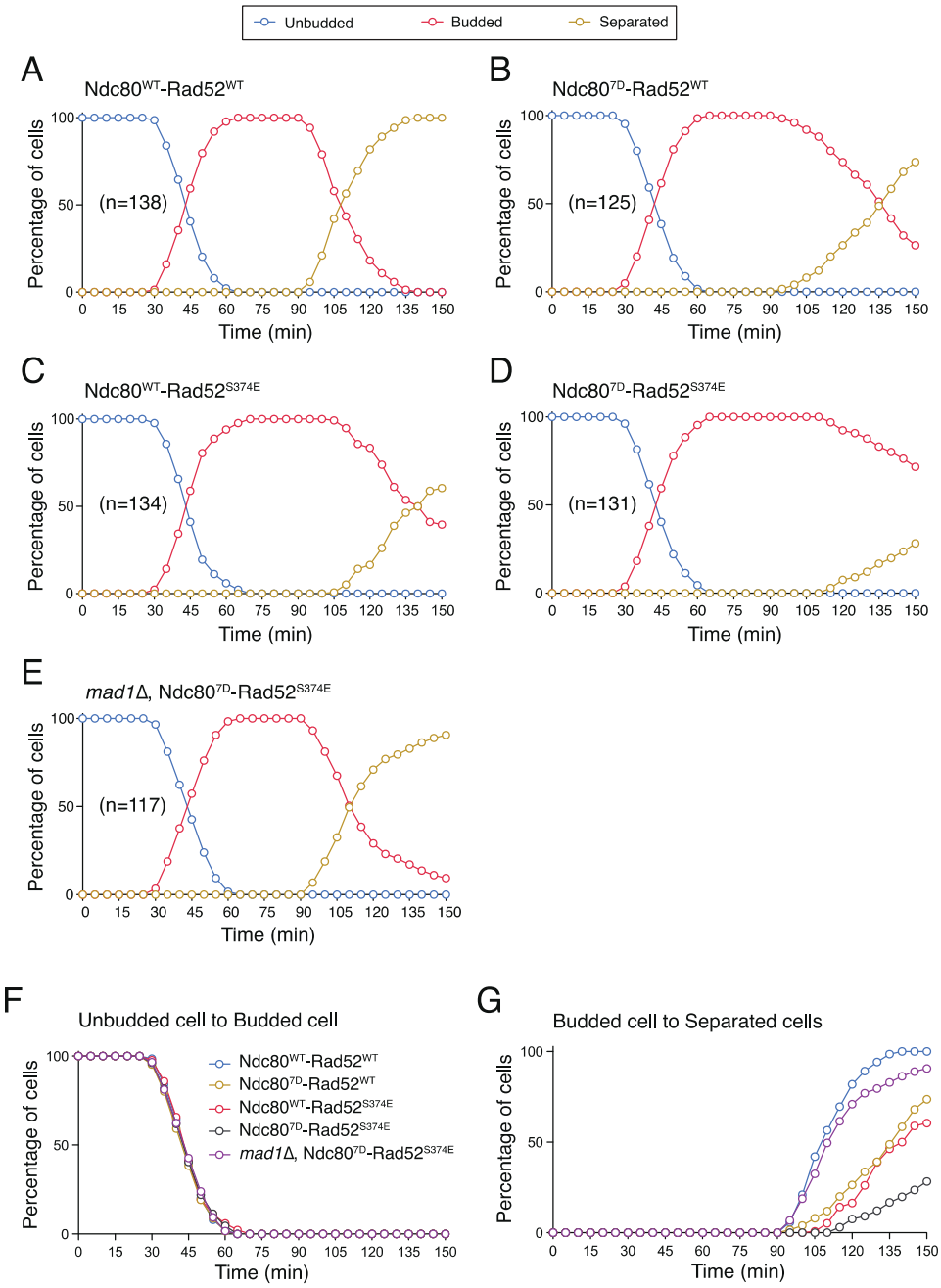
Unbudded
Budded
Separated
A
Ndc80WT-Rad52WT
(n=138)
B
Ndc807D-Rad52WT
(n=125)
C
Ndc80WT-Rad52S374E
(n=134)
D
Ndc807D-Rad52S374E
(n=131)
E
mad1Δ, Ndc807D-Rad52S374E
(n=117)
Percentage of cells
Time (min)
F
Unbudded cell to Budded cell
Ndc80WT-Rad52WT
Ndc807D-Rad52WT
Ndc80WT-Rad52S374E
Ndc807D-Rad52S374E
mad1Δ, Ndc807D-Rad52S374E
G
Budded cell to Separated cells

H

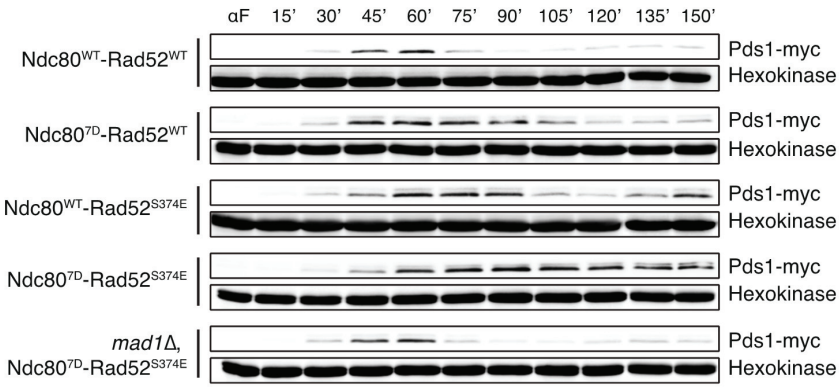
αF 15' 30' 45' 60' 75' 90' 105' 120' 135' 150'
Ndc80WT-Rad52WT
Ndc807D-Rad52WT
Ndc80WT-Rad52S374E
Ndc807D-Rad52S374E
mad1Δ, Ndc807D-Rad52S374E
Pds1-myc
Hexokinase

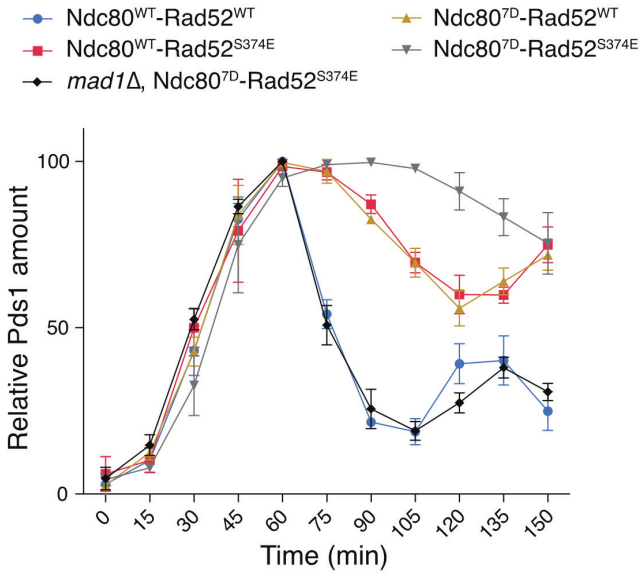
Ndc80WT-Rad52WT
Ndc80WT-Rad52S374E
mad1Δ, Ndc807D-Rad52S374E
Ndc807D-Rad52WT
Ndc807D-Rad52S374E
Relative Pds1 amount
100
50
0
0 15 30 45 60 75 90 105 120 135 150
Time (min)

Fig. 25 Ipl1-dependent phospho-mimicking mutants of Ndc80 and Rad52 show synergetic effect on SAC activation.

(A-H) Mitosis of Ndc80^{7D}-Rad52^{S374E} cells was severely delayed by SAC activation. Ndc80^{WT}-Rad52^{WT}, Ndc80^{7D}-Rad52^{WT}, Ndc80^{WT}-Rad52^{S374E}, Ndc80^{7D}-Rad52^{S374E} and *mad1*Δ Ndc80^{7D}-Rad52^{S374E} cells were grown in 2% raffinose containing YP media, treated with α-factor and 2% galactose for 3 hr at log phase and released to fresh 2% galactose containing YP media. (A-E) Cell morphology images were taken every 5 min by microscopy. Indicated numbers mean counted cell numbers for each strain. (F,G) Kinetics of Unbudded to Budded and kinetics of Budded to Separated are compared in five strains. (H) Samples were taken every 15 min after release from α-factor arrest. Immunoblot assay was conducted with an anti-myc antibody. Highest value in each trial was used as 100% standard to normalize the relative amount of Pds1 (lower panel). Data represent the mean±SD of triplicate cultures.

activator gene *MAD1* (**Fig. 25E, F, G**), suggesting that both of Ndc80^{7D} and Rad52^{S374E} affect to the mitotic progression via SAC pathway. Thus Ipl1-dependent phosphorylation of multiple target proteins induces higher stimulation of SAC activation.

Ipl1-dependent phospho-mimicking mutants of Ndc80 and Rad52 affect to SAC activation via kinase activity of Mps1

To further confirm whether the phospho-mimicking mutations on Ndc80 and Rad52 are the direct upstream signal of Mps1, Mps1 activity was suppressed by treatment of reversine, which is an inhibitor for human Mps1 (Santaguida et al., 2010). Before using reversine for physiological research of yeast cells, I confirmed whether reversine is compatible to yeast system. Mps1-dependent phosphorylation of Rad52 was remarkably decreased by reversine treatment in *in vitro* kinase assay (**Fig. 26A**). It clearly suggests that reversine efficiently suppressed kinase activity of yeast Mps1. Thus, the effect of Mps1 suppression was examined in cells expressing Ndc80^{7D}-Rad52^{S374E} by reversine treatment. As shown in Supplementary **Fig. 26B, C, and D**, although defect of cell cycle progression was not perfectly recovered by reversine treatment, reversine reduced Budded to Separated kinetics delay of cells expressing Ndc80^{7D}-Rad52^{S374E} in a dose-dependent manner. To check the reversine effect on SAC activation, Pds1 degradation assay was performed using 10 μM revesine. Suppression of Pds1 degradation in cells expressing Ndc80^{7D}-Rad52^{S374E} was also attenuated by reversine treatment (**Fig. 26E**), suggesting that mitotic arrest by Ndc80^{7D}-Rad52^{S374E} expression is achieved through Mps1 activation, which is the upstream signal of SAC activation. In addition, it was also confirmed that human Mps1 inhibitor reversine can be used for inhibition of yeast Mps1 activity. It can be an adaptable way for the research of mitotic regulation to suppress Mps1 activity in *Saccharomyces cerevisiae*.

From these data, I defined that Rad52 is a novel downstream substrate of Ipl1 and Ipl1 phosphorylates Rad52 to control a major mitotic kinase Mps1 for accurate regulation of mitosis.

Furthermore, Rad52 is also phosphorylated by Mps1 to help mitotic activity of Mps1 during mitosis. Thus, Rad52 is a newly identified key component in mitosis and SAC pathway.

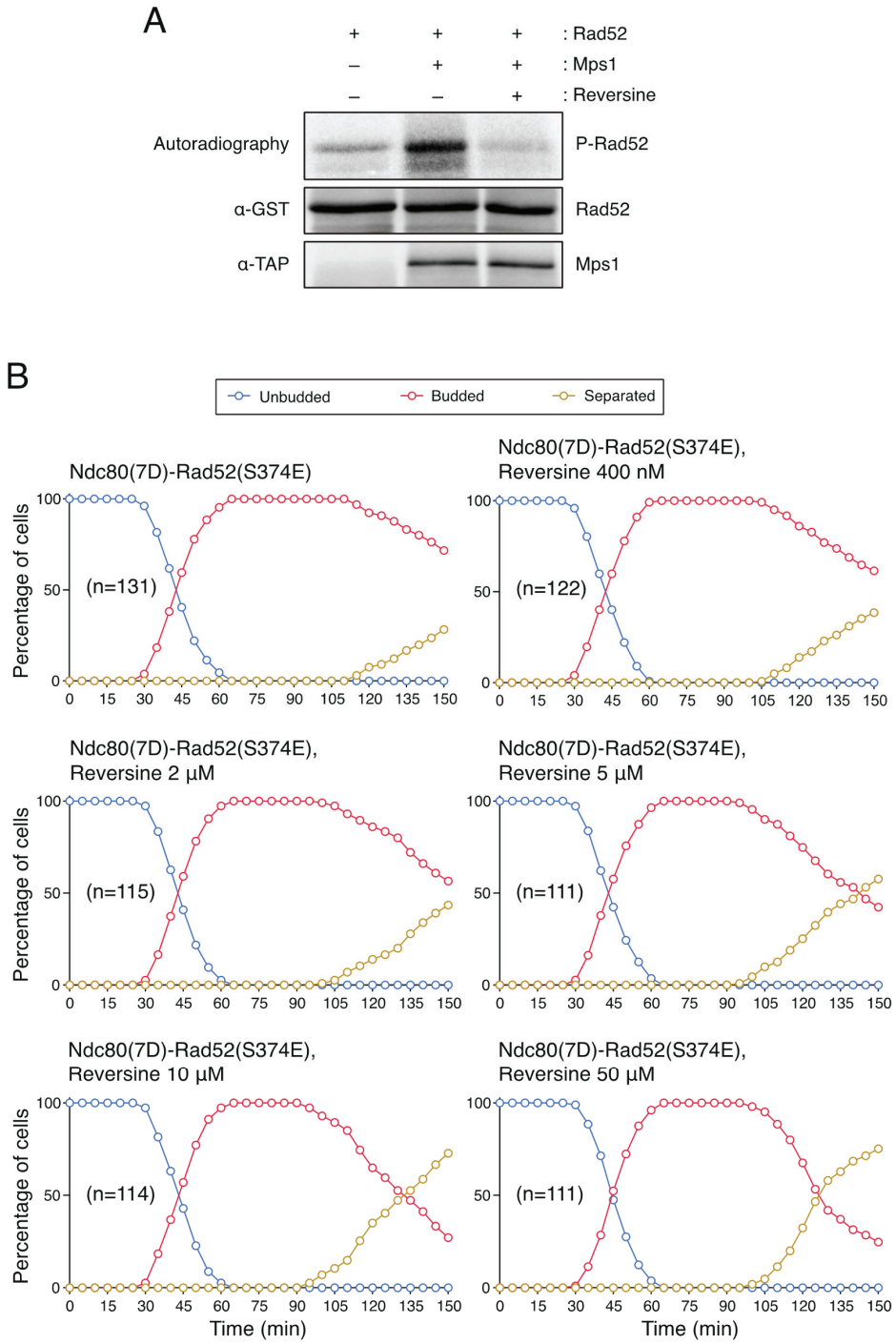
A
+ + + : Rad52
– + + : Mps1
– – + : Reversine
Autoradiography
P-Rad52
α-GST
Rad52
α-TAP
Mps1
B
Unbudded
Budded
Separated
Ndc80(7D)-Rad52(S374E)
Ndc80(7D)-Rad52(S374E), Reversine 400 nM
Ndc80(7D)-Rad52(S374E), Reversine 2 μM
Ndc80(7D)-Rad52(S374E), Reversine 5 μM
Ndc80(7D)-Rad52(S374E), Reversine 10 μM
Ndc80(7D)-Rad52(S374E), Reversine 50 μM
Percentage of cells
(n=131)
(n=122)
(n=115)
(n=111)
(n=114)
(n=111)
0 15 30 45 60 75 90 105 120 135 150
Time (min)

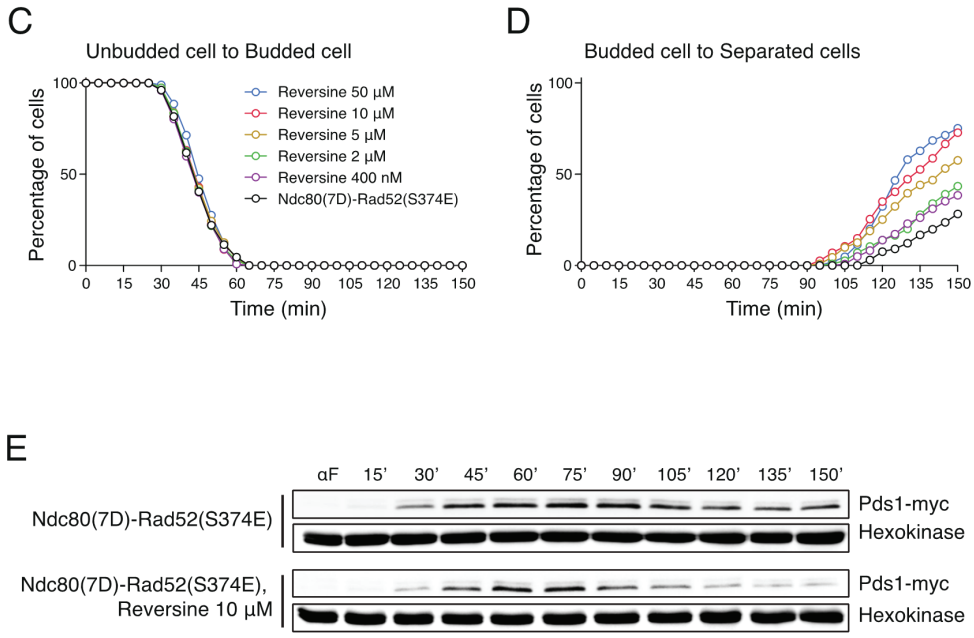
C
Unbudded cell to Budded cell
Percentage of cells
100
50
0
0 15 30 45 60 75 90 105 120 135 150
Time (min)
Reversine 50 µM
Reversine 10 µM
Reversine 5 µM
Reversine 2 µM
Reversine 400 nM
Ndc80(7D)-Rad52(S374E)
D
Budded cell to Separated cells
Percentage of cells
100
50
0
0 15 30 45 60 75 90 105 120 135 150
Time (min)
E
αF 15’ 30’ 45’ 60’ 75’ 90’ 105’ 120’ 135’ 150’
Ndc80(7D)-Rad52(S374E)
Pds1-myc
Hexokinase
Ndc80(7D)-Rad52(S374E),
Reversine 10 µM
Pds1-myc
Hexokinase

Fig. 26 Mitotic delay by Ndc80^{7D}-Rad52^{S374E} expression is recovered by Mps1 inhibition by reversine treatment.

(A) Kinase activity of yeast Mps1 was suppressed by reversine. *In vitro* kinase assay was performed with purified Rad52 from *E. coli* and immunoprecipitated Mps1 from *S. cerevisiae*. Immunoblot assay was conducted with an anti-GST antibody for the C-terminus-truncated Rad52 and an anti-mouse IgG for Mps1. 10 μM reversine in DMSO or same volume of DMSO was treated to mixtures for kinase reaction. (B-D) Reversine recovered mitotic delay of Ndc80^{7D}-Rad52^{S374E} cells in a dose-dependent manner. Ndc80^{7D}-Rad52^{S374E} cells were grown in 2% raffinose containing YP media, treated with α-factor and 2% galactose for 3 hr at log phase and released to fresh 2% galactose containing YP media including indicated concentration of reversine. (B) Cell morphology images were taken every 5 min by microscopy. Indicated numbers mean counted cell numbers for each reversine-treated condition. (C, D) Kinetics of Unbudded to Budded and kinetics of Budded to Separated are compared in six reversine-treated conditions. (E) Defect of Pds1 degradation by Ndc80^{7D}-Rad52^{S374E} expression was recovered by 10 μM reversine treatment. Ndc80^{7D}-Rad52^{S374E} cells were grown in 2% raffinose containing YP media, treated with α-factor and 2% galactose for 3 hr at log phase and released to fresh 2% galactose containing YP media with or without 10 μM reversine. Samples were taken every 15min after release from α-factor arrest. Immunoblot assay was conducted with an anti-myc antibody.

3. Discussion

Regulation mechanism of chromosome segregation and SAC activation has been investigating in many organisms. However, how kinase activity of inner kinetochore associated Ipl1 controls the localization of Mps1, which is distant from kinetochores, is poorly understood. In present study, I demonstrate that Ipl1 phosphorylates Rad52 to regulate the kinetochore-localization of Mps1. Furthermore, I also defined that Mps1-dependent phosphorylation of Rad52 is necessary to activate SAC, when spindle-kinetochore interactions are damaged.

Interestingly, Mps1 target residues of Rad52 are on the Ipl1 consensus sequences (**Fig. 17A, C**). This residue-sharing phenomenon of Ipl1 and Mps1 was already reported. Ndc80 has Ipl1 target residues on N-terminus (Akiyoshi et al., 2009). In other research, however, some of Ipl1 target residues on N-terminus of Ndc80 were defined as Mps1 target residue (Kemmler et al., 2009). It can be interpreted that Ipl1 and Mps1 have crosstalk via shared substrates or these two kinases evolutionally share the target residues, because substrates have physiologically related functions. Furthermore, these common features of Ndc80 and Rad52 may suggest that Rad52 is working with Ipl1 and Mps1 as same way as Ndc80 in regulation of mitosis. Consistent with this, it was confirmed that kinetochore-localized Ipl1-dependent phospho-mimicking mutant of Rad52 shows similar mitotic delay with Ipl1-dependent phospho-mimicking mutant of Ndc80 (**Fig. 25B, C, H**) and combination of Ipl1-dependent phospho-mimicking mutations of Rad52 and Ndc80 synergistically stimulates SAC activation (**Fig. 17D, G, H**). Thus, these results mean that Rad52 acts as an upstream regulator in mitotic pathway including Ndc80.

Although I have shown that the phosphorylation of Rad52 by Mps1 is a key signal to activate SAC, the precise mechanism is still unclear. However, I can make a prediction from my data and previous reports. The SAC-related function of Rad52, which is regulated by Mps1-dependent phosphorylation, seems to be not based on signal transduction to the downstream of

SAC pathway, because other SAC-related proteins such as Spc105 and Bub1 are also direct substrates of Mps1 (London and Biggins, 2014; London et al., 2012; Shepperd et al., 2012). Additionally, despite that the kinetochore-tethered Mps1 activates SAC under normal condition (Ito et al., 2012; Jelluma et al., 2010), Mps1 accumulated to the kinetochores in *rad52-3A* cells cannot activate SAC even in nocodazole-treated media (Fig. 3.5A and Fig. 3.8C, D). This result suggests that Rad52 phosphorylated by Mps1 is essential for SAC activation, even though Mps1 is already localized to the kinetochores. Thus, it is possible that Mps1-dependent phosphorylation of Rad52 assists accessibility of Mps1 to other substrates for SAC activation. In addition, I also discovered that Mps1-dependent phospho-mimicking Rad52 ($Rad52^{S86E,T96E,S136E}$) and phosphorylated wild-type Rad52 were degraded in the proteasome-dependent manner (**Fig. 20A**). It is presumable that Rad52 phosphorylated by Mps1 may be related to the ubiquitin/proteasome-dependent protein degradation. Consistent with this, E3 ubiquitin ligase APC/C-mediated degradation of Cdc20 in MCC is necessary for SAC activation (Ge et al., 2008; Hwang et al., 1998; Sudakin et al., 2001). Hence, I inferred that phosphorylated Rad52 by Mps1 assists the function of Mps1 for the MCC formation and Cdc20 degradation in APC/C-dependent manner to activate SAC.

Despite that the kinetochore accumulation of Mps1 is stimulated by Ipl1-dependent phosphorylation of Rad52, I observed that Mps1 is still partially accumulated to the kinetochores in *rad52-5A* and even *rad52*Δ cells (**Fig. 22C**). This observation indicates that, although the regulation of Mps1 is largely dependent on Rad52, Rad52 is not the only factor for kinetochore-binding process of Mps1. Given that an outer kinetochore subunit Ndc80 has been reported as an Mps1-binding protein in yeast and human cell (Kemmler et al., 2009; Martin-Lluesma et al., 2002; Saurin et al., 2011), it is likely that recruited Mps1 by Rad52 tightly binds to the kinetochore via physical interaction with Ndc80. Furthermore, contrary to Rad52, non-Ipl1/Aurora-phosphorylable mutant of Ndc80 does not affect the accumulation of Mps1 to the kinetochores (Nijenhuis et al., 2013), suggesting that Ndc80 acts as a direct binding platform for

Mps1 localization and Rad52 acts as a major Ipl1-dependent regulatory factor in Mps1 accumulation pathway to the kinetochore. Thus, deletion of *RAD52* does not cause total disruption of kinetochore-binding affinity of Mps1 that is supplied by physical interaction with Ndc80.

In total, this study demonstrates that Rad52 controls Mps1 localization and SAC activation as a novel regulator for accurate mitotic regulation. Especially, present work provides the insight for 'missing link' of Mps1 regulation by Ipl1. Thus, defining the precise mechanism that regulates Mps1 by Ipl1-dependent phosphorylated Rad52 will be interesting subject for future work.

4. Material and Methods

4.1. Yeast Growth Condition

Yeast cells were grown at 30°C in YPD or SC medium lacking amino acids as required. For all chemical treatments, cells were grown to mid-log phase (OD_{600} = 0.7-1.0) and diluted to OD_{600} = 0.5. Chemical-treated cells were incubated in 30°C for 3 hr.

4.2. Construction of Plasmid

Sequence-mutated Rad52 expression vectors [p415ADH-RAD52 (K10,11,220R)-RFP, p416ADH-RAD52 (S86A,T96A,S136A,T349A,S374A)-HA, p416ADH-RAD52 (S86A,T96A,S136A)-HA, p416ADH-RAD52 (S136A,T349A,S374A)-HA, p416ADH-RAD52 (S86A,T96A,T349A,S374A)-HA, p416ADH-RAD52 (S86A,T96A,S136A,S374A)-HA, p416ADH-RAD52 (S86A,T96A,S136A,T349A,)-HA, p416ADH-RAD52 (S374A)-HA, p416ADH-RAD52 (S86E,T96E,S136E)-HA, p416GPD-RAD52 (S86E,T96E,S136E)-HA] were constructed by SLIC-based sequence substitution cloning (Jeong et al., 2012).

Chromosomal RAD52 integration vectors [p305ADH-RAD52-HA, p305ADH-RAD52 (S86A,T96A,S136A)-HA, p305ADH-RAD52 (S86A,T96A,S136A,T349A,S374A)-HA, p305ADH-RAD52-myc, p305ADH-RAD52 (S86A,T96A,S136A)-myc, p305ADH-RAD52 (S86A,T96A,S136A,T349A,S374A)-myc, p305ADH-RAD52 (S374A)-myc, p306ADH-RAD52-HA, p306ADH-RAD52 (S86A,T96A,S136A)-HA, p306ADH-RAD52 (S86A,T96A,S136A,T349A,S374A)-HA, p306ADH-RAD52 (S374A)-HA] were constructed as follows: DNA sequences for HA-tagged Rad52 variants were digested by XbaI and XhoI from Rad52 expression vectors, ligated to XbaI- and XhoI- digested p305ADH or p306ADH. For constructing integration vectors for myc-tagged Rad52, myc sequence was substituted for HA sequence by XmaI and XhoI digestion and ligation.

Chromosomal NDC80-RAD52 integration vectors [p305GAL-NDC80-RFP-RAD52-HA, p305GAL-NDC80-RFP-RAD52 (S374E)-HA, p305GAL-NDC80-RFP-RAD52 (S86A, T96A, S136A, S74E)-HA, p305GAL-NDC80 (T21D, S37D, T54D, T71D, T74D, S95D, S100D)-RFP-RAD52-HA, p305GAL-NDC80 (T21D, S37D, T54D, T71D, T74D, S95D, S100D)-RFP-RAD52 (S374E)-HA] were constructed as follows: DNA fragments of sequence-mutated NDC80 and Rad52 were constructed by SLIC-based sequence substitution cloning. p305ADH vector was digested by XbaI and XhoI. All DNA fragments for Chromosomal NDC80-RAD52 integration vector (digested p305GAL, NDC80-RFP, RAD52-HA) were ligated by SLIC-based cloning.

For in vitro kinase assay, bacterial vectors for expressing fusion proteins [pGEX-4T-1-yRAD52, pGEX-4T-1-yRAD52 (S86A,T96A,S136A,T349A,S374A), pGEX-4T-1-yRAD52 (S136A,T349A,S374A), pGEX-4T-1-yRAD52 (S86A,T96A,T349A,S374A), pGEX-4T-1-yRAD52 (S86A,T96A,S136A,S374A), pGEX-4T-1-yRAD52 (S86A,T96A,S136A,T349A), pGEX-4T-1-IPL1, pGEX-4T-1-IPL1 (K133R), pGEX-4T-1-hRAD52, pGEX-4T-1-AURORA B] were constructed as follows: All protein sequences were amplified using specific primers that were designed to insert SalI and NotI sites at the ends of PCR construct. Yeast Rad52 variant sequences were amplified from Rad52 expression vectors, and IPL1 ORF sequence was amplified from yeast genomic DNA. To make bacterial vectors for expressing kinase-dead mutant of Ipl1, pRS416ADH-IPL1(K133R)-HA was constructed by SLIC-based sequence substitution cloning, and IPL(K133R) sequence was amplified and cloned into pGEX-4T-1. cDNAs synthesized from HEK293T cell mRNAs were used as a template for PCR amplification of human Rad52 and Aurora B. All PCR constructs were digested by SalI and NotI, and ligated with pGEX-4T-1. For Mps1 kinase assay, p416ADH-MPS1-TAP was constructed by PCR-based cloning. EcoRI and XmaI sites-inserted MPS1 ORF sequence was amplified from yeast genomic DNA. Amplified MPS1 ORF was digested by EcoRI and XmaI, and ligated with

p416ADH-TAP. p416ADH-MPS1 (D550A)-TAP was constructed by SLIC-based sequence substitution cloning.

4.3. Measurement of Growth Curve

All growth curves were measured by using yeast strains carrying vectors, which are indicated in figures. Cells were grown at 30°C in SC media lacking amino acids as required and diluted to OD_{600} = 0.2-0.25. OD_{600} was measured every 1 hr during incubation at 30°C.

4.4. Measurement of DNA Contents

DNA contents measurement by flow cytometry was performed as previously described (Haase and Reed, 2002). Approximately 1x107 cells were harvested and fixed with 5 ml of 70% ethanol for 1 hr at room temperature. Fixed cells were collected and washed once with 1 ml of distilled water and transferred to microfuge tube. 0.5 ml of 2 mM RNase solution (2 mg/ml RNase A in 50 mM Tris, pH 8.0, 15 mM NaCl, boiled for 15 min) was treated to harvested cells for 2-3 hr at 37°C. After removing RNase solution, 0.2 ml of pepsin solution (5 mg/ml pepsin in 1 ml distilled water, 4.5 µl HCl) was directly treated to collected cells for 0.5-1 hr at 37°C. Cells were collected by centrifugation and re-suspended to 0.5 ml of 50 mM Tris, pH 7.5. This sample can be analyzed immediately or stored at 4°C for few days. To analyze DNA contents, 50 µl of sample solution was added to 1 ml of SYTOX green solution (1 mM SYTOX green (Invitrogen) in 50 mM Tris, pH 7.5) and this mixture was sonicated for few minutes at low power. DNA contents were measured by FACS Canto cytometer (BD Biosciences) using 488 nm excitation filter and 510 nm emission filter.

4.5. Fluorescence and Time-lapse Microscopy

Fluorescence microscopy was performed on a Nikon Eclipse Ti inverted microscope and DeltaVision microscope (Applied Precision). Cells were grown to OD_{600} = 0.7-1.0 in SC media

at 30°C. For sample fixation, 1x107 cells were harvested and treated with 1 ml of paraformaldehyde solution (4% paraformaldehyde, 3.4% sucrose in distilled water) for 15 min at room temperature. Fixed cells were collected by centrifugation and washed twice with PBS. Washed cells were resuspended to 0.5 ml PBS. Fixed samples can be analyze immediately or stored at 4°C for few days. To visualize Nuclear DNA, Fixed samples were directly treated with 2 μg/ml DAPI (Invitrogen). To attach cells on plates, 96-well glass bottom plate (Metrical Bioscience) for Nikon Eclipse Ti inverted microscope and coverglass bottom dish (SPL) for DeltaVision microscope were pre-treated with 5 μg/ml concanavalin A (Sigma-Aldrich). For fluorescence quantification of Mps1-GFP, acquired images were analyzed by ImageJ software. Fluorescence intensity was quantified by manual selection of Mps1-GFP signals colocalized with Ndc80-RFP signals, and background intensity was obtained at random position that was not colocalized with Ndc80-RFP signals. The relative fluorescence intensity was calculated by subtracting background intensity from fluorescence intensity of Mps1-GFP.

Time-lapse microscopy of living cells was performed using DeltaVision microscope. Cells grown to OD_{600} = 0.7-1.0 were used for asynchronous time-lapse microscopy immediately or cell cycle synchronization. 150 μM α-factor was treated for 3 hr to synchronize cell cycle to G1 phase and washed twice with fresh media. Washed cells were resuspended to fresh media, and fluorescence images were acquired in environmental chamber of DeltaVision microscope. To maintain cell growth, environmental chamber was heated to 30°C while time-lapse images were acquired.

4.6. Serial Dilution Assay

Cells carrying indicated vectors were grown to OD_{600} = 1.0-2.0 in SC media lacking amino acid as required and adjusted to OD_{600} = 0.75 with distilled water for the first dilution. Four 10-fold serial dilutions were prepared by using the first dilution sample. For MMS sensitivity test, 3 μl of five serial dilution samples were subsequently spotted on media plates in

the absence or presence of 0.01% MMS and incubated at 30°C for 3 days. For UV sensitivity test, 3 μl of five serial dilution samples were subsequently spotted on two media plates, and one of them was exposed to 100 J/m2 UV light by using UV crosslinker (UVP HL-2000 Hybrilinker). Both plates were incubated at 30°C for 3 days.

4.7. Western Blot Assay

To measure cell cycle-dependent Pds1-myc amount, cells were cultured in 25 ml YPD to OD_{600} = 1.0 and mixed with 25 ml fresh YPD to dilute cell density. 150 μM α-factor was treated for 3 hr to synchronize cell cycle to G1 phase and washed twice with YPD. Washed cells were resuspended to 100 ml YPD, and 1x108 cells were harvested for the zero time point. Remaining cultures were incubated at 30°C, and 1x108 cells were harvested every 30 min from the zero time point. Harvested cells were washed twice with PBS and resuspended to 100 μl lysis buffer (150 mM NaCl, 50 mM Tris, pH 7.5, 0.15% NP-40, 1 mM phenylmethylsulfonyl fluoride, 1 mM benzamidine, 1 μg/ml leupeptin, 1 μg/ml pepstatin). Cells were disrupted by bead-beating using a cell pellet volume equivalent of 0.5 mm glass beads. Lysates were clarified by centrifugation at 14,000 RPM for 10 min on 4°C pre-cooled microcentrifuge. Protein concentration was determined by Bradford assay.

Cells harboring plasmids for expressing wild-type and mutant Rad52 were cultured in SC lacking amino acid as required. 10 ml cultures were harvested at OD_{600} = 1.0 and washed twice with pre-cooled PBS. Washed cells were resuspended to 100 μl lysis buffer with phosphatase inhibitors (10 mM sodium fluoride, 20 mM β-glycerolphosphate, 10 mM sodium orthovanadate, 10 mM sodium pyrophosphate). Cells were disrupted as described above. For λ phosphatase assay, lysate was incubated with 600 units of λ phosphatase (New England Biolabs), 1X NEB buffer for PMP, and 1 mM MnCl2 at 30°C for 2 hr.

MG-132 treatment was carried out as previously described (Liu et al., 2007). Cells were cultured in special SC-Ura medium (0.17% yeast nitrogen base without amino acids and

ammonium sulfate, 0.1% proline, appropriate amino acids, 2% glucose). Cultures were reinoculated to this media with 0.003% SDS and grown at 30°C for 3 hr. 50 μM MG-132 (A.G. Scientific) was treated to cultures and incubated at 30°C for 3 hr. Cell harvest and lysis were performed as described above.

SDS-PAGE analysis was performed with 8% separating gel for Pds1-myc and Rad52-HA. To isolate phosphorylated Rad52 clearly, 6% separating gel containing 20 μM Phos-tag (NARD institute) and 100 μM MnCl2 was also used. Immunoblots were performed with an anti-HA antibody (Santa cruz) for HA-tagged proteins, an anti-GFP antibody (Santa cruz) for GFP-tagged proteins, an anti-mouse IgG antibody (Sigma-Aldrich) for TAP-tagged proteins, and an anti-hexokinase antibody (United States Biological) for endogenous hexokinases.

4.8. *in vitro* Kinase Assay

For Ipl1 kinase assay, Ipl1 and Rad52 variants were purified from E. coli by GST affinity purification. 3.5 μg of GST-Ipl1 or GST-Ipl1 kinase-dead mutant was incubated with 2.5 μg of Rad52 variant, kinase buffer (25 mM HEPES, pH 7.6, 10 mM MgCl2, 5 mM β-glycerolphosphate, 50 μM ATP in distilled water), and 4 μCi [γ-32P]-ATP at 30°C for 60 min. Reaction was terminated by boiling at 95°C with 1x SDS sample buffer, and the samples were subjected to SDS-PAGE. The incorporation of 32P was visualized using BAS 2500 (Biorad). Aurora B and human Rad52 were purified from E. coli by GST affinity purification, and 3.5 μg of GST-Aurora B and 2.5 μg of human Rad52 were used for Aurora B kinase assay.

For Mps1 kinase assay, Mps1 was purified from S. cerevisiae by immnoprecipitation. 50 ml of cells expressing wild-type or kinase-dead mutant of Mps1 were cultured to OD_{600} = 1.0 at 30°C. Cell harvest and lysis were performed as described in Immunoprecipitation Assay, and lysate was incubated with 25 μl of IgG-conjugated agarose beads (GE healthcare) at 4°C for 3 hr. 10 μl of washed IgG-conjugated agarose beads were incubated with 5 μg of Rad52 variant, kinase buffer, and 4 μCi [γ-32P]-ATP at 30°C for 60 min. For reversine treated kinase assay, 10

μM reversine in DMSO or same volume of DMSO was treated to kinase reaction mixture. Subsequent steps were performed as described above. For human Mps1 kinase assay, 0.1 μg of active human Mps1 (abcam) was incubated with 5 μg of human Rad52.

Table 4 Yeast strains used in this study

Strain	Genotype	Source
HY1619	*MATa his3Δ1 leu2Δ0 met15Δ0 ura3Δ0 rad52Δ::kanMX4 leu2::pADH-RAD52-HA:LEU2*	This study
HY1620	*MATa his3Δ1 leu2Δ0 met15Δ0 ura3Δ0 rad52Δ::kanMX4 leu2::pADH-RAD52(S86A, T96S, S136A)-HA:LEU2*	This study
HY1621	*MATa his3Δ1 leu2Δ0 met15Δ0 ura3Δ0 rad52Δ::kanMX4 leu2::pADH-RAD52(S86A, T96S, S136A, T349A, S374A)-HA:LEU2*	This study
HY1622	*MATa his3Δ1 leu2Δ0 met15Δ0 ura3Δ0 rad52Δ::kanMX4 leu2::pADH-RAD52-HA:LEU2 PDS1-myc:HIS3*	This study
HY1623	*MATa his3Δ1 leu2Δ0 met15Δ0 ura3Δ0 rad52Δ::kanMX4 leu2::pADH-RAD52(S86A, T96S, S136A)-HA:LEU2 PDS1-myc:HIS3*	This study
HY1624	*MATa his3Δ1 leu2Δ0 met15Δ0 ura3Δ0 rad52Δ::kanMX4 leu2::pADH-RAD52(S86A, T96S, S136A, T349A, S374A)-HA:LEU2 PDS1-myc:HIS3*	This study
HY1625	*MATa his3Δ1 leu2Δ0 met15Δ0 ura3Δ0 rad52Δ::kanMX4 leu2::pADH-RAD52-HA:LEU2 NDC80-GFP:HIS3 SPC29-RFP:URA3*	This study
HY1626	*MATa his3Δ1 leu2Δ0 met15Δ0 ura3Δ0 rad52Δ::kanMX4 leu2::pADH-RAD52(S86A, T96S, S136A)-HA:LEU2 NDC80-GFP:HIS3 SPC29-RFP:URA3*	This study
HY1627	*MATa his3Δ1 leu2Δ0 met15Δ0 ura3Δ0 rad52Δ::kanMX4 leu2::pADH-RAD52(S86A, T96S, S136A, T349A, S374A)-HA:LEU2 NDC80-GFP:HIS3 SPC29-RFP:URA3*	This study

HY1628	*MATa his3Δ1 leu2Δ0 met15Δ0 ura3Δ0 IPL1-GFP:HIS3 [p416ADH-RAD52-RFP]*	This study
HY1629	*MATa his3Δ1 leu2Δ0 met15Δ0 ura3Δ0 SLI15-GFP:HIS3 [p416ADH-RAD52-RFP]*	This study
HY1637	*MATa his3Δ1 leu2Δ0 met15Δ0 ura3Δ0 rad52Δ::kanMX4 MPS1-GFP:LEU2 NDC80-RFP:HIS3*	This study
HY1638	*MATa his3Δ1 leu2Δ0 met15Δ0 ura3Δ0 rad52Δ::kanMX4 leu2::pADH-RAD52-HA:LEU2 MPS1-GFP:HIS3 NDC80-RFP:URA3*	This study
HY1639	*MATa his3Δ1 leu2Δ0 met15Δ0 ura3Δ0 rad52Δ::kanMX4 leu2::pADH-RAD52(S86A, T96S, S136A)-HA:LEU2 MPS1-GFP:HIS3 NDC80-RFP:URA3*	This study
HY1640	*MATa his3Δ1 leu2Δ0 met15Δ0 ura3Δ0 rad52Δ::kanMX4 leu2::pADH-RAD52(S86A, T96S, S136A, T349A, S374A)-HA:LEU2 MPS1-GFP:HIS3 NDC80-RFP:URA3*	This study
HY1641	*MATa his3Δ1 leu2Δ0 met15Δ0 ura3Δ0 rad52Δ::kanMX4 leu2::pADH-RAD52(S374A)-myc:LEU2 MPS1-GFP:HIS3 NDC80-RFP:URA3*	This study
HY1642	*MATa his3Δ1 leu2Δ0 met15Δ0 ura3Δ0 rad52Δ::kanMX4 [p416ADH-RAD52(S86E, T96E, S136E)-HA]*	This study
HY1643	*MATa his3Δ1 leu2Δ0 met15Δ0 ura3Δ0 rad52Δ::kanMX4 [p416GPD-RAD52(S86E, T96E, S136E)-HA]*	This study
HY1648	*MATa his3Δ1 leu2Δ0 met15Δ0 ura3Δ0 leu2::pGAL-NDC80-RFP-RAD52-HA:LEU2 MPS1-GFP:HIS3*	This study
HY1649	*MATa his3Δ1 leu2Δ0 met15Δ0 ura3Δ0 leu2::pGAL-NDC80-RFP-RAD52(S374E)-HA:LEU2 MPS1-GFP:HIS3*	This study
HY1650	*MATa his3Δ1 leu2Δ0 met15Δ0 ura3Δ0 leu2::pGAL-NDC80-RFP-RAD52-HA:LEU2 PDS1-myc:HIS3*	This study

HY1651	*MATa his3Δ1 leu2Δ0 met15Δ0 ura3Δ0 leu2::pGAL-NDC80-RFP-RAD52(S374E)-HA:LEU2 PDS1-myc:HIS3*	This study
HY1652	*MATa his3Δ1 leu2Δ0 met15Δ0 ura3Δ0 leu2::pGAL-NDC80-RFP-RAD52(S86A, T96A, S136A, S374E)-HA:LEU2 PDS1-myc:HIS3*	This study
HY1653	*MATa his3Δ1 leu2Δ0 met15Δ0 ura3Δ0 mad1Δ::URA3 leu2::pGAL-NDC80-RFP-RAD52(S374E)-HA:LEU2 PDS1-myc:HIS3*	This study
HY1654	*MATa his3Δ1 leu2Δ0 met15Δ0 ura3Δ0 leu2::pGAL-NDC80(T21D, S37D, T54D, T71D, T74D, S95D, S100D)-RFP-RAD52-HA:LEU2 PDS1-myc:HIS3*	This study
HY1655	*MATa his3Δ1 leu2Δ0 met15Δ0 ura3Δ0 leu2::pGAL-NDC80(T21D, S37D, T54D, T71D, T74D, S95D, S100D)-RFP-RAD52(S374E)-HA:LEU2 PDS1-myc:HIS3*	This study
HY1656	*MATa his3Δ1 leu2Δ0 met15Δ0 ura3Δ0 mad1Δ::URA3 leu2::pGAL-NDC80(T21D, S37D, T54D, T71D, T74D, S95D, S100D)-RFP-RAD52(S374E)-HA:LEU2 PDS1-myc:HIS3*	This study
HY1667	*MATa ade2- 1 ura3-1 his3-11,15 trp1-1 leu2-3,112 can1-100 leu2::tetR-GFP:LEU2 CEN5::tetO2X112:HIS3 rad52Δ::TRP1 ura3::pADH-RAD52-HA:URA3*	This study
HY1668	*MATa ade2- 1 ura3-1 his3-11,15 trp1-1 leu2-3,112 can1-100 leu2::tetR-GFP:LEU2 CEN5::tetO2X112:HIS3 rad52Δ::TRP1 ura3::pADH-RAD52(S86A, T96A, S136A)-HA:URA3*	This study
HY1669	*MATa ade2- 1 ura3-1 his3-11,15 trp1-1 leu2-3,112 can1-100 leu2::tetR-GFP:LEU2 CEN5::tetO2X112:HIS3 rad52Δ::TRP1 ura3::pADH-RAD52(S86A, T96A, S136A, T349A, S374A)-HA:URA3*	This study
HY1670	*MATa ade2- 1 ura3-1 his3-11,15 trp1-1 leu2-3,112 can1-100 leu2::tetR-GFP:LEU2 CEN5::tetO2X112:HIS3 rad52Δ::TRP1 ura3::pADH-RAD52(S374A)-HA:URA3*	This study

Table 5 Oligonucleotide primers used in this study

Primer name	Sequence (5' to 3')
RAD52-F(SLIC)	GCTATACCAAGCATACAATCAACTTCTAGATTGGTGTGTTGTTGATGAATGAAATTATGG
RAD52-R(SLIC)	AGACATCGTATGGGTAAAAGATGTTAATTAACCCGGGGATCCGTCGACCAGTAGGCTTGC
RAD52(S86A,T96A)-F	GGAAAGTTTGCCATAGGGTGTACTGCAATTGTTCGTGTTGCGTTGACTAGCGGG
RAD52(S86A,T96A)-R	CCCGCTAGTCAACGCAACACGAACAATTGCAGTACACCCTATGGCAAACTTTCC
RAD52(S136A)-F	GCCTTGAAAAGAGCTTTGAGAGGGTTTGGT
RAD52(S136A)-R	ACCAAACCCTCTCAAAGCTCTTTTCAAGGC
RAD52(T349A)-F	TCCATTAGGCACGCCGTTGATCAGACTACG
RAD52(T349A)-R	CGTAGTCTGATCAACGGCGTGCCTAATGGA
RAD52(S374A)-F	ACCGCGAGGGATGCTGTCTATGAAAAATTT
RAD52(S374A)-R	AAATTTTTCATAGACAGCATCCCTCGCGGT
RAD52(S374E)-F	ACCGCGAGGGATGAGGTCTATGAAAAATTT
RAD52(S374E)-R	AAATTTTTCATAGACCTCATCCCTCGCGGT

PDS1-F2	AGAAGGCCTCGATCCTGAAGAACTAGAGGACTTAGTTACTGGTCGACGGATCCCCGGGTT
PDS1-R1	ACGTGTATATATGTTGTGTGTATGTGAATGAGCAGTGGATTCGATGAATTCGAGCTCGTT
IPL1-2(SalI)	CAGAGTCGACGA**ATG**CAACGCAATAGTTTA
IPL1+1104R (NotI)	AGTCGCGGCCGC**CTA**TAACCGCTTATTTTCCCAAA
IPL1(K133R)-F	ATTTGCGCACTGAGAGTAATGGAGAAG
IPL1(K133R)-R	CTTCTCCATTACTCTCAGTGCGCAAAT
MPS1 -2(EcoRI)	TCAGGAATTCACATGTCAACAAACTCATTC
MPS1-F(SLIC)	GCTATACCAAGCATACAATCAACTTCTAGA ATCTCAAAACAAACATGTCAACAAACTCAT
MPS1-R(SLIC)	TTTTCCATCTTCTCTTCCATGGATTAATTAACCCGGGGATCCGTCGACC AATTTTGTAAT
MPS1(D580A)-F	TTAAAAATCATTGCTTTTGGTATAGCAAAC
MPS1(D580A)-R	GTTTGCTATACCAAAAGCAATGATTTTTAA
RAD52-2(SalI)	CAGAGTCGACTCATGAATGAAATTATGGAT
RAD52+1416R(NotI)	AGTCGCGGCCGCTCAAGTAGGCTTGCGTGCATGCA
AuroraB-2(SalI)	CAGAGTCGACGGATGGCCCAGAAGGAGAAC

AuroraB+1038R (NotI)	AGTCGCGGCCGCTCAGGCGACAGATTGAAGGGCAG
Rad52_human-2(SalI)	CAGAGTCGACAGATGTCTGGGACTGAGGAA
Rad52_human+1257R (NotI)	AGTCGCGGCCGCTTAAGATGGATCATATTTCCTTT
NDC80-300F(SLIC)	GCTATACCAAGCATACAATCAACTTCTAGA TAAAGATGTAAGCAGTCTATTGCGATTAGC
NDC80+2073R (SLIC)	TGAAAAGTTCTTCTCCTTTACTGTTAATTAACCCGGGGATCCGTCGACCATTTGTTACGTTATGTTCAG TTTCAAACTC
NDC80(T21D)-F	GACCCTCATCGGTTTGATTCCCAAATACCAACT
NDC80(T21D)-R	AGTTGGTATTTGGGAATCAAACCGATGAGGGTC
NDC80(S37D)–F	TTGAGGAGAAGAAACGACACGAATCAAGGTCTA
NDC80(S37D)–R	TAGACCTTGATTCGTGTCGTTTCTTCTCCTCAA
NDC80(T54D)–F	AGTATTGCCAGGAATGATATAAGCGGGACTGGC
NDC80(T54D)–R	GCCAGTCCCGCTTATATCATTCCTGGCAATACT
NDC80(T71,74D)–F	AATAAAAATAAGAGGGATAGAAGCGACGTTGCAGGAGGTACA
NDC80(T71,74D)–R	TGTACCTCCTGCAACGTCGCTTCTATCCCTCTTATTTTTATT
NDC80(S95, 100D)–F	TCCAACAGTAGAAACGACGTCAGCAGATTAGATATAAATCAACTTGGC

NDC80(S95, 100D)–R	GCCAAGTTGATTTATATCTAATCTGCTGACGTCGTTTCTACTGTTGGA
NDC80-GAL1-F(SLIC)	CGTCAAGGAGAAAAAACCCCGGATTCTAGA ACCCGTTTCTATAAATGCAAAGCTCAACAA
tCYC1-p305-R(SLIC)	GGGAACAAAAGCTGGGTACCGGGCCC TCTATATTACCCTGTTATCC

CONCLUSION

In first part of this study, I demonstrate that Rad52 has novel functions for the activation of SAC and the regulation of mitosis using *RAD52* deletion strain. *rad52*Δ strain showed growth defect and G2/M phase accumulation, which are the evidences of mitotic arrest. In addition, growth defect to *rad52*Δ strain was related to different domain with the domains for homologous recombination. By the Pds1 degradation assay, it was also confirmed that *rad52*Δ strain could not activate SAC under spindle damage condition. Strikingly, by using *CEN5*-GFP system, I demonstrated that deletion of *RAD52* led to chromosome mis-alignment, which causes improper chromosome inheritance and aneuploidy. From these results, it is clearly verified that Rad52 is a novel regulator for SAC activation and proper mitotic regulation. Present study discovers unknown regulatory component of pathway for proper chromosome segregation and it will contribute to improve the understanding of regulation mechanism for mitosis.

In second part of this study, I demonstrate that Rad52 controls Mps1 localization by Ipl1-dependent phosphorylation and contribute SAC activation by Mps1-dependent phosphorylation. By *in vitro* kinase assay, it was confirmed that Ipl1 phosphorylates Rad52 at serine 374 and Mps1 phosphorylates Rad52 at three residues, which are serine 86, threonine 96, and serine 136. To identify the function of phosphorylation by Ipl1 and Mps1, the physiological effect of non-phosphorylable mutants of Rad52 were examined. As a result, I verified that Mps1-dependent phosphorylation of Rad52 is crucial for SAC activation under spindle damage condition and Ipl1-dependent phosphorylation of Rad52 is related to the regulation of Mps1 localization. By using Ndc80-conjugated Rad52^{S374E}, which imitates Ipl1-dependent phosphorylation of Rad52 at kinetochores, it was confirmed that Ipl1-dependent phosphorylated Rad52 accumulated Mps1 to kinetochores and activates SAC without induction of spindle damage. Furthermore, by using Ndc80^{7D}-conjugated Rad52^{S374E}, which imitates Ipl1-dependent phosphorylation of multiple substrates, it was verified that Ipl1 regulates mitosis via multiple substrates. In addition, it was also defined that Aurora B kinase and human Mps1 phosphorylate human Rad52. Thus, I

presume that novel Rad52 functions for mitotic regulation, which are controlled by Ipl1 and Mps1, are conserved to human system. From these results, it is clearly verified that Rad52 has dual functions for SAC activation and mitotic regulation, which are controlled by Ipl1-dependent or Mps-dependent phosphorylation. Present study will provide further insight for undefined Mps1-recruiting mechanism, which is controlled by the kinase activity of Ipl1.

Taken together, present study supports the model in **Fig. 27**. As a major mitotic kinase, Ipl1 regulates progression of mitosis at higher hierarchy of mitotic regulatory pathway. Recently, it has been reported that Mps1 localization to kinetochores is important during unperturbed mitosis (Heinrich et al., 2012; Maure et al., 2007; Nijenhuis et al., 2013). Thus, Ipl1 phosphorylates Rad52 at serine 374 to regulate Mps1 localization. Ipl1-dependent Phosphorylated Rad52 accumulates Mps1 to the kinetochores and accumulated Mps1 binds to outer kinetochore component Ndc80 for accurate mitosis (Kemmler et al., 2009; Martin-Lluesma et al., 2002; Saurin et al., 2011). When spindle is damaged, unattached kinetochores are localized close to Ipl1 and substrates of Ipl1 are highly phosphorylated (Foley and Kapoor, 2012). In this condition, Mps1 is highly accumulated to kinetochores by Ipl1-dependent phosphorylated Rad52. Kinetochore-bound Mps1 are changed to active form (Dou et al., 2015) and phosphorylates Rad52 at serine 86, threonine 96, and serine 136. Mps1-dependent phosphorylated Rad52 assists Mps1 function to activate SAC and SAC is activated to repair spindle damage.

In summary, present study demonstrates that Rad52 does not just play a role in DNA damage repair by homologous recombination activity. Through its ability to accumulate Mps1 to the kinetochores and activate SAC, Rad52 is a vital component of chromosome bi-orientation and is essential for spindle damage repair by SAC. In conclusion, Rad52 is a novel regulatory

component of chromosome segregation in yeast mitosis. It would be interesting to confirm and extend the present findings in other eukaryotic cells.

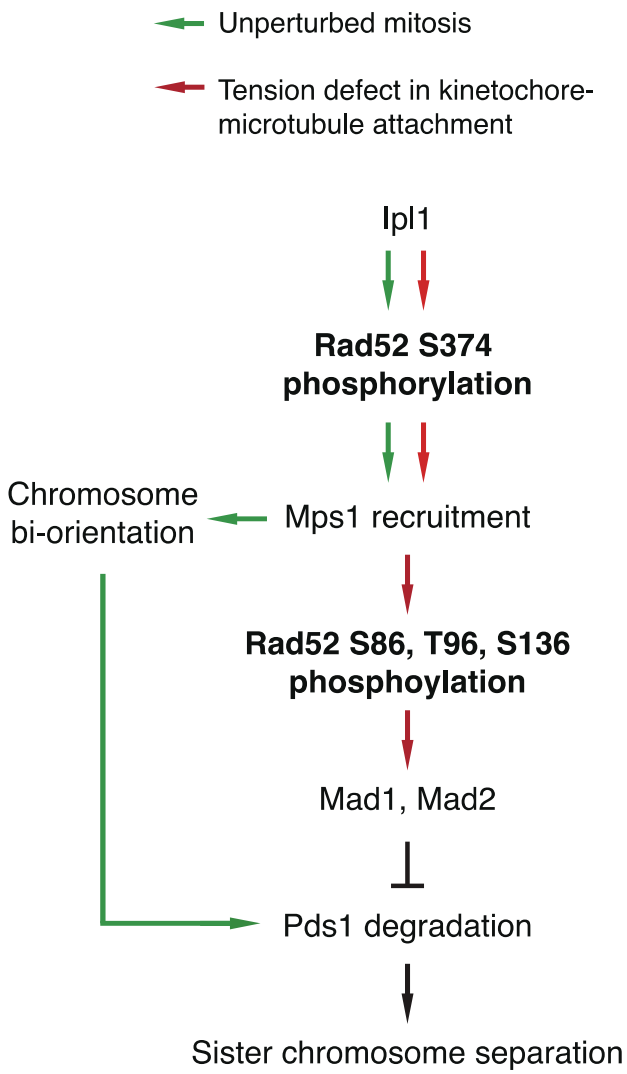

Fig. 27 The model for Mps1 regulation and SAC activation by Rad52.

When tension between kinetochore and microtubule is absent, Ipl1 phosphorylates S374 of Rad52. Ipl1-dependent phosphorylated Rad52 recruits Mps1 to the kinetochore for the regulation of mitosis. Mps1 on the kinetochore phosphorylates S86, T96, and S136 of Rad52. Mps1-dependent phosphorylation of Rad52 acts as a SAC activation signal.

REFERENCE

Akiyoshi, B., Nelson, C.R., Ranish, J.A., and Biggins, S. (2009). Analysis of Ipl1-mediated phosphorylation of the Ndc80 kinetochore protein in Saccharomyces cerevisiae. In Genetics, pp. 1591-1595.

Alexandru, G., Zachariae, W., Schleiffer, A., and Nasmyth, K. (1999). Sister chromatid separation and chromosome re-duplication are regulated by different mechanisms in response to spindle damage. EMBO J *18*, 2707-2721.

Altmannova, V., Eckert-Boulet, N., Arneric, M., Kolesar, P., Chaloupkova, R., Damborsky, J., Sung, P., Zhao, X., Lisby, M., and Krejci, L. (2010). Rad52 SUMOylation affects the efficiency of the DNA repair. Nucleic Acids Research *38*, 4708-4721.

Alver, B., Kelly, M.K., and Kirkpatrick, D.T. (2013). Novel checkpoint pathway organization promotes genome stability in stationary-phase yeast cells. In Mol Cell Biol, pp. 457-472.

Andrews, B., and Measday, V. (1998). The cyclin family of budding yeast: abundant use of a good idea. In Trends Genet, pp. 66-72.

Araki, Y., Gombos, L., Migueleti, S.P.S., Sivashanmugam, L., Antony, C., and Schiebel, E. (2010). N-terminal regions of Mps1 kinase determine functional bifurcation. J Cell Biol *189*, 41-56.

Bloom, J., Cristea, I.M., Procko, A.L., Lubkov, V., Chait, B.T., Snyder, M., and Cross, F.R. (2011). Global analysis of Cdc14 phosphatase reveals diverse roles in mitotic processes. Journal of Biological Chemistry *286*, 5434-5445.

Bock, L.J., Pagliuca, C., Kobayashi, N., Grove, R.A., Oku, Y., Shrestha, K., Alfieri, C., Golfieri, C., Oldani, A., Dal Maschio, M.*, et al.* (2012). Cnn1 inhibits the interactions between the KMN complexes of the yeast kinetochore. Nat Cell Biol *14*, 614-624.

Buvelot, S., Tatsutani, S.Y., Vermaak, D., and Biggins, S. (2003). The budding yeast Ipl1/Aurora protein kinase regulates mitotic spindle disassembly. J Cell Biol *160*, 329-339.

Carmena, M., Wheelock, M., Funabiki, H., and Earnshaw, W.C. (2012). The chromosomal passenger complex (CPC): from easy rider to the godfather of mitosis. Nat Rev Mol Cell Biol *13*, 789-803.

Cheeseman, I.M., Anderson, S., Jwa, M., Green, E.M., Kang, J.s., Yates, J.R., Chan, C.S.M., Drubin, D.G., and Barnes, G. (2002). Phospho-regulation of kinetochore-microtubule attachments by the Aurora kinase Ipl1p. Cell *111*, 163-172.

Cimini, D., Howell, B., Maddox, P., Khodjakov, A., Degrassi, F., and Salmon, E.D. (2001). Merotelic kinetochore orientation is a major mechanism of aneuploidy in mitotic mammalian tissue cells. J Cell Biol *153*, 517-527.

Cohen-Fix, O., Peters, J.M., Kirschner, M.W., and Koshland, D. (1996). Anaphase initiation in Saccharomyces cerevisiae is controlled by the APC-dependent degradation of the anaphase inhibitor Pds1p. Genes & Development *10*, 3081-3093.

Cottingham, F.R., and Hoyt, M.A. (1997). Mitotic spindle positioning in Saccharomyces cerevisiae is accomplished by antagonistically acting microtubule motor proteins. J Cell Biol *138*, 1041-1053.

D'Amours, D., and Jackson, S.P. (2002). The Mre11 complex: at the crossroads of dna repair and checkpoint signalling. In Nat Rev Mol Cell Biol, pp. 317-327.

Dewar, H., Tanaka, K., Nasmyth, K., and Tanaka, T.U. (2004). Tension between two kinetochores suffices for their bi-orientation on the mitotic spindle. Nature *428*, 93-97.

Dou, Z., Liu, X., Wang, W., Zhu, T., Wang, X., Xu, L., Abrieu, A., Fu, C., Hill, D.L., and Yao, X. (2015). Dynamic localization of Mps1 kinase to kinetochores is essential for accurate spindle microtubule attachment. In Proceedings of the National Academy of Sciences, pp. E4546-4555.

Dudáš, A., and Chovanec, M. (2004). DNA double-strand break repair by homologous recombination. In Mutation Research/Reviews in Mutation Research, pp. 131-167.

Emanuele, M.J., Lan, W., Jwa, M., Miller, S.A., Chan, C.S.M., and Stukenberg, P.T. (2008). Aurora B kinase and protein phosphatase 1 have opposing roles in modulating kinetochore assembly. J Cell Biol *181*, 241-254.

Foley, E.A., and Kapoor, T.M. (2012). Microtubule attachment and spindle assembly checkpoint signalling at the kinetochore. Nat Rev Mol Cell Biol *14*, 25-37.

Fraschini, R., Formenti, E., Lucchini, G., and Piatti, S. (1999). Budding yeast Bub2 is localized at spindle pole bodies and activates the mitotic checkpoint via a different pathway from Mad2. J Cell Biol *145*, 979-991.

Ge, S., Skaar, J., and Pagano, M. (2008). APC/C- and Mad2-mediated degradation of Cdc20 during spindle checkpoint activation. Cell Cycle *8*, 167-171.

Geymonat, M., Spanos, A., Smith, S.J.M., Wheatley, E., Rittinger, K., Johnston, L.H., and Sedgwick, S.G. (2002). Control of mitotic exit in budding yeast. In vitro regulation of Tem1 GTPase by Bub2 and Bfa1. J Biol Chem *277*, 28439-28445.

Glotzer, M., Murray, A.W., and Kirschner, M.W. (1991). Cyclin is degraded by the ubiquitin pathway. Nature *349*, 132-138.

Haase, S.B., and Reed, S.I. (2002). Improved flow cytometric analysis of the budding yeast cell cycle. Cell Cycle *1*, 132-136.

Heinrich, S., Windecker, H., Hustedt, N., and Hauf, S. (2012). Mph1 kinetochore localization is crucial and upstream in the hierarchy of spindle assembly checkpoint protein recruitment to kinetochores. J Cell Sci *125*, 4720-4727.

Hu, F., and Elledge, S.J. (2002). Bub2 is a cell cycle regulated phospho-protein controlled by multiple checkpoints. In Cell Cycle, pp. 351-355.

Huang, B., and Huffaker, T.C. (2006). Dynamic microtubules are essential for efficient chromosome capture and biorientation in S. cerevisiae. J Cell Biol *175*, 17-23.

Hustedt, N., Gasser, S.M., and Shimada, K. (2013). Replication checkpoint: tuning and coordination of replication forks in s phase. In Genes (Basel), pp. 388-434.

Hwang, L.H., Lau, L.F., Smith, D.L., Mistrot, C.A., Hardwick, K.G., Hwang, E.S., Amon, A., and Murray, A.W. (1998). Budding yeast Cdc20: a target of the spindle checkpoint. Science *279*, 1041-1044.

Ito, D., Saito, Y., and Matsumoto, T. (2012). Centromere-tethered Mps1 pombe homolog (Mph1) kinase is a sufficient marker for recruitment of the spindle checkpoint protein Bub1, but not Mad1. Proc Natl Acad Sci U S A *109*, 209-214.

Janke, R., Herzberg, K., Rolfsmeier, M., Mar, J., Bashkirov, V.I., Haghnazari, E., Cantin, G., Yates, J.R., and Heyer, W.-D. (2010). A truncated DNA-damage-signaling response is activated after DSB formation in the G1 phase of Saccharomyces cerevisiae. In Nucleic Acids Research, pp. 2302-2313.

Jelluma, N., Dansen, T.B., Sliedrecht, T., Kwiatkowski, N.P., and Kops, G.J.P.L. (2010). Release of Mps1 from kinetochores is crucial for timely anaphase onset. J Cell Biol *191*, 281-290.

Jeong, J.-Y., Yim, H.-S., Ryu, J.-Y., Lee, H.S., Lee, J.-H., Seen, D.-S., and Kang, S.G. (2012). One-step sequence- and ligation-independent cloning as a rapid and versatile cloning method for functional genomics studies. Appl Environ Microbiol *78*, 5440-5443.

Jin, F., Liu, H., Li, P., Yu, H.-G., and Wang, Y. (2012). Loss of Function of the Cik1/Kar3 Motor Complex Results in Chromosomes with Syntelic Attachment That Are Sensed by the Tension Checkpoint. PLoS Genet *8*, e1002492.

Kagawa, W., Kurumizaka, H., Ishitani, R., Fukai, S., Nureki, O., Shibata, T., and Yokoyama, S. (2002). Crystal structure of the homologous-pairing domain from the human Rad52 recombinase in the undecameric form. Mol Cell *10*, 359-371.

Kalantzaki, M., Kitamura, E., Zhang, T., Mino, A., Novák, B., and Tanaka, T.U. (2015). Kinetochore-microtubule error correction is driven by differentially regulated interaction modes. In Nat Cell Biol.

Keating, P., Rachidi, N., Tanaka, T.U., and Stark, M.J.R. (2009). Ipl1-dependent phosphorylation of Dam1 is reduced by tension applied on kinetochores. J Cell Sci *122*, 4375-4382.

Kemmler, S., Stach, M., Knapp, M., Ortiz, J., Pfannstiel, J., Ruppert, T., and Lechner, J. (2009). Mimicking Ndc80 phosphorylation triggers spindle assembly checkpoint signalling. EMBO J *28*, 1099-1110.

Lee, M.S.M., and Spencer, F.A.F. (2004). Bipolar orientation of chromosomes in Saccharomyces cerevisiae is monitored by Mad1 and Mad2, but not by Mad3. Proc Natl Acad Sci U S A *101*, 10655-10660.

Liakopoulos, D., Kusch, J., Grava, S., Vogel, J., and Barral, Y. (2003). Asymmetric loading of Kar9 onto spindle poles and microtubules ensures proper spindle alignment. Cell *112*, 561-574.

Liang, F., and Wang, Y. (2007). DNA damage checkpoints inhibit mitotic exit by two different mechanisms. In Mol Cell Biol, pp. 5067-5078.

Liu, C., Apodaca, J., Davis, L.E., and Rao, H. (2007). Proteasome inhibition in wild-type yeast Saccharomyces cerevisiae cells. BioTechniques *42*, 158-160- 162.

Liu, D., Vader, G., Vromans, M.J.M., Lampson, M.A., and Lens, S.M.A. (2009). Sensing chromosome bi-orientation by spatial separation of aurora B kinase from kinetochore substrates. Science *323*, 1350-1353.

Liu, D., Vleugel, M., Backer, C.B., Hori, T., Fukagawa, T., Cheeseman, I.M., and Lampson, M.A. (2010). Regulated targeting of protein phosphatase 1 to the outer kinetochore by KNL1 opposes Aurora B kinase. J Cell Biol *188*, 809-820.

London, N., and Biggins, S. (2014). Mad1 kinetochore recruitment by Mps1-mediated phosphorylation of Bub1 signals the spindle checkpoint. Genes & Development *28*, 140-152.

London, N., Ceto, S., Ranish, J.A., and Biggins, S. (2012). Phosphoregulation of Spc105 by Mps1 and PP1 regulates Bub1 localization to kinetochores. Curr Biol *22*, 900-906.

Malvezzi, F., Litos, G., Schleiffer, A., Heuck, A., Mechtler, K., Clausen, T., and Westermann, S. (2013). A structural basis for kinetochore recruitment of the Ndc80 complex via two distinct centromere receptors. EMBO J *32*, 409-423.

Martin-Lluesma, S., Stucke, V.M., and Nigg, E.A. (2002). Role of Hec1 in Spindle Checkpoint Signaling and Kinetochore Recruitment of Mad1/Mad2. Science *297*, 2267-2270.

Maure, J.-F., Kitamura, E., and Tanaka, T.U. (2007). Mps1 kinase promotes sister-kinetochore bi-orientation by a tension-dependent mechanism. Curr Biol *17*, 2175-2182.

Miller, R.K., Matheos, D., and Rose, M.D. (1999). The cortical localization of the microtubule orientation protein, Kar9p, is dependent upon actin and proteins required for polarization. J Cell Biol *144*, 963-975.

Mitra, S., Gómez-Raja, J., Larriba, G., Dubey, D.D., and Sanyal, K. (2014). Rad51-Rad52 mediated maintenance of centromeric chromatin in Candida albicans. In PLoS Genet, pp. e1004344.

Musacchio, A., and Salmon, E.D. (2007). The spindle-assembly checkpoint in space and time. In Nat Rev Mol Cell Biol, pp. 379-393.

Nakajima, Y., Cormier, A., Tyers, R.G., Pigula, A., Peng, Y., Drubin, D.G., and Barnes, G. (2011). Ipl1/Aurora-dependent phosphorylation of Sli15/INCENP regulates CPC–spindle interaction to ensure proper microtubule dynamics. J Cell Biol *194*, 137-153.

Nijenhuis, W., von Castelmur, E., Littler, D., De Marco, V., Tromer, E., Vleugel, M., van Osch, M.H.J., Snel, B., Perrakis, A., and Kops, G.J.P.L. (2013). A TPR domain-containing N-terminal module of MPS1 is required for its kinetochore localization by Aurora B. J Cell Biol *201*, 217-231.

Ohouo, P.Y., Bastos de Oliveira, F.M., Liu, Y., Ma, C.J., and Smolka, M.B. (2013). DNA-repair scaffolds dampen checkpoint signalling by counteracting the adaptor Rad9. In Nature, pp. 120-124.

Pereira, G., Manson, C., Grindlay, J., and Schiebel, E. (2002). Regulation of the Bfa1p-Bub2p complex at spindle pole bodies by the cell cycle phosphatase Cdc14p. J Cell Biol *157*, 367-379.

Ruchaud, S., Carmena, M., and Earnshaw, W.C. (2007). Chromosomal passengers: conducting cell division. Nat Rev Mol Cell Biol *8*, 798-812.

Santaguida, S., Tighe, A., D'Alise, A.M., Taylor, S.S., and Musacchio, A. (2010). Dissecting the role of MPS1 in chromosome biorientation and the spindle checkpoint through the small molecule inhibitor reversine. J Cell Biol *190*, 73-87.

Saurin, A.T., van der Waal, M.S., Medema, R.H., Lens, S.M.A., and Kops, G.J.P.L. (2011). Aurora B potentiates Mps1 activation to ensure rapid checkpoint establishment at the onset of mitosis. Nat Comms *2*, 316-.

Schleiffer, A., Maier, M., Litos, G., Lampert, F., Hornung, P., Mechtler, K., and Westermann, S. (2012). CENP-T proteins are conserved centromere receptors of the Ndc80 complex. Nat Cell Biol *14*, 604-613.

Schwartz, K., Richards, K., and Botstein, D. (1997). BIM1 encodes a microtubule-binding protein in yeast. In Mol Biol Cell, pp. 2677-2691.

Seong, C., Sehorn, M.G., Plate, I., Shi, I., Song, B., Chi, P., Mortensen, U., Sung, P., and Krejci, L. (2008). Molecular anatomy of the recombination mediator function of Saccharomyces cerevisiae Rad52. J Biol Chem *283*, 12166-12174.

Shepperd, L.A., Meadows, J.C., Sochaj, A.M., Lancaster, T.C., Zou, J., Buttrick, G.J., Rappsilber, J., Hardwick, K.G., and Millar, J.B.A. (2012). Phosphodependent recruitment of Bub1 and Bub3 to Spc7/KNL1 by Mph1 kinase maintains the spindle checkpoint. Current Biology *22*, 891-899.

Shimogawa, M.M., Widlund, P.O., Riffle, M., Ess, M., and Davis, T.N. (2009). Bir1 is required for the tension checkpoint. In Mol Biol Cell, pp. 915-923.

Shirayama, M., Matsui, Y., and Toh-E, A. (1994). The yeast TEM1 gene, which encodes a GTP-binding protein, is involved in termination of M phase. Mol Cell Biol *14*, 7476-7482.

Shou, W., Seol, J.H., Shevchenko, A., Baskerville, C., Moazed, D., Chen, Z.W., Jang, J., Shevchenko, A., Charbonneau, H., and Deshaies, R.J. (1999). Exit from mitosis is triggered by Tem1-dependent release of the protein phosphatase Cdc14 from nucleolar RENT complex. Cell *97*, 233-244.

Stegmeier, F., Visintin, R., and Amon, A. (2002). Separase, polo kinase, the kinetochore protein Slk19, and Spo12 function in a network that controls Cdc14 localization during early anaphase. Cell *108*, 207-220.

Sudakin, V., Chan, G.K., and Yen, T.J. (2001). Checkpoint inhibition of the APC/C in HeLa cells is mediated by a complex of BUBR1, BUB3, CDC20, and MAD2. J Cell Biol *154*, 925-936.

Symington, L.S. (2002). Role of RAD52 epistasis group genes in homologous recombination and double-strand break repair. Microbiol Mol Biol Rev *66*, 630-670.

Tytell, J.D., and Sorger, P.K. (2006). Analysis of kinesin motor function at budding yeast kinetochores. In J Cell Biol, pp. 861-874.

Visintin, R., Prinz, S., and Amon, A. (1997). CDC20 and CDH1: a family of substrate-specific activators of APC-dependent proteolysis. Science *278*, 460-463.

Wang, E., Ballister, E.R., and Lampson, M.A. (2011). Aurora B dynamics at centromeres create a diffusion-based phosphorylation gradient. J Cell Biol *194*, 539-549.

Yamagishi, Y., Sakuno, T., Goto, Y., and Watanabe, Y. (2014). Kinetochore composition and its function: lessons from yeasts. FEMS Microbiol Rev *38*, 185-200.

Yamagishi, Y., Yang, C.-H., Tanno, Y., and Watanabe, Y. (2012). MPS1/Mph1 phosphorylates the kinetochore protein KNL1/Spc7 to recruit SAC components. Nat Cell Biol *14*, 746-752.

Yeh, E., Yang, C., Chin, E., Maddox, P., Salmon, E.D., Lew, D.J., and Bloom, K. (2000). Dynamic positioning of mitotic spindles in yeast: role of microtubule motors and cortical determinants. Mol Biol Cell *11*, 3949-3961.

Zimniak, T., Fitz, V., Zhou, H., Lampert, F., Opravil, S., Mechtler, K., Stolt-Bergner, P., and Westermann, S. (2012). Spatiotemporal regulation of ipl1/aurora activity by direct cdk1 phosphorylation. Curr Biol *22*, 787-793.

국문초록

염색체 bi-orientation 은 세포분열과정에서 복제된 한쌍의 염색체가 두 개의 딸세포로 나누어질 때 염색체의 수를 정확하게 유지하고 세포가 지속적으로 생존할 수 있도록 하는데 필수적인 과정이다. 진핵세포는 세포분열과정에서 염색체 bi-orientation 을 정확하게 조절하기 위한 기작들을 진화적으로 발전시켜 왔고, 특히 Aurora B 인산화 단백질은 spindle 과 kinetochore 의 연결 상태를 점검하고 spindle assembly checkpoint (SAC)을 활성화시키는데 핵심적인 역할을 한다고 연구되었다. 본 연구에서 사용된 *Saccharomyces cerevisiae* 에서는 Aurora B 인산화 단백질의 출아효모 상응 단백질인 Ipl1 이 인산화 과정을 통해 SAC 을 조절한다고 알려져 있다. 세포분열 중에 spindle 과 kinetochore 가 제대로 연결되지 않으면, Ipl1 은 이러한 비정상적인 연결을 감지하고 SAC 을 활성화시키는 인산화 단백질인 Mps1 을 spindle 과의 연결이 손상된 kinetochore 쪽으로 위치하도록 조절한다. Kinetochore 에 위치한 Mps1 은 Mad1 과 Mad2 등의 SAC 단백질을 kinetochore 로 불러들이고, Knl1 과 Bub1 을 인산화시켜 SAC pathway 를 활성화시킨다. 이렇게 활성화된 SAC 은 metaphase 에서 anaphase 로의 전환을 억제하고 비정상적인 spindle 과 kinetochore 의 연결을 수정한다. 최근의 연구에 따르면 여러종류의 암세포에서 SAC 이 제대로 작동하지 못하도록 하는 돌연변이들이 발견되고 있기 때문에, SAC 의 자세한 조절기작을 연구하는 것은 암세포 형성과정에 대한 이해를 넓혀줄 것으로 기대된다.

Rad52 는 세포 내에서 일어나는 상동재조합 과정에서 핵심적인 역할을 수행하는 것으로 알려진 단백질이다. S phase 에서 일어나는 DNA 복제과정 중에는 내외부적인 다양한 원인으로 DNA double strand break (DSB)가 발생한다. 이러한 DSB 는 세포가 유전정보를 유지하고 생존하는데 치명적인 문제점으로 작용하기

때문에 대부분 Rad52 를 통한 수리기작으로 복원된다. 이렇게 DSB 의 수리를 위한 Rad52 의 기능들은 이미 오랫동안 연구되어 왔지만, Rad52 가 추가적으로 가지고 있을 새로운 기능들에 대한 연구는 미흡한 것이 사실이다. 본연구는 Rad52 가 SAC 과 Ipl1 complex 를 구성하는 유전자들과 유전적 연관성을 가지고 있음을 발견함으로써 Rad52 의 새로운 기능이 mitosis 과 관련이 있을 가능성을 확인하였고, *RAD52* 유전자가 제거된 균주를 이용하여 Rad52 단백질이 spindle 이 손상된 환경에서는 SAC 을 활성화하고, 일반적인 세포분열과정에서는 염색체 bi-orientation 을 조절하는 핵심적인 역할을 수행함을 확인하였다. 또한 본 연구에서 밝힌 기능들은 진핵세포에서 잘 알려진 상동염색체 재조합 기능이나 *Candida albicans* 에서 알려진 kinetochore 구조를 유지하는 기능과는 무관한 추가적인 것임을 확인하였다. 이와 함께, Rad52 가 핵심적인 mitosis 조절 인산화 단백질인 Ipl1 과 SAC 을 활성화시키는 인산화 단백질인 Mps1 에 의해서 인산화가 이루어지는 새로운 기질 단백질임을을 in vitro kinase assay 를 통해 확인하였다. Rad52 가 mitosis 를 조절하는 정확한 기작을 알기 위해서, Ipl1 또는 Mps1 에 의해서 인산화가 되지 않는 돌연변이 단백질들과 지속적으로 인산화가 되어 있는 효과를 나타내는 돌연변이 단백질들을 세포 내에서 발현시켜 생리적인 효과를 관찰하였다. 그 결과, Ipl1 은 Rad52 를 인산화시킴으로써 Mps1 을 kinetochore 쪽으로 위치하도록 조절하고, Mps1 은 Rad52 를 인산화시킴으로써 spindle 이 손상된 상황에서 SAC 이 활성화되도록 조절한다는 것을 밝혀 내었다. 이러한 연구 결과를 통하여, 본 연구는 Rad52 가 염색체 분열이 정확하게 일어날 수 있도록 조절하는 중요한 역할을 수행하고 있음을 확인하고, mitosis 조절 기작의 세부적인 이해를 제공하였다.